Drilling Fluid Engineering

Pål Skalle

Pål Skalle

Drilling Fluid Engineering

Contents

Download free eBooks at bookboon.com

1   Introduction

The simplest drilling fluid is a dirty mixture of water and clay, often referred to as mud. The drilling fluid in the drilling process can be seen as the equivalent to the blood in the human body, the mud pump is the heart, and the drilled out shale (cuttings) represent the slag products. At the surface, we find the mud cleaning system which corresponds to the kidney and the lungs. In the mud cleaning system the cuttings are removed by means of a sieve, the shale shaker.

Mud is basically a fluid (water or oil) circulated to bring cuttings out of the wellbore. Two important qualities of the fluid are needed for mud to achieve all its tasks:

- **Viscosity**: Water and oil has a viscosity of around 1 cP (centiPoise), which is far too little to transport the cuttings out. A component is needed to increase the viscosity. The main viscosifyers are clay and polymer, presented in Chapter 3.
- **Density**: Water and oil have a density of around 1 kg/l, which in most cases is too little to counter high pore pressure. It may in fact become necessary to increase it to twice the pressure of a water column. The main density giver is Barite ($BaSO_4$), a mineral often found as evaporites (with a specific density of 4.2 kg/l), or, soluble salts (brines).

Clay and polymers react with water, while Barite does not, and is therefore referred to as the inert phase.

1.1   Nine distinct mud systems

For mud to manage its many tasks, a broad range of different fluid systems have been developed. The July issue of World Oil (a list of general references are found in Chapter 9) presents all drilling fluids and additives (approximately 5000 different additives). Nine distinct mud systems are defined here. The first seven are water-based, while the eighth is oil-based. The ninth category is a specialized one in which air or gas is the continuous fluid. The 9 categories are:

1. *Non dispersed.* These may consist of spud muds, natural muds and other lightly treated systems generally used for shallow wells or top-hole drilling.
2. *Dispersed.* At greater depths or where hole-conditions may be problematic, muds are often dispersed, typically by means of lignosulphonates or other deflocculants. These and similar products are also effective filtrate reducers.

3. *Calcium treated.* Divalent cations such as calcium and magnesium, when added to a mud, inhibit the swelling of formation clays and shale, and are therefore added to control sloughing shale, hole enlargement and to prevent formation damage. Hydrated lime, gypsum (calcium sulphate) and calcium chloride are principal ingredients of calcium systems. *Gyp systems* (note: Gyp = gypsum) usually have a pH of 9.5 to 10.5 and an excess gyp concentration of 2 to 4 lb/bbl; *Lime systems* have an excess lime concentration of 1 to 15 lb/bbl and a pH of 11.5 to 12.0.

4. *Polymer.* Muds incorporating long-chain, high-molecular-weight chemicals are effective in increasing viscosity, flocculating muds, reducing filtrate loss and stabilizing the formation. Various types of polymers are available for this purpose, including Bentonite extenders. Bio polymers and cross-linked polymers are also used and have good shear-thinning properties at low concentrations.

5. *Low solids.* This includes systems in which the amount and type of solids are controlled. Total solids should not range higher than about 6% to 10% by volume (and clay < 3% by volume). One primary advantage of low-solids systems is that they significantly improve the rate of penetration.

6. *Saturated salt.* Include several groups: *Saturated salt systems* have a chloride ion concentration of 189 000 ppm. *Saltwater systems* have a chloride content from 6 000 to 189 000 ppm, and at its lower level are usually referred to as *brackish* or *seawater systems.*

7. *Workover.* Completion and workover fluids are specialized systems designed to minimize formation damage, and be compatible with acidizing and fracturing operations (acid soluble) and capable of inhibiting swelling clays that reduce formation permeability. Density is obtained through dissolved salt to avoid long term settling.

8. *Oil/synthetic.* Oil-based fluids are used for high temperature wells, deviated holes and wells where pipe sticking and hole stabilization is a problem. They consist of two types of systems:

    1) *Invert emulsion muds* are water-in-oil fluids and have water as the dispersed phase and oil as the continuous phase. They may contain up to 50% water in the liquid phase. Emulsifier (commonly fatty acids amine derivatives, high-molecular-weight soaps), and water concentrations are varied to control rheological and electrical stability;

    2) *Synthetic fluids* are designed to duplicate the performance of oil-based muds, without the environmental hazards. Primary types of synthetic fluids are esters, poly alpha olefins and food grade paraffin. They are environmentally friendly, can be discharged offshore and are non-sheening and biodegradable.

9. *Air, mist, foam and gas.* Four basic operations are included in this specialized category according to the IADC. These include:

   1) Dry air drilling, which involves injecting dry air or gas into the wellbore at rates capable of achieving annular velocities that will remove cuttings;

   2) Mist drilling involves injecting a foaming agent into the air stream, which mixes with produced water and lifts drill cuttings;

   3) Stable foam uses chemical detergents and polymers and a foam generator to carry cuttings in fast-moving air stream;

   4) Aerated fluids rely on mud with injected air (which reduces the hydrostatic head) to remove drilled solids from the wellbore.

1.2   The four main tasks of a drilling fluid

Mud has many important functions and corresponding necessary properties. Chapter 5, 6, 7 and 8 will take you through the four most important ones.

The two single most important functions are to 1) remove the cuttings away from under the bit and 2) transport them from the bottom to the surface. The two functions are studied in Chapter 5 and 6. Flushing the cuttings from the bottom require a high flushing effect. This is achieved by inserting small jet nozzles in the rock bit and thereby creating a large pressure drop. Typically 50% of the pump pressure is placed here for this very purpose. The other 50% is pure friction loss through the thin, long drill string through and the concentric hole between the wellbore and the drill pipe. The wellbore is made up by the drilling bit, and the concentric hole is referred to as the annulus.

Friction loss is an important sub task of Task 2, and is studied separately in Chapter 4. Here it will be revealed that the viscosity of drilling fluids is not a constant parameter for a given drilling fluid; it varies with shear rate (which is created by the pumping action of the mud pumps). Viscosity of the mud is in fact surprisingly high at low pump rates, but decreases with increasing pump flow rates.

Task 3: Controlling the pump pressure loss in the annulus. This pressure loss has an additional importance compared to other friction drops; annular friction pressure adds itself onto the hydrostatic wellbore pressure and may create difficult conditions from time to time. This topic will be discussed in Chapter 7.

Task 4: Maintaining a stable wellbore. This task includes two sub tasks; chemical stability and mechanical stability. Chapter 8 will reveal the details.

The drilling fluid must be designed to take care of other tasks also, such as;

- Cool and lubricate the bit and the drill string
- Avoid loosing mud into natural or induced cracks
- Bring information back to the surface

1.3   About this book

This book aims to present the procedure of how to apply fluid mechanics on drilling challenges, and to explain the related physics involved and the different engineering approaches. All students with an interest in Petroleum Engineering can read this book without special preparations besides fluid mechanics.

This book does not give many references to scientific papers. Most of the information in this book is found in relevant textbooks plus web pages from major oil companies and major drilling fluid service companies. Many of the companies have their own Best Practices Manuals. Details about Drilling Fluid Engineering are found in such textbooks and manuals, listed under References (Chapter 9).

2 Mud circulation loop and its components

Mud is circulated through a wellbore to bring the cuttings to the surface. Here cuttings are separated out so that clean mud can be reinjected into the well.

2.1   The mud loop and solids control

A typical circulation system on a stationary, offshore drilling platform is presented in Figure 2-1, while Figure 2-2 presents a circulation system; on a floating drilling unit. The mud is mixed and prepared in the mud pits consisting of several large tanks, each typically 60 m³ large. One or two of the tanks are in active use during drilling, while the others are for transfer and storing of fluids. One reserve pit is for kill mud, where the density is kept typically at 0.25 kg/l above the density in the active pits. Both density and rheology are maintained in the active mud pits. Typical total volume of offshore mud pits are 200 m³, and with a surface area of typically 50 m². Here a vertical height of two cm corresponds to a volume of 1000 liters! In the surface mud system in Figure 2-1, we see two pumps in parallel. On offshore rigs today it is more common with three or four.

From the pumps, a high-pressure output line leads up to the drill floor, where, on the standpipe, a multi-task junction is found, called the standpipe manifold. Here the driller can read the standpipe pressure, and is almost identical with the pump pressure, reduced only by pipe friction in the short distance between the pump and the standpipe manifold.

On its return to the surface, the mud is directed through a wide settling tank, where the largest particles are allowed to settle out. On other rigs this tank is called the sand trap, positioned in front of the shale shakers as an over-flow tank.
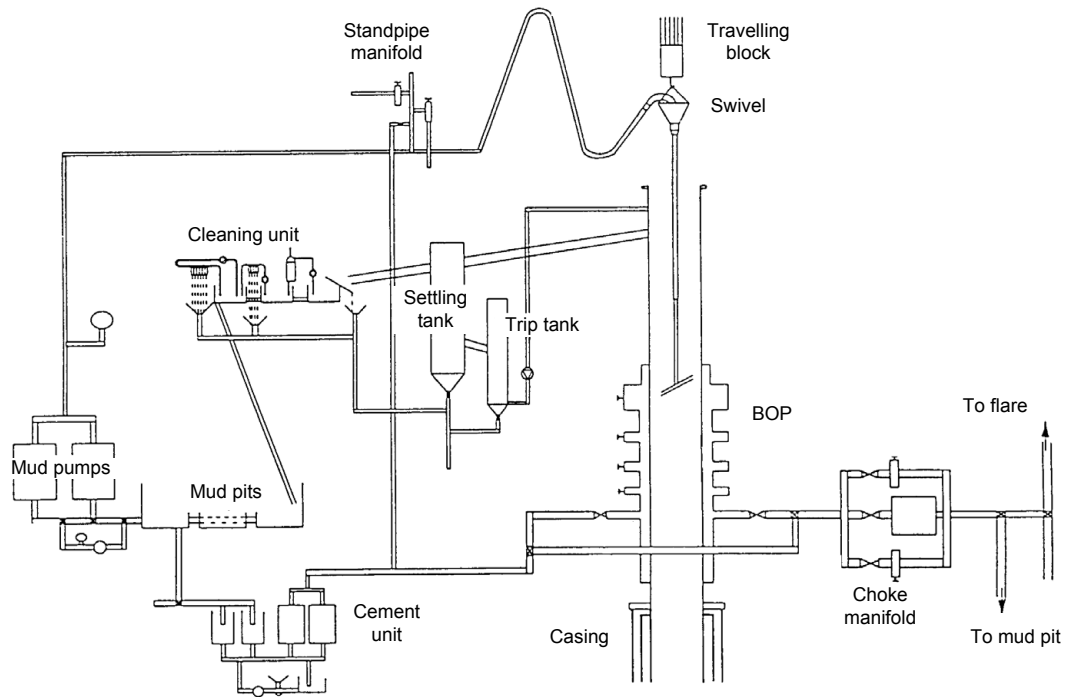
Figure 2-1: The surface mud flow path and the cleaning unit. For cementing operations and for killing operations the smaller cement pump is applied.

Download free eBooks at bookboon.com
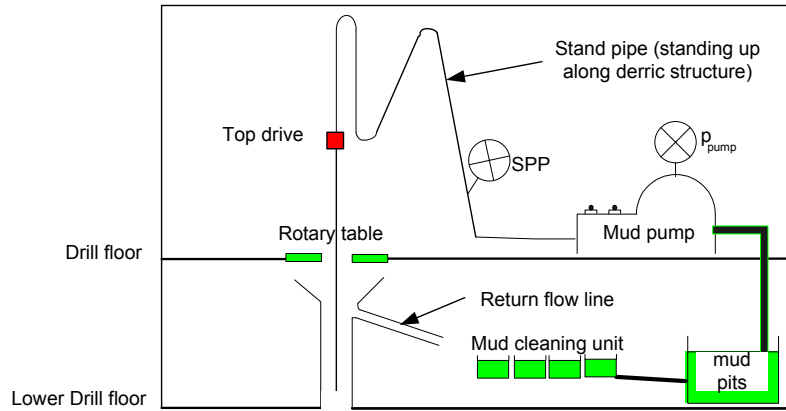
Figure 2-2: Mud circulation system on a floater.

Drilled out solids are separated from the drilling fluid and discarded in the mud-cleaning system. Figure 2-3 presents a typical mud-cleaning unit.
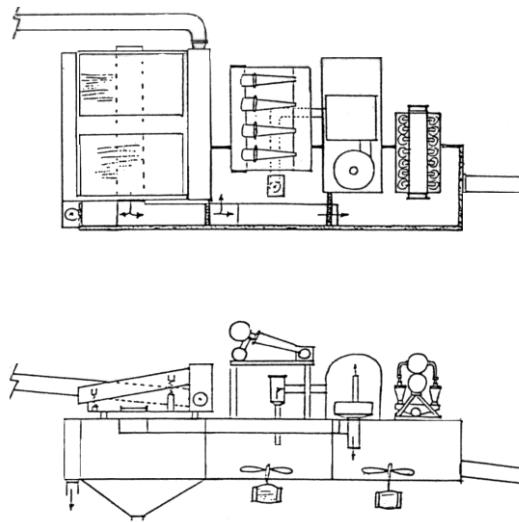
Figure 2-3: Horizontal and vertical projection of a mud cleaning unit.

In a complete mud cleaning system, the following cleaning methods may be included:

1. Settling
2. Dilution
3. Mechanical separation
4. Chemical treatment

Each method exhibits certain advantages and disadvantages. The most efficient form of solids control is a combination of several methods. Settling can remove particles down to colloidal size, but settling is time consuming and impractical. Mechanical separation can remove particles of sizes down to 5 mm as shown in Table 2-1.

Shale shaker	Can remove solids > 68 μ (200 mesh)
Desander	Dependent on size of the cone, can remove solids > 30 μ
Desilter	Dependent on size of the cone, can remove solids> 15 μ
Centrifuge	Can remove colloidal solids > 5 μ

Table 2-1: Mechanical cleaning equipment.

Shakers are the most common cleaning method. With the quality and fineness of shaker filter screens available today, other cleaning methods have become almost obsolete. With a 60 mesh and a 300 mesh filter screen in series, 99% of the cuttings are removed. A 60 mesh filter screen removes the largest cuttings and protects the extremely fine second filter screen from wear and tear. The Mesh – size system is presented in Table 2-2.

Low gravity solids (LGS) enter the mud through dispersed or disintegrated cuttings and has a density of 1.8–2.8 kg/l. If its content (LGSC) is increasing above a certain limit, solids control must be intensified.

Mesh	Wire Diameter	Opening Width	Smallest particle size removed
	Inches	Microns	Microns
10	.0250	2108	2000
20	.0160	863	800
60	.0072	230	205
100	.0045	140	125
120	.0037	117	105
200	.0030	74	68
325	.0018	44	40

Table 2-2: Important parameters for square Mesh shakers (Mesh # = # of openings pr. inch).

One issue with fine filter screens is the wear of filter screens; monitoring and maintenance is required.

2.2   The mud pump

Pumping drilling fluids through kilometre long pipe systems will result in large hydraulic friction, and correspondingly powerful mud pumps are required. One typical pump is shown in Figure 2-3.
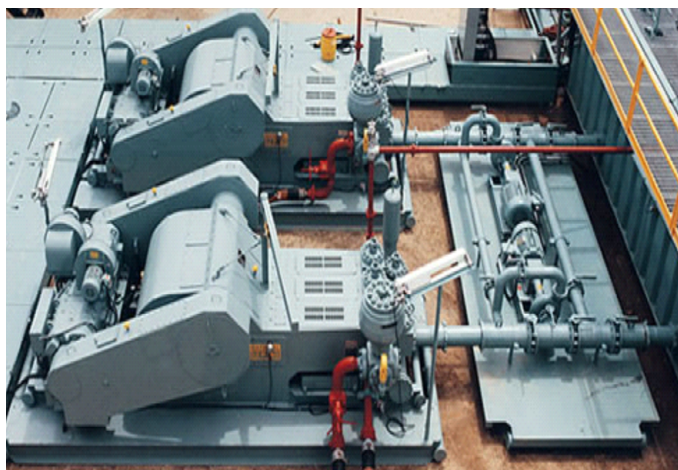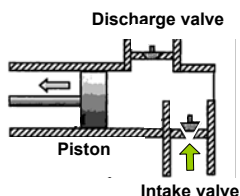
Figure 2-3: Two blue painted triplex (triplex means three pistons working in parallel), single acting piston pumps (single acting means acting only during on one of the two stroke directions). A single acting piston is shown to the left.

When it comes to hydraulic friction and to Task 1, removal of crushed cuttings, it will be necessary to know the characteristics of a mud pump. Figure 2-4 shows the pumps characteristics. The pump is limited by its maximum pressure, $p_{p,max}$, for each liner size, its maximum flow rate for each liner size, q_{max}, and its maximum effect, $E_{p,max}$ (the latter parameter is the same for all liners). The pump characteristics are divided into two different operating ranges: Range I is defined through the pump's smallest liner, and range II includes the rest of the liners. Table 2-2 presents a typical pump characteristic for large sized mud pumps.
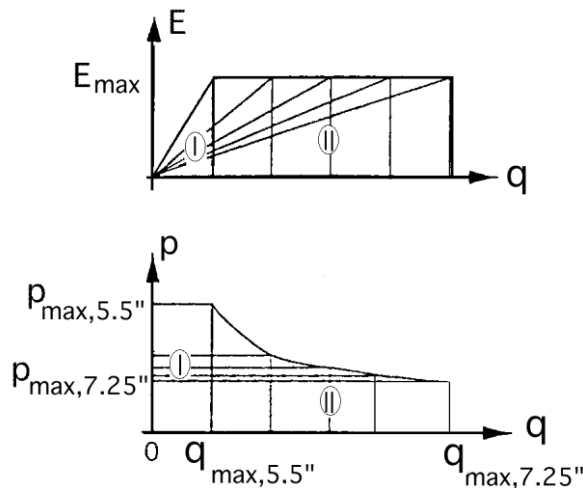
Figure 2-4: Pump characteristics. The two numbers I and II indicate the two operating ranges of the pump. Range I is represented by the smallest liner, in which the pump pressure can be manipulated to be held constant if desired, for instance at the maximum recommended pressure for the 5.5″ diameter liner.

Parameter:	Unit:	Data:							
Liner size	in	5 1/2	5 3/4	6	6 1/4	6 1/2	6 3/4	7	7 1/4
Discharge pressure	psi bar	5555 383.0	5085 350.6	4670 322	4305 296.8	3980 274.4	3690 254.4	3430 236.5	3200 220.6
Pump flow rate	GPM m^3/s	444 .0280	486 .0307	529 .0334	574 .0362	621 .0392	669 .0422	720 .0454	772 .0487
Power	Hp	1439.0	1441.8	1441.3	1441.7	1442.0	1440.3	1440.8	1441.3

Table 2-3: Characteristics of a 1600 Hp mud pump, rated at 120 SPM (max is 140).

The effect of the pump is equal to approximately 2000 Hp when running at its maximum design speed (140 spm). It is recommended to run it at a lower maximum, e.g. 120 spm. The resulting effect, 1440 Hp, is also the nominal effect of the pump. The pumps effect can be expressed in SI units or in OFU (Watt (W) or Horsepower (Hp) respectively):

$$E_{pump} = q \cdot p_{pump} \quad (W) \tag{2.1}$$

To obtain effect in horsepower (Hp) when applying OFU, q is given in GPM and p in psi:

$$E_{pump} = \frac{q \cdot p_{pump}}{1714} \, (Hp) \tag{2.2}$$

Other useful conversions are presented in Chapter 10.5.

3   Drilling fluid viscosity control

Clay and polymers play an important role in drilling fluid viscosity control and are therefore given special attention here. Clay plays in addition a central role for wellbore stability (Chapter 8).

3.1   Clay chemistry

The group of minerals classified as clays can be described chemically as aluminium silicates. Since the elements that constitute the clays account for more than 80% of the earth mass (aluminium 8.1%, silicon 27.7% and oxygen 46.6%) it can be readily accepted that every stage of drilling a hole brings us in contact with clay. Clay and shale thus account for more than 75% of all sediments. Type and quantity of clay minerals is one of the most important features for chemical and mechanical properties of sedimentary rock. A compositional example of sediments vs. depth is shown in Table 3-1.

Depth (m)	2 000	2 200	2 400	2 600	2 800
Quartz	10	15	55	40	75
Feldspar	12	15	8	10	6
Calcite	11	-	2	10	5
Pyrite	5	-	2	10	4
Smectite	22	25	8	5	-
Illite	22	25	10	10	5
Chlorite	10	5	6	-	-
Kaolinite	8	15	10	15	5
CEC	28	22	14	8	3

Table 3-1: Mineralogy of typical sediments at different depths. Top of the reservoir starts at 2 400 m. Mineralogy is presented in % (CEC is a relative measure of water-shale reactivity).

The selection of the drilling fluid is often related to the reactions between the fluid and the rock, as these reactions can influence the stability of the bore hole. Thus, an understanding of clay is important both in the selection of a drilling fluid system and for the optimization of bore hole stability. The most important clay properties for a drilling fluid engineer are shown in Table 3-2.

Property	Kaolinite	Mica	Montmorillonite	Attapulgite	Chlorite
Crystal structure	sheet	sheet	sheet	sheet	sheet
Particle shape	hexagonal plate	extensive plates	flake	needle	plate
Particle size, mm	5–0.5		2–0.1	1–0.1	5–0.1
Surface Area:		10^5–0.5			
BET-N$_2$ m^2/g	15–25	50–110	300–800	200	140
BET-H$_2$O, m^2/g	3–15	-	200–800	-	-
CEC, meq/100 g	-	10–40	80–150	15–25	10–40
Viscosity in water	Low	Low	High	High	Low
Effect of salt	Flocculates	Flocculates	Flocculates	None	Flocculates

Table 3-2: Properties of common clays.

Bentonite is the generic name applied to a mixture of minerals that predominantly contains the mineral Montmorillonite. The associated minerals are typically other clays, such as mica, kaolinite and quartz. Clay is often formed by the *in-situ* alternation of volcanic ash in the presence of water. The salinity and chemical composition of water and ash can give rise to different types of clay.

3.1.1   Structure of Montmorillonite

Montmorillonite is an aluminium silicate, in which the silicon-oxygen sandwich is a layer of aluminium hydroxide, as shown in Figure 3-1.
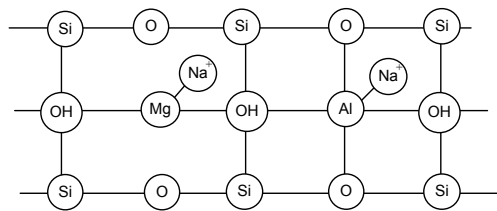

Figure 3-1: A principle and simplified structure of one unit layer of Montmorillonite, 10 Angstroms thick.

Three essential characteristics of this crystal are responsible for the special properties of Montmorillonite:

1. Some of the aluminium in the lattice structure are, during creation, replaced with ions of a lower charge (electron valence) such as magnesium (from 3 to 2). The *substitution*, without any other change of structure, creates negative surface charges in the lattice.

2. The negative charge sites created in the clay sheet by magnesium substitution are partly balanced by close association of positively charged ions (cations), normally Na^+. When the negative charge arises in the aluminium layer, the silica layers act as a barrier that prevents effective neutralisation of either the cations or the charge sites on the clay surface. The creation of these charged ions and charged clay surfaces creates very strong attractive forces for polar water molecules that readily force themselves in between the unit layers. The unique feature of Montmorillonite is thus potential for the individual sheets to separate as more water is attracted. In other clay minerals, the bonds formed between unit layers are stronger and they do not separate. One clay particle consist normally of hundreds of stacked unit layers.

3. The loosely held cations give rise to the property known as the *cation exchange capacity*. The attached ions can be exchanged or replaced by other ions present in the surrounding water. The ability of one type of cation to replace another depends on the nature of the involved cations and their relative concentrations. The common cations will replace each other (when present in equal concentration) in the following order:

$$Al^{3+} > Mg^{2+} > Ca^{2+} > H^+ > K^+ > Na^+$$
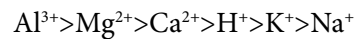
The cation exchange capacity (CEC) is easily determined by measuring the adsorption of a cationic organic dye called methylene blue.

The nature of the cations in the exchange positions can affect the hydration properties of the mineral. The most common exchangeable cations are sodium and calcium. The sodium ion has only one single positive charge. In a Montmorillonite only containing sodium exchangeable ions, the clay has a capacity for infinite expansion and even separation of the sheets down to single sheets, which are only 10 Angstroms thick. A multivalent ion, such as calcium (valence = 2), associates with two sheets, so the expansion is limited to a maximum spacing between the sheets of about 17 A, see Figure 3-2.
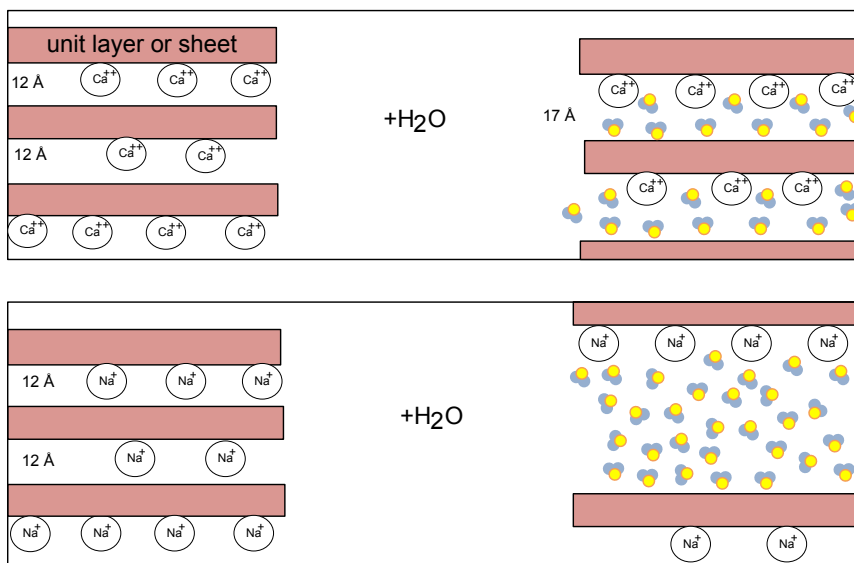
Figure 3-2: Hydration of Calcium Montmorillonite (upper) and Sodium Montmorillonite (lower).

3.1.2   Interaction between clay particles

The forces acting on the clay particles can be described as either repulsive or attractive forces. The particles may interact due to Brownian motion. Whether they will agglomerate or not will depend on the summation of the repulsive and the attractive forces.

Repulsive electrical forces

The clay particles have been described as small crystals that have a negative surplus charge (a partly compensating charge is provided by the ions in solution that are electrostatically attracted to the surface). When two negatively charged particles approach each other, there will be repulsion between the particles that will become larger the closer the particles approach each other.

However, since thickness of the electrostatic layer can be compressed by electrolytes, then, as the electrolyte (dissolved salt) level is increased, the particles can more easily approach each other, as shown in Figure 3-3.
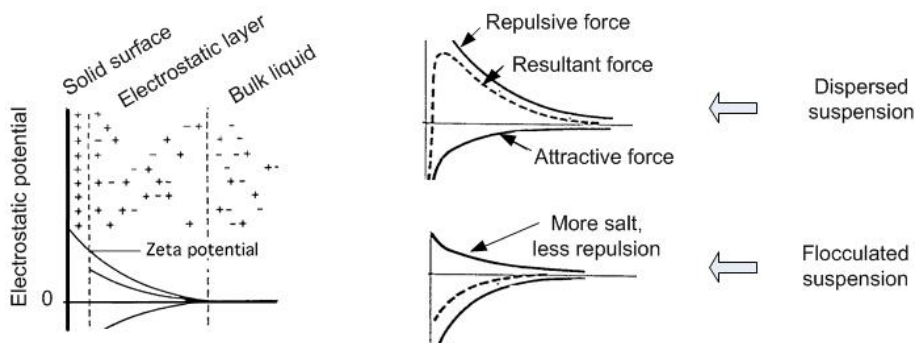
Figure 3-3: Bulk solution is neutral. Salt compresses the electrostatic layer and affects the attractive and repulsive forces between clay particles.

Download free eBooks at bookboon.com

Attractive van der Waals forces

van der Waals forces arise through the attraction of the spontaneous dipoles being set up due to distortion of the cloud of electrons around each atom. This is illustrated in Figure 3-4. For a large assemblage of atoms, such as in a clay platelet, this force can be significant as it is additive. The attractive force decays very rapidly with distance; inversely proportional to the distance cubed (l/d³), but it is essentially independent of the electrolyte concentration.

Two atoms with symmetrical clouds of electrons and hence no attractive force between the atoms.

Spontaneous distortion of the electron cloud sets up dipole attractive forces.
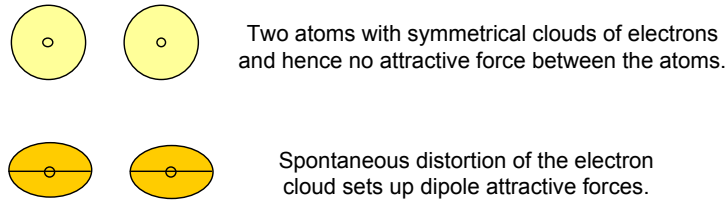
Figure 3-4: Illustration of the origins of van der Waals attractive forces in any two materials close to each other.

Resulting associations

The associations between clay particles are caused by repulsive/attractive forces and are important as they affect important properties, such as viscosity, yield and fluid loss, exemplified in Figure 3-5. The terms describing the associations are as follows:

Deflocculated or dispersed; an overall repulsive force between clay particles, which carry the same net negative charge.

Flocculated Systems; there are net attractive forces between the particles.

*Aggregated Systems***;** the clay consists of a basic sheet structure or unit layer, and the crystals consist of assemblages of the sheets, one upon the other.
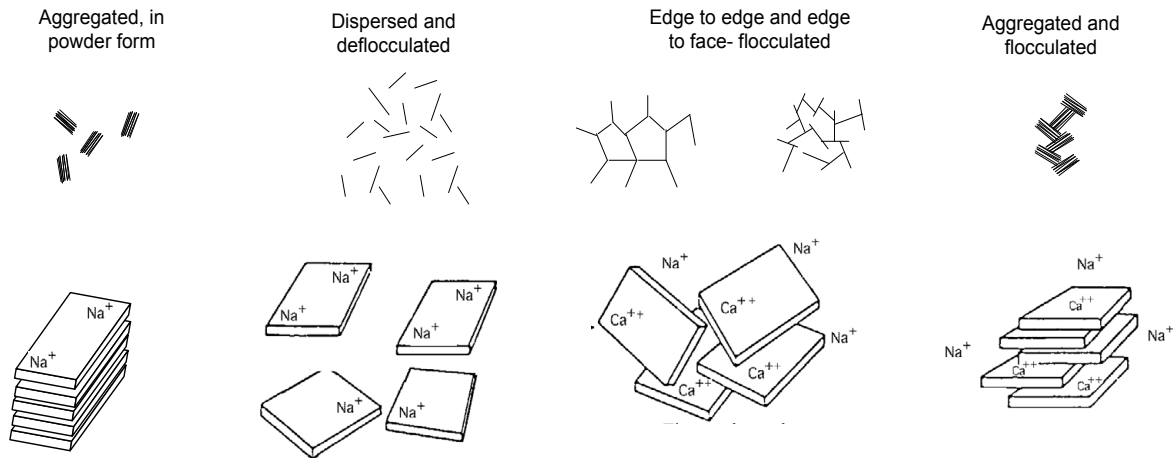
Figure 3-5: Modes of particle association of clay.

3.2   Polymer chemistry

3.2.1   Fundamental structure of polymers

A polymer consists of basic units (monomers) that are chemically joined together (polymerized), to form chains as shown in Figure 3-6.
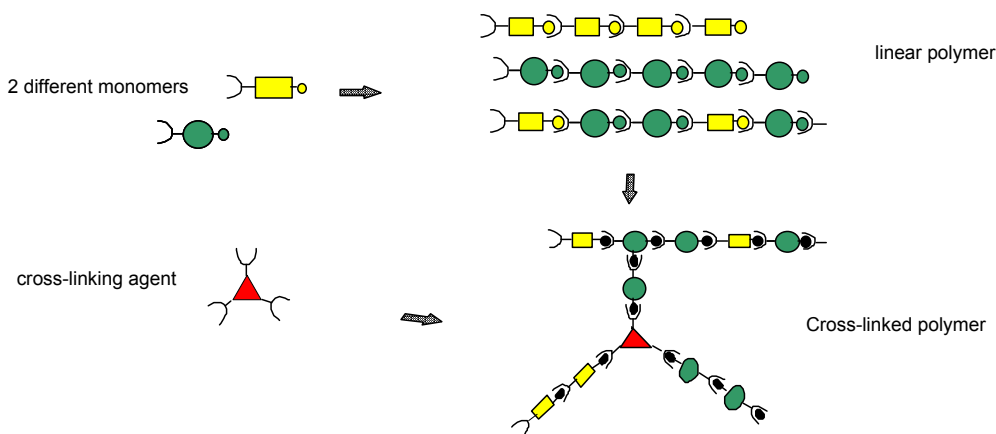
Figure 3-6: Fundamental polymer structure.

The molecular weight (MW) or chain length can be impressively long, up to 50 millions! Assuming a typical monomer diameter is 7 A, a 50 million MW polymer is 3.5 cm long. Polymers can be divided into three groups; non-ionic, anionic (-) and cationic (+). More than one type of monomer group may be present in the same molecule. Since the groups are either weakly basic or acidic, the charged nature of most of the groups is dependent on the pH value of the drilling fluid and will change from non-ionic to cationic or anionic respectively (just like charged clay).

The ionic strength of the fluid affects the electrostatic repulsion between the charges. An increased level of electrolyte will change the balance between the repulsive and attractive forces and allows molecules of equal charges to approach each other. A negatively charged polymer will change its configuration from an extended polymer in fresh water, where charge repulsions are stretching the molecule, to a tightly-coiled structure in a saline solution, where the repulsive forces are lower. This is shown schematically in Figure 3-7. The change in molecular shape will change the physical properties of the polymer in the solution. The coiled up polymer will present a smaller surface for interacting with the water or with other polymer molecules, and thus produce lower viscosity. A non-ionic polymer should be essentially unaltered by salt.

Multivalent ions can act as bridging agents by reacting with more than one charged group on the molecule. Unhydrated cement will feed the drilling fluid with soluble calcium ions and a high alkalinity (pH > 7). Calcium ions (Ca^{++}) react with anionic (-) polymers such as CMC and cause bridging or flocculation. The extent of the reaction is a function of the concentration of the double valens ions and of the pH of the solution.

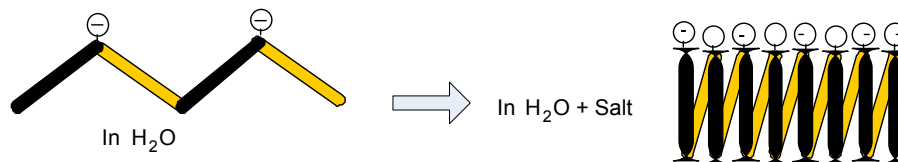In H_2O In H_2O + Salt

Figure 3-7: Effect of electrolyte concentration on polymer configuration.

3.2.2   Classification of polymers

A rough classification of polymers and some of its associated properties are:

> A. Synthetic polymers
>   1. Copolymer, like Vinylacetat-meleic-anhydrid (VAMA).
>   2. Polyakrylonitril, like PHPA = partially hydrolyzed polyacrylacetat

B. Natural polymers (polysaccharides)

1. Cellulose

    a) CMC (Sodium Carboxylmetyl cellulose). From wood pulp. Anionic.

    b) HEC (Hydroxyletyl cellulose). Non-ionic

    c) PAC (Poly-ionic cellulose)

2. Starch (of corn). Non-ionic.

3. Guar. Non-ionic.

4. Biopolymers, like Sugar + microorganisms. X-C-polymers. Weakly anionic.
   MW = 2 – 50 mill.

The most common applications of polymers are viscosity building: Polymers are applied as viscosifyers simply by dissolving high-molecular-weight-polymers in water. Natural polymers will start to degrade when exposed to heat. Already at 80 ^{o}C biocides are required to slow the decomposition rate down. Above 100 ^{o}C, natural polymers are difficult to apply, since the rate of adding polymer to maintain viscosity becomes intolerable. As wells become deeper, thermal stability becomes an important performance characteristics of polymers. Synthetic polymer-chemistry has made its most significant contribution to the drilling industry in high-temperature/high-pressure applications. From the early 1990s, numerous synthetic polymers proved technically capable and cost effective at high bottom hole temperatures and pressures. Synthetic polymers specifically formulated for deflocculating, fluid-loss-control, and gel inhibition at high temperature proved to have a wide utility. Using WBM at these hostile conditions would have been impossible without natural, modified, and synthetic polymers.

The application of polymers is described more detailed in Chapter 3.5.

3.3   Rheology of drilling fluids

Rheology models and rheology measurements in the drilling industry has been influenced by the 2-speed rotational viscometer (Fann VG meter), which has been applied in the oil field. The objective behind the use of this viscometer was to simplify rheology control in the field. Today, however, as the petroleum industry has evolved in all aspects, the need for higher quality rheology control has arisen. Now a 6-speed viscometer is the norm. Therefore, three different approaches to determine rheology constants are presented:

-   2 data points oil field approach
-   2 data points standard approach
-   6 data points regression approach

Flow curve or rheogram is a plot of shear stress readings vs. shear rate, obtained in a rotational viscometer. Table 3-3 presents an example of readings, with the corresponding flow curve in Figure 3-9. Due to the geometry and calibration of the Fann VG viscometer the true shear stress, τ_w, is obtained by multiplying the obtained readings with the correction factor of 1.07. This constant is normally ignored and thus the readings (q) are incorrectly assumed equal to the shear stress (t).

The test results in Table 3-3 will be used to exemplify different rheology models, together with Figure 3-8.

Symbol	RPM	θ		$\dot{\gamma}$	t = τ	τ_w
Unit	rpm	(-)		s⁻¹	lb/100 ft²	Pa
Data	600	140		1022	149.4	71.5
	300	98		511	104.9	50.8
	200	78		340	83.2	39.8
	100	54		170	57.6	27.6
	6	16		10.2	17.1	8.2
	3	13		5.1	13.9	6.7
	3 ₁₀″	23		5.1	24.5	11.7
	3 ₁₀′	48		5.1	51.2	24.5

Table 3-3: Shear stress readings (q) in a 6-speed rotational Fann VG viscometer. The two lower data points, representing gel strength, build up after 10 seconds and 10 minutes quiescence.
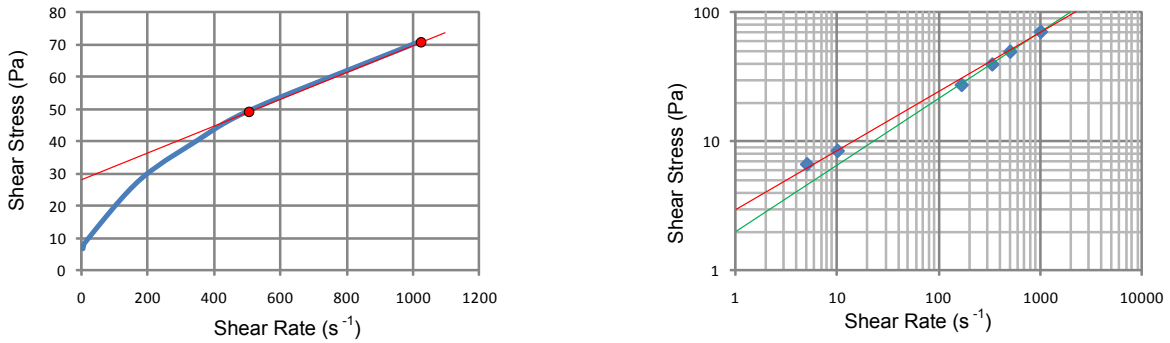
Figure 3-8: Example of flow curve (left). Flow curve in log-log plot (right).
Data taken from Table 3-3.

The viscosity of a fluid expresses its resistance to flow. Fluids with a constant viscosity for all shear rates are called Newtonian fluids. Non-Newtonian fluids are those in which the shear stress is not linearly related to the shear rate $\dot{\gamma}$. Shear rate expresses the intensity of shearing action in the pipe, or change of velocity between fluid layers across the flow path:

$$\dot{\gamma} = -\frac{dv}{dr} \tag{3.1}$$

Common rheological models are:

Newtonian model: $\qquad \tau = \mu\dot{\gamma}$ $\qquad\qquad\qquad\qquad$ (3.2)

Bingham plastic model: $\qquad \tau = \tau_y + \mu_{pl}\dot{\gamma}$ $\qquad\qquad\qquad$ (3.3)

Power law model: $\qquad \tau = K\dot{\gamma}^n$ $\qquad\qquad\qquad\qquad$ (3.4)

Herschel & Bulkley model: $\qquad \tau = \tau_y + K\dot{\gamma}^n$ $\qquad\qquad\qquad$ (3.5)
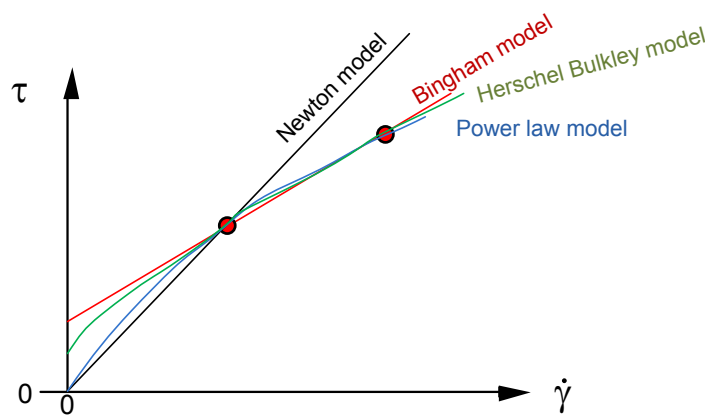
Figure 3-9: The flow curve of four different rheological models of four different fluid samples.

The principle shape of the four rheological models is shown in Figure 3-9, and their parameters are determined as follows:

Newtonian model; 2 data points, standard approach

One constant is sufficient to describe this model. For the Newtonian fluid readings at 300 RPM are selected:

$$\mu_{300} = \frac{\tau_{300}}{\dot{\gamma}_{300}} = \frac{50.1}{511} = 0.098 \ Pas = 98 \ cP \tag{3.6}$$

Bingham model; 2 data points, oil field approach

The Fann VG viscometer is calibrated to suit the Bingham model. The shear rate at 300 is designed to be equal to one shear rate unit, making eqn (3.7) simply a difference between two numbers:

$$\mu_{pl} = \theta_{600} - \theta_{300} = 140 - 98 = 42 \ cP = 0.042 \ Pas \tag{3.7}$$

$$\tau_y = \theta_{300} - \mu_{pl} = 98 - 42 = 56 \ lb/100 \ ft^2 = 26.8 \ Pa \tag{3.8}$$

Bingham model; 2 data points, standard approach

After converting to SI-units and including the conversion factor of 1.067 in Table 3-3, the viscosity is defined by the slope of the curve:

$$\mu_{pl} = \frac{\tau_{600} - \tau_{300}}{\dot{\gamma}_{600} - \dot{\gamma}_{300}} = \frac{71.5 - 50.1}{1022 - 511} = \frac{21.4}{511} = 0.04199 \; Pas$$

(3.9)

The yield point is found by solving eqn (3.3):

$$\tau_y = \tau_{600} - \mu_{pl} \cdot \dot{\gamma}_{600} = 71.5 - 0.04199 \cdot 1022 = 28.6 \; Pa$$

(3.10)

Note that oil field and conventional standard procedures give identical results with respect to by including the 1.067 factor.

Power law model; 2 data points, standard approach

In order to find the two constants, take the logarithm of eqn (3.4) for two different data points. Both resulting equations contain n and K. Solving for n yields:

$$n = \frac{\log \tau_{600} - \log \tau_{300}}{\log \dot{\gamma}_{600} - \log \dot{\gamma}_{300}} = \frac{\log \dfrac{\tau_{600}}{\tau_{300}}}{\log \dfrac{\dot{\gamma}_{600}}{\dot{\gamma}_{300}}} = \frac{\log \dfrac{71.5}{50.1}}{\log 2} = 3.32 \cdot \log \frac{71.5}{50.1} = 0.514$$

(3.11)

With known n, solving eqn (3.4) for K yields:

$$K = \frac{\tau}{\dot{\gamma}^n} = \frac{71.5}{1022^{0.514}} = 2.3 \; Pa$$

(3.12)

After also checking the Oil Field Approach we note that n is identical in the two approaches, while K is around 6.7% lower in the Oil Field Approach.

Herschel Bulkley model; 3 data points, oil field approach

Since this model contains 3 unknowns we need minimum 3 data points. The yield point is found through either reading τ_y from the flow curve plot after extending it to $\gamma = 0$, or simply assuming

$$\tau_y = \tau_3 = 3 \; Pa$$

(3.13)

The equation can now be solved in a log-log plot with 3 + 1 (τ_y) data points. The slope of the line defines n and K can be found from:

$$K = \left(\tau_2 - \tau_y \right) / \left(\dot{\gamma}_2^n - \dot{\gamma}_y^n \right) = (71.5 - 3) / 1022^{0.5} = 0.6$$

Herschel & Bulkley model; 3 data points, standard approach

Select three data points and apply standard iteration procedure to solve the tree equations.

6 data points, regression approach

One reason for using the two upper data points is the remarkable quality of the Bingham model. It turns out that after long periods of still standing, the gel strength of the fluid approaches the yield point, t_y (obtained through the two upper readings). This is clearly demonstrated through Table 3-3. After 10 minutes the gel strength has climbed to 48 lb/100 ft^2, whereas the yield point is 56 lbs/100 ft^2. But the yield point is therefore true only under such conditions; long stationary periods.

Now a days there is no excuse for not applying all six readings to determine the constants through curve fitting (regression analysis). A detailed description of how to do this is presented in Chapter 10.6.

Other known rheological models are:

$$\text{Collins-Graves} \qquad \tau = (\tau_y + K\dot{\gamma})(1 - e^{-\beta\dot{\gamma}}) \tag{3.14}$$

$$\text{Robertson-Stiff} \qquad \tau = K(\dot{\gamma}_y + \dot{\gamma})^n \tag{3.15}$$

$$\text{Casson} \qquad \tau = \left[\sqrt{\tau_y} + \sqrt{\mu \cdot \dot{\gamma}} \right]^2 \tag{3.16}$$

These models are in little use in conjunction with drilling fluids.

3.4   Filtration control

Darcy's law governs filtration of liquids through porous media. However, fluid loss from the wellbore will decrease with time, since the permeability decreases continuously as particles make a tighter filter. In Figure 3-10, the spurt loss occurs at the start of a filter test, a test which is made on an initially clean filter paper, mimicking porous sandstone. After the spurt loss, the filtrate volume becomes proportional to the square root of time.
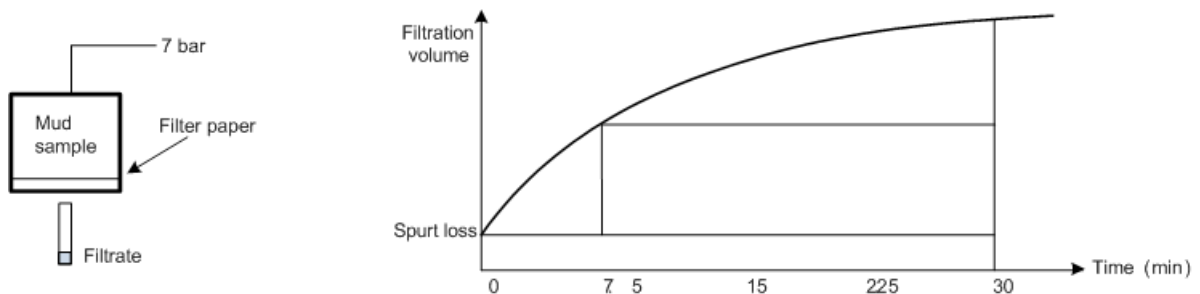

Figure 3-10: Filter press test results.

It is common to simplify laboratory procedures by decreasing test duration to 1/4 of the standard 30 minutes. The accumulated filtrate volume can be predicted from eqn (3.17);

$$q_{filtrate} = q_{spurt\,loss} + C \cdot \sqrt{t} \tag{3.17}$$

For example, the 30 minute filtrate volume is predicted by measuring the filtrate volume at 7.5 minutes. The value obtained, must be doubled since $\sqrt{30}\,/\,\sqrt{7.5} = 2$.

In the well, spurts loss may be large when drilling through highly permeable rocks, unless the mud contains particles of the size required to bridge the pores of the rock, and thus establish an improved filter somewhat ahead of the bit. Only particles of a certain size relative to the pore size can make bridges. Particles larger than the pore opening cannot enter the pores, and are swept away by the mud stream. Particles considerably smaller than the opening invade the formation unhindered. Particles of a certain critical size are caught in bottlenecks in the flow channels (which vary enormously along the flow paths), and form a bridge inside the porous wall. Once a primary bridge is established, successively smaller particles are trapped, and thereafter only the filtrate (liquid) may invade the formation. The spurt loss period is very brief; it is a matter of seconds.

As a result of the process just described, three zones of mud particles are established in a permeable formation. This is shown in Figure 3-11.

External filter cake

Internal filter, made up by particles invaded mainly through spurt loss

Uncontaminated formation

Figure 3-11: Invasion of a permeable formation by particles in the mud.

The outer filter cake can be made by emulsified water droplets in oil based mud (left) and water based mud (right). In the context of building a tighter filter it is important to supply the mud with a particle size distribution in relation to the pore size distribution of the porous formation to be drilled through. Mean particle size should be 1/3–1/7 of mean pore throat size as indicated in Figure 3-12. Barite and drilled particles, classified in Table 3-4, will always be available and prefect for filter building. However, at the same time these particles will interfere with the filter cake building process.
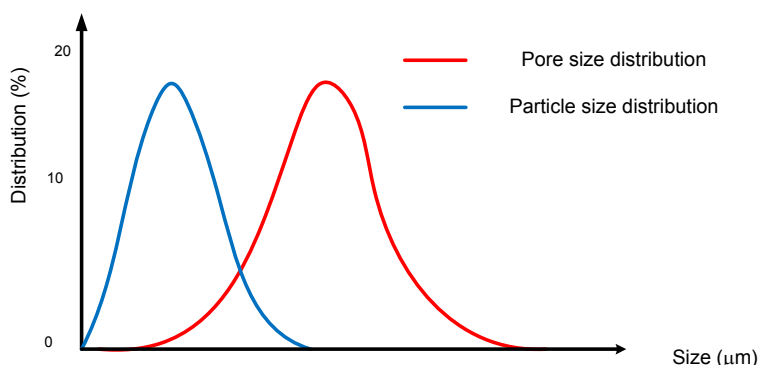
Figure 3-12: How to, by means of particles, create an internal filter which is pictured in Figure 3-11. The pore size distribution is determined by a scanning microscope analysis of a thin-section of a core sample.

1. Coarse	Particles greater than 2 000 microns	Cuttings
2. Intermediate	Particles between 250–2 000microns	Cuttings
3. Mediums	Particles between 74–250 microns	Cuttings
4. Fines	Particles between 44–74 microns	Barite, sand from cutt.
5. Ultrafine	Particles between 2–44 microns	Barite, silt from cutt.
6. Colloidal	Particles less than 2 microns	Bentonite, polymers

Table 3-4: Drilled solids classified by particle size.

In the context of building a filter cake, a dispersed mud is the preferred mud state. Bentonite in flocculated state will experience high water loss and lead to a thick, soft filter cake. By the addition of a thinning agent (deflocculator or thinner) a thin, strong and low permeable cake will form. As a generalization, it may be said that cake permeability of flocculated muds are in the order of 10^{-2} mD, those of untreated fresh-water muds are in the order of 10^{-3} mD and filter cakes of muds treated with dispersants are in the order of 10^{-4} mD.

3.5   Additives

In the next sub Chapter the most common additives are presented and summarized at the end of this Chapter.

3.5.1   Viscosity control

Important viscosity control additives are:

Bentonite extender: A simple method to increase the viscosity of Bentonite suspensions is to extend the Bentonite into a partly flocculated state. Anionic polymers mixed into WBM will react with Bentonite as indicated in Figure 3-13 (Flocculants). For the polymer to function as an extender the molecular weight must be medium high and the concentration in the ultra low range (0.05–0.10 PPB).
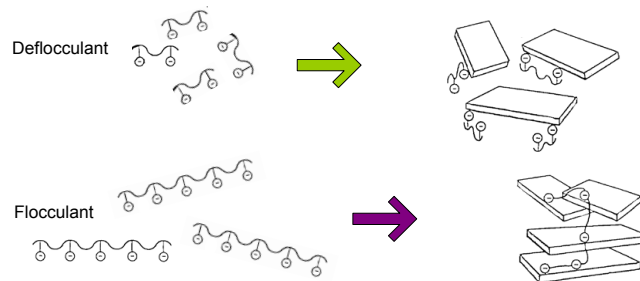
Figure 3-13: Low molecular weight polymers act as deflocculants (upper). High MW polymers act as flocculants. Polymeric flocculants are used in "clear-water" drilling, where the drilled solids are made larger by the flocculants and then removed.

Dispergator: The advantages of maintaining a dispersed mud system are two-fold:

1. Easier to control the viscosity
2. Fluid loss becomes optimal

To maintain a system in a dispersed (deflocculated) state the repulsive forces must be maximised. The negative charges on the clay particles can be maximized in three ways:

a) High pH level:
    A pH above 8.0 will increase the number of negative groups on the clay edges. Thus, maintaining an alkaline pH condition with caustic soda will stabilize the clay system. At high pH level, negative charges will predominate.

b) Adding deflocculant or thinner:

There is a wide range of chemicals known as deflocculant or thinner, which have a wide range of chemical structure. However, they can all be described as negatively charged polymers. Figure 3-13 illustrates the mechanism whereby a short chain of negatively charged polymer can neutralise a positive charge on the edge, and increase the negative charge density on the clay platelet. Some common chemicals are chrome lignosulphonate, tannin and lignite. Since the deflocculants are reacting with the positive sites on the edges, and the edge surface area is a relatively small proportion of the total, the chemicals can be effective at low concentrations.

c) Fine particles act as dispersants:

Other fine particulate solids, such as calcium carbonate, barites or drilled out fines, are all inert, and will act essentially as physical hinders for clays to flocculate. Such particles are called dispersants.

Flocculants (Clay free/clear water drilling): The process is initiated by creating larger lumps of clay particles as illustrated in Figure 3-13. Then the particles are separated out by means of gravity. Conditions are similar to those mentioned under Bentonite Extension, but polymer concentration must be in the low range (0.1–0.3 ppb), added after the shale shaker.

3.5.2 Fluid loss control

Fluid loss to permeable formations is reduced through increasing the viscosity of the fluid phase. Non-ionic, low MW polymers are applied, and will therefore become an integrated part of the fluid phase. They do not interact with the solids. The filtrate from filtration tests in the filter press is a surprisingly clear fluid, consisting of water and the fluid loss additives, which are in the size range of molecules. The practical topic of fluid loss is presented in Chapter 3.4.

3.5.3 Hydraulic friction reducers

Some special polymer suspensions provide much lower friction than the base fluid's rheology predicts. This is explained by a layer of base fluid being formed along the pipe wall during flowing. When small molecules like polymers are suspended in liquids, they will perform a stochastic movement referred to as Brownian movement. The suspended particles have 6 degrees of freedom, and will normally diffuse equally in all directions. However, close to the wall one freedom of movement is removed, only diffusion away from or along the wall is possible. An additional effect is caused by the shear stress field. The shear stress in the fluid reaches a maximum at the wall, leading to stretching effects of the polymers. The resulting viscosity near the wall will approach the base fluid's viscosity under certain conditions. Figure 3-14 illustrates the phenomenon, while Table 3-5 summarises the features and friction effects of these special polymer solution.

Entrance flow   Developed flow
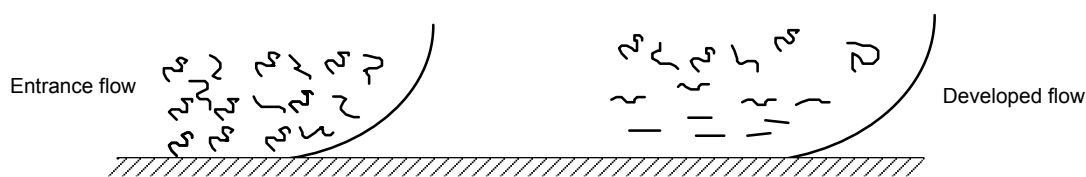
Figure 3-14: Polymers as drag reducers; low viscosity develops at the wall.

Mixture No	Composition	Parameter: Unit:	Weight PPG	Pressure drop psi	PV cP	YP lb/100 ft^2
1	Brine of CaCl$_2$	Data:	11.0	706	1.5	-
1+	6 ppb HEC		10.8	265	3.5	2.5
2	Base (dispersed Bentonite) 2	Data:	8.5	548	8.5	8.5
2+	ppb HEC		8.4	165	13.0	15.0

Table 3-5: Properties and friction pressure in pipe flow with HEC added to two base fluids.

3.5.4   Summary of additives

In addition to viscosifyers and to rheology control agents, there are several more groups of additive. We refer to the classification of additives published by World Oil once a year as presented below. They also publish the name and characteristics of more than 3000 additives.

Alkalinity, pH control: Lime, caustic soda and bicarbonate of soda, control the degree of acidity of a fluid.

Bactericides: Para formaldehyde, caustic soda, lime and starch preservatives are commonly used to reduce bacteria count.

Calcium removers: Caustic soda, soda ash, bicarbonate of soda and certain polyphosphates make up the majority of chemicals designed to prevent and overcome the contaminating effects of anhydrite, gypsum and calcium sulphates.

Corrosion inhibitors: Hydrated lime and amine salts are often added to check corrosion.

Defoamers: Products designed to reduce foaming action, particularly in brackish and saturated saltwater mud.

Emulsifiers: Surface active agents create a heterogeneous mixture of two liquids.

Filtrate reducers: Filtrate, or fluid loss reducers – such as Bentonite clays, CMC (sodium carboxyl methyl cellulose) and pre gelatinized starch – reduces the tendency of the liquid phase of the drilling fluid to pass into the formation.

Flocculants: Salt, hydrated lime, gypsum and sodium tetra phosphates are used to cause colloidal particles in suspension to group into bunches, or "flocks», causing solids to settle out.

Foaming agents: Surfactants (foamers) permit air or gas drilling through water-bearing formations.

Lost circulation materials: Lost circulation additives plug the zone of loss in the formation.

Lubricants: Oils, graphite, powder and soaps reduce torque and increase horsepower transmitted to the bit by reducing the coefficient of friction.

Pipe-freeing agents: Detergents, soaps, oils and surfactants are intended to be spotted in an area of suspected pipe sticking to reduce friction, increase lubricity and inhibit formation swelling.

Shale control inhibitors: Gypsum, sodium silicate and calcium lignosulfonate, as well as lime and salt, are used to control swelling or hydrous disintegration of shale.

Surface active agents: Reduce the interfacial tension between contacting surfaces (water/oil, water/air, etc.).

4   Hydraulic friction in the circulating system

The objective of estimating hydraulic friction in the circulation system is three-fold:

1. Determine the total frictional loss at its maximum design flow rate, so that the required pump size can be selected
2. Determine pressure loss thorough the nozzles in the bit to enable determination of optimal nozzle size and thus achieving proper cleaning effect on bottom
3. Establish ECD in the annulus in order to stay inside the pressure window

To reach these goals we rely on three types of knowledge:

- The fluid flow system and drilling engineering operations (Chapter 2)
- Rheology of drilling fluids (Chapter 3)
- The governing equation of fluid mechanics (this Chapter)

We will therefore now go through hydraulic friction losses in pipes and annuli, for laminar and turbulent flow, for three different rheology models;

- Newtonian
- Bingham plastic
- Power law

Not only losses in pipe flow will be covered, but also singularity losses, i.e. losses through sudden expansions or restrictions, like in the rock bit nozzles. Since we are dealing with pipe flow, we apply cylindrical coordinates. The basic equations will initially also be presented in Cartesian coordinates. Cartesian velocity components in the x, y and z direction are denoted v_x, v_y and v_z, while resultant axial flow is simply denoted v, sometimes v_z or v_x. Governing equations of fluid mechanics are summarized in Chapter 10.4, in microscopic and macroscopic views. The microscopic view is characterized by observing the flow behaviour as it develops inside the pipe, and thereby allowing us to observe from one position in the flow profile continuously, referred to as the Langrangian view. The macroscopic view or the Eularian view involves a control volume and keeping track of what is entering and what is leaving the control volume.

4.1   Head loss

Before going to friction loss, we introduce an expression from the fluid mechanics course, and some useful definitions. Bernoulli's law can be expressed in terms of fluid head (in meters). Return to pressure by multiplying with ρg:

$$\frac{p_1}{\rho g} + \frac{v_1^2}{2g} + z_1 + h_{pump} = \frac{p_2}{\rho g} + \frac{v_2^2}{2g} + z_2 + h_f \qquad (4.1)$$

The different parts of eqn (4.1) represent for left to right; pressure head, velocity head, gravity or potential energy head and pump head. To the far right the friction loss head is added, referred to as head-loss. Head loss is demonstrated in Figure 4-1.

In a flow systems the total head is composed of energy input, while the hydraulic head is the total head minus the effect of the velocity head:

Total head = $h_o = z + p\,/\,\dot{\gamma} + \overline{v}^2\,/\,2g$ = energy grade line (EGL)
Hydraulic head = $z + p\,/\,\dot{\gamma}$ = hydraulic grade line (HGL)
                                            = the height in a piczometric tube

Figure 4-1 demonstrates all expressions.
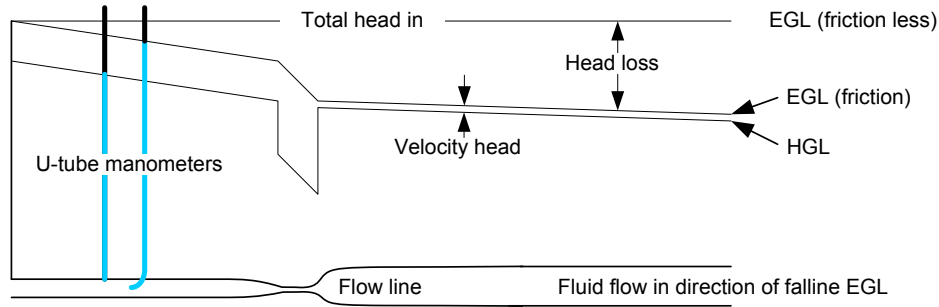
Figure 4-1: Important expressions involved in the evaluation of pipe flow.

4.2   Laminar flow

We start with the simplest case; laminar pipe flow. Since our analysis will assume steady state flow, it will either be laminar or turbulent flow (Figure 4-2 demonstrates the significance of it). Flow regime is determined through the Reynolds number:

$$N_{Re} = \rho vd / \mu \tag{4.2a}$$

The flow turns from laminar into a transition flow at 1800, and fully turbulent flow is developed at 2100.

Below N_{Re} = 1800, laminar flow will prevail in slick steel pipes, while above 3000 turbulent flow is fully developed. Figure 4-10 in Chapter 4.3 demonstrates how the flow lines behave in the transition zone. If the pipe wall is not slick but has a certain roughness, turbulent flow will develop at a much lower Reynolds number.

High mixing energy causes high mechanical energy loss. The mixing length or entrance length, L_e, before flow is fully developed (has obtained a constant flow profile), is given through eqn. (4.2b) and (4.2c):

$$L_e \approx D \cdot 0.06 \, N_{Re} \text{ for laminar flow} \tag{4.2b}$$

$$L_e \approx D \cdot 4.4 \left(N_{Re}\right)^{1/6} \text{ for turbulent flow} \tag{4.2c}$$
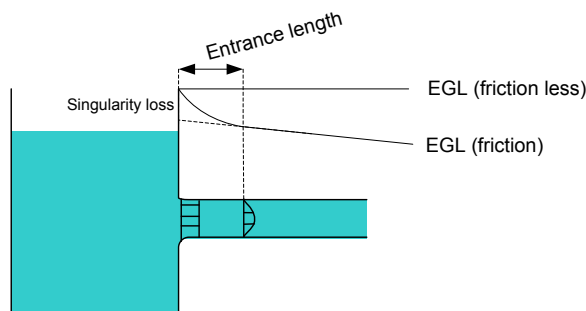
Figure 4-2: After entrance effects flow reaches a stationary flow profile.

4.2.1 Pipe flow

The simplest rheology model is the Newtonian model.

Newtonian model

In this chapter the complete derivation is carried out for the Newtonian rheology model. The complete sets of resulting equations for all three types of rheological models are gathered in Chapter 10.5.

Hydraulic flow problems are solved by solving the five basic equations:

1. *Equation of state* relates fluid density to pressure and temperature. For practical purposes liquids are incompressible, we therefore assume that the density is constant.
2. *Constitutive material equation* characterizes fluid behaviour in laminar flow. Fluids subjected to shear rate will resist deformation resulting in shear stress:

$$\tau = -\mu \frac{dv_x}{dr} = \mu \cdot \dot{\gamma} \tag{4.3}$$

The strain rate; $\dot{\gamma} = -\frac{dv_x}{dr}$, across the pipe is the velocity gradient or the rate of shear.

3. *Continuity equation* is the law of conservation of mass. A general form of the continuity equation states the difference between the input and output of mass to a small volume element:

$$- \frac{\partial \rho}{\partial t} = \nabla(\rho v) = \frac{\partial}{\partial x}(\rho v_x) + \frac{\partial}{\partial y}(\rho v_y) + \frac{\partial}{\partial z}(\rho v_z) \tag{4.4}$$

when expressed in Cartesian coordinates. For incompressible fluids, eqn (4.4) simplifies to:

$$\frac{\partial v_x}{\partial x} + \frac{\partial v_y}{\partial y} + \frac{\partial v_z}{\partial z} = 0 \tag{4.5}$$

4. Momentum equation, or Newton's second law of motion for viscous flow is called the Navier-Stoke equation:

$$\frac{\partial v}{\partial t} + \frac{\mu \nabla^2 v}{\rho} = -\frac{\nabla p}{\rho} + g \tag{4.6}$$

Expressed in cylindrical coordinates the eqn. of motion (only the axial component (x-direction) is of interest) for steady state, constant density and constant viscosity yields:

$$0 = -\frac{\partial p}{\partial x} + \mu \left[\frac{1}{r} \frac{\partial}{\partial r} r \left(-\frac{\partial}{\partial r} v_x + \frac{\partial^2}{\partial x^2} v_x \right) + \frac{1}{r^2} \frac{\partial^2 v_x}{\partial \theta^2} \right] + \rho g_x \tag{4.7}$$

Both $\frac{\partial p}{\partial x}$ and $\frac{\partial v_x}{\partial r}$ are negative since ∂p and ∂v decreases for increasing x and r values respectively.

5. Energy equation or law of conservation of energy is interesting only for problems involving temperature change.

Except for the energy equation, all the other four equations are needed. By assuming that an incompressible, Newtonian fluid is flowing at steady-state in a horizontal pipe, the term $\partial^2 v_x / \partial \theta^2$ becomes 0 in the momentum equation since the flow is symmetrical about the pipe axis. Under these circumstances the state, continuity and momentum equations simplify to:

state: $\qquad \frac{\partial \rho}{\partial t} = o \qquad\qquad$ since ρ = constant $\hfill (4.8)$

continuity: $\qquad \frac{\partial v}{\partial x} = 0 \qquad\qquad$ since $v_y = v_z = 0$ ($v_x = v$) $\hfill (4.9)$

momentum: $\qquad \frac{dp}{dx} = \mu \left[\frac{1}{r} \frac{\partial}{\partial r} \left(r \cdot -\frac{\partial v}{\partial r} \right) + \frac{\partial^2 v}{\partial x^2} \right] + \rho g_x \hfill (4.10)$

Leaving ρg_x out (for horizontal flow) and substituting eqn (4.9) into eqn (4.10) yields:

$$\frac{dp}{dx} = -\frac{\mu}{r} \frac{\partial}{\partial r} \left(r \cdot \frac{\partial v}{\partial r} \right) \tag{4.11}$$

Separating and integrating eqn (4.11) from r = 0 to r = r:

$$\int_0^r \frac{r}{\mu} \cdot \frac{dp}{dx} \partial r = -\int_0^{\frac{\partial v_x}{\partial r}} r \partial\left(\frac{\partial v}{\partial r}\right)$$
(4.12)

At r = 0, $\frac{\partial v}{\partial r} = 0$, resulting in the following expression:

$$\frac{1}{2} \cdot \frac{r^2}{\mu}\frac{dp}{dx} = -r\left(\frac{\partial v}{\partial r}\right)$$
(4.13)

Separating

$$\frac{\partial v}{\partial r} = -\frac{r}{2\mu} \cdot \frac{dp}{dx}$$
(4.14)

Combining eqn (4.3), $\tau = -\mu \frac{dv_x}{dr}$ and (4.14) gives this expression:

$$\tau_r = \frac{r}{2} \cdot \frac{dp}{dx}$$
(4.15)

Integrating eqn (4.14) from r to R, where v = 0 (no slip):

$$\int_{v_x(r)}^0 \partial v_x = -\frac{dp}{dx \cdot 2\mu} \cdot \int_r^R r \partial r$$
(4.16)

and solving for v yields the parabolic eqn (4.17) as shown in Figure 4-3:

$$v_x(r) = -\frac{dp/dx}{4\mu}\left(R^2 - r^2\right)$$
(4.17)
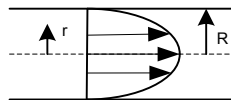
Figure 4-3: Eqn (4.17) presented graphically.

A third integration along r to include total flow over the cross sectional area;

$$q = \bar{v} \cdot A = \bar{v} \cdot \pi\ r^2$$
(4.18)

Eqn (4.18) on a differential form yields:

$$dq = v \cdot 2\pi r dr$$
(4.19)

Integrating from r = 0 to R yields:

$$q = \frac{\pi R^4 \cdot dp / dx}{8\mu}$$

(4.20)

Integrating along the x-direction and letting q = $\bar{v}$ A = $\bar{v}$ * π/4*d², gives the pressure change along L;

$$\Delta p = \frac{32\mu\bar{v}L}{d^2}$$

(4.21)

Eqn (4.21) is known as the Hagen-Poiseuille equation for laminar pipe flow. The pressure loss Dp is due to viscous stress only, and is linearly proportional to flow rate or average velocity and to length of pipe.

For the Bingham model (and Power law model) the procedure is identical, only boundary conditions are different as indicated in Figure 4-4.
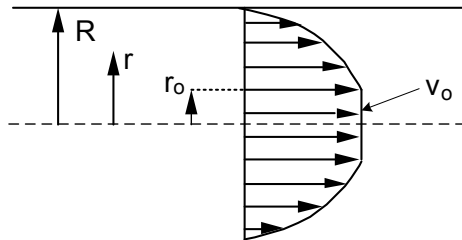
Figure 4-4: Flow profile for laminar flow of a fluid obeying the Bingham rheology model.

Radius r_o is calculated from eqn (4.6) by using $\tau = \tau_y$ at $r = r_o$.

$$r_o = \frac{2 \cdot \Delta x \cdot \tau_y}{\Delta p}$$ (4.23)

Derivation of pressure loss for laminar pipe flow, through macroscopic view:

The same results as achieved above in the previous paragraph can be achieved through a macroscopic view.
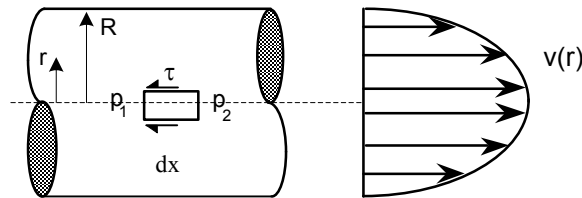
Figure 4-5: A fluid element in pipe flow.

Conservation of momentum of the flow element in Figure 4-5 shows that for steady state flow, shear and pressure forces are the only forces acting and must be equal to each others:

$$(p_1 - p_2) \cdot A = \int \tau(r) \cdot dA = \int \tau(r) \cdot 2\pi r dr$$ (4.24)

Taking $\tau(r)$ as a constant for a given r, integration leads to:

$$\Delta p \cdot \pi r^2 = \tau(r) \cdot 2\pi r \cdot \Delta x$$ (4.25)

Solving for $\tau(r)$:

$$\tau(r) = \frac{r}{2} \cdot \frac{\Delta p}{\Delta x}$$ (4.26)

For r = R (at the wall (w)):

$$\tau_w = \frac{R}{2} \cdot \frac{\Delta p}{\Delta x}$$ (4.27)

Eqn (4.27) is graphically shown in Figure 4-6:
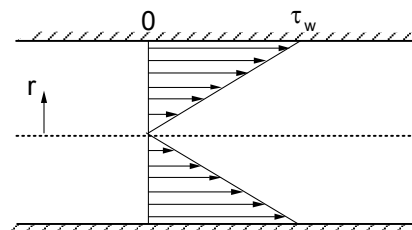
Figure 4-6: Shear stress distribution in a liquid flowing laminarly through a pipe.

Similarly for slot flow;

$$\tau_w = \frac{d_0 - d_i}{4} \cdot \frac{dp}{dx}$$

(4.28)

These two equations are referred to as the universal pressure loss equations since they are valid for all rheologies. And the macroscopic view give the same result as the microscopic (see eqn (4.15)).

4.2.2   Annular flow

Newtonian fluids

Flow in between two concentric pipes can be treated either as flow in true concentric pipes, or in a simplified manner, as flow between two parallel plates. For narrow annuli the deviation between true and parallel flow is highest, and here the losses may become a large portion of total loss, significant errors are introduced. By presenting both solutions we can pursue this difference.

The simplified annular flow between two parallel plates is shown in Figure 4-7:
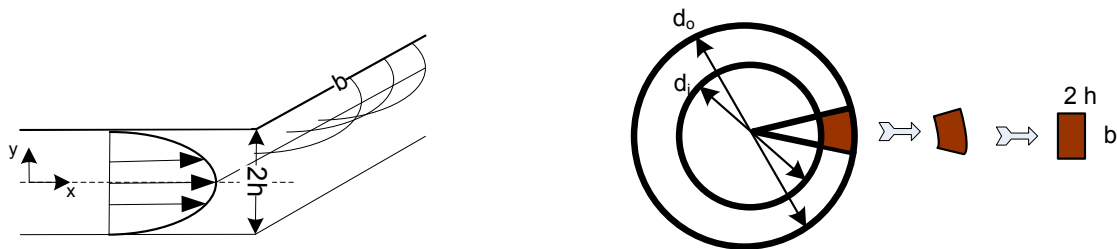
Figure 4-7: Geometry and velocity profile for flow between two parallel plates

Navier Stoke form of the momentum equation:

$$\rho\left(u \frac{\partial v_x}{\partial x} - v \frac{\partial v_y}{\partial y} \right) = -\frac{\partial p}{\partial x} + \rho g_x + \mu\left(\frac{\partial^2 v_x}{\partial x^2} + \frac{\partial^2 v_x}{\partial y^2} \right)$$

(4.29)

For steady state flow the continuity equation shows that in the x-y dimension $\frac{\partial v_x}{\partial x} = \frac{\partial v_y}{\partial y} = 0$ and $\frac{\partial v_x}{\partial y} \neq 0$, then eqn (4.29) reduces to:

$$\rho(0 + 0) = -\frac{\partial p}{\partial x} + \mu\left(0 + \frac{\partial^2 v_x}{dy^2} \right)$$

Separating and integrating from 0 to y:

$$\int \partial^2 v_x = \frac{1}{\mu} \frac{dp}{dx} \int dy^2$$

(4.30)

Integration yields:

$$v_x = \frac{1}{\mu}\frac{dp}{dx}\frac{y^2}{2} + C_1 y + C_2 \tag{4.31}$$

By referring to Figure 4-7, y= h for $v_x = 0$, eqn (4.31) gives $C_1 = 0, \quad C_2 = -\frac{dp}{dx}\cdot\frac{h^2}{2\mu}$, and eqn (4.31) takes the form:

$$v_x = -\frac{dp}{dx}\frac{h^2}{2\mu}\left(1 - \frac{y^2}{h^2}\right) \tag{4.32}$$

If the channel has width b, the volume flow becomes:

$$q = \int_{-h}^{+h} v(y)\, b\, dy = \frac{bh^3}{3\mu}\left[-\frac{d}{dx}(p + \rho g z)\right] \tag{4.33}$$

Solving for average pipe velocity:

$$\bar{v} = \frac{q}{bh} \quad = \quad \frac{h^2}{3\mu}\left[-\frac{d}{dx}(p + \rho g z)\right] \tag{4.34}$$

The wall shear stress in developed channel flow is a constant (at y = h):

$$\tau_w = \mu\left|\frac{dv_x}{dy}\right| = h\left[-\frac{d}{dx}(p + \rho g z)\right] \tag{4.35}$$

This may be made non dimensional as a friction factor:

$$f_M = 4 \cdot \frac{8\tau_w}{\frac{1}{2} \cdot \rho \bar{v}^2} = \frac{24\mu}{\rho \bar{v}\, h} = \frac{24}{N_{\text{Re}}}$$

(4.36)

Finally we convert slot flow to annular flow by converting width (breadth) to radius. If we follow the center line of the gap, the average breadth can be expressed as the periphery:

$$b = 3.14\,(d_o + d_1)\,/\,2$$

(4.37)

The hydraulic diameter is defined as:

$$d_{hydr} = \frac{4A}{perimeter} = \frac{4 \cdot 2hb}{2b + 4h}$$

(4.38)

For infinite breadth eqn (4.38) approaches 4h. Inserting h = ¼ * d_{hyd} in eqn (4.36), combining with eqn (4.34) and solving for dp/dx yields;

$$\frac{dp}{dx} = 48\,\frac{\bar{v}\mu}{d_{hydr}^2}$$

(4.39)

The exact solution of annular flow results from the true flow profile in the annular space between two concentric cylinders is shown in Figure 4-8.
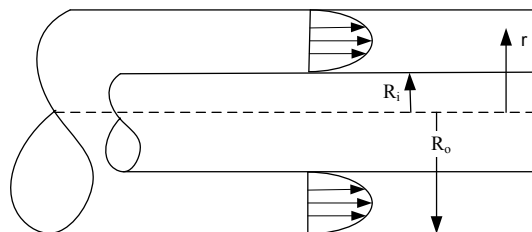
Figure 4-8: Geometry and flow profile for flow through a concentric annulus.

Since we do not know where the velocity has its maximum (where $\partial v_x / \partial r = 0$) we make an unbound integration of eqn. (4.16) and obtain

$$v_x(r) = -\frac{r^2}{4\mu}\frac{dp}{dx} - \frac{C_1}{\mu}\ln r + C_2$$

(4.40)

At r = R_0 and r = R_i → v(r) = 0 (no slip), and eqn. (4.40) becomes;

$$v_x(r) = \frac{1}{4\mu}\left[(R_0^2 - r^2) - (R_0^2 - R_i^2)\frac{\ln \dfrac{R_0}{r}}{\ln \dfrac{R_0}{R_i}} \right]\frac{dp}{dx}$$

(4.41)

Hence, the flow rate is:

$$q = \int_{R_i}^{R_0} v_x 2\pi r \cdot dr = \frac{\pi}{8\mu}\frac{dp}{dx}\left[R_0^4 - R_i^4 - \frac{(R_0^2 - R_i^2)^2}{\ln\frac{R_0}{R_i}}\right]$$ (4.42)

It is seen that for $R_i \to 0$ (pipe flow), eqn. (4.42) reduces to eqn. (4.20). Expressing the flow rate in terms of average flow velocity and solving eqn. (4.41) for dp/dx gives:

$$\frac{\Delta p}{\Delta x} = \frac{32\,\mu\bar{v}}{d_L^2}$$ (4.43)

where

$$d_L^2 = d_0^2 + d_i^2 - \frac{d_0^2 - d_i^2}{\ln\frac{d_0}{d_i}}$$ (4.44)

Note that eqn (4.43) reduces to the corresponding pipe flow equation eqn (4.21) as $d_i \to 0$.

4.2.3   Shear rate and effective viscosity

In some situations it may be useful to find the shear rate at the pipe wall, to compare with a rheometer shear stress. Eqn (4.27) is valid for all rheologies. Combining Eqn. (4.27) and (4.21) yields:

$$\dot{\gamma}_w = \frac{8\bar{v}}{d}$$ (4.45)

In similar manner it may be shown that for the Power law model:

$$\dot{\gamma}_w = \frac{8\bar{v}}{d} \cdot \frac{3n+1}{4n}$$ (4.46)

and for Bingham fluids

$$\dot{\gamma}_w = \frac{8\bar{v}}{d} + \frac{\tau_0}{3\mu_{pl}}$$ (4.47)

It is also possible to apply the Newtonian pressure loss equations for other rheological models when expressing them through the equivalent Newtonian viscosity. The equivalent viscosity is often referred to as effective or apparent viscosity. For Bingham plastic, the equivalent viscosity for circular pipes is found by comparing eqn. (4.21) with the Bingham fluid loss equation (see Chapter 10.5):

$$\frac{32 \cdot \mu_{eff} \cdot L \cdot \bar{v}}{d^2} = \frac{32 \cdot \mu_p \cdot L \cdot \bar{v}}{d^2} + \frac{16 \cdot \tau_y \cdot L}{3d}$$ (4.48)

Solving for μ_{eff} yields:

$$\mu_{eff} = \mu_{pl} + \frac{\tau_y \cdot d}{6 \cdot \bar{v}}$$

(4.49)

Chapter 10.5 summarises hydraulic friction equations for all rheologies.

4.2.4   Laminar pressure loss example

The following example will summarize much of what has been presented so far in Chapter 4. Starting with viscometer data in Table 3-5 and operational data in Figure 4-9:

200 m

q_{pump}= 4000 lpm (two pumps)

d_{DC} = 9 " = 0.229 m

d_{bit} = 26 ½" = 0.673 m
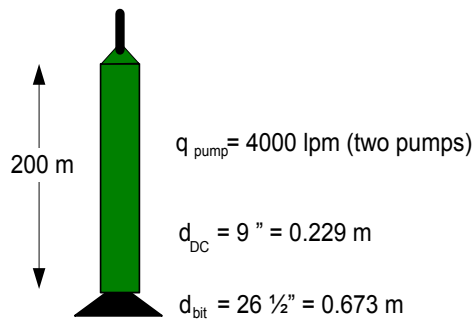
Figure 4-9: Example data; flow around DC. Rheology as in Figure 3-9.

The task in this example is to find Δp along the DC annulus, for two models: Bingham and Universal.

$$\bar{v} = q/A = \frac{0.0667}{0.3145} = 0.212 \, m/s$$

$$A_{DC-OH} = \frac{\pi}{4}\left(0.673^2 - 0.229^2\right) = 0.3145 \, m^2$$

$$q = 4000 \cdot \frac{1}{1000 \cdot 60} = 0.0667 \, m^2/s$$

Bingham (2 data points, SI approach):

$$\mu_{pl} = 0.0417 \, Pas$$

$$\tau_o = 28.5 Pa$$

$$\mu_{eff} = \mu_{pl} + \frac{\tau_o(d_o - d_i)}{8\bar{v}} = 0.0417 + \frac{28.5\,(0.673 - 0.229)}{8 \cdot 0.212} = 7.50 \, Pas$$

At low shear rates the yield point plays a major role. And it leads to extremely low Reynolds numbers:

$$N_{Re} = \frac{\rho \bar{v} d_{hydraulic}}{\mu_{eff}} = \frac{1000 \cdot 0.212 \cdot 0.444}{7.5} = 12.5$$

$$\Delta p_{ann} = \frac{48 \cdot 0.0417 \cdot 200 \cdot 0.212}{(0.444)^2} + \frac{6 \cdot 200 \cdot 28.5}{0.444} = 430 + 77\,027 = 77\,457 \, Pa = \underline{0.8 \, bar}$$

Universal:

$$\dot{\gamma} = \frac{12\,\bar{v}}{d_{hydraulic}} = \frac{12 \cdot 0.212}{0.444} = 5.7 \, s^{-1}$$

τ_w from graph in Figure 39 can be reads to 7 Pa.

$$\Delta p_{ann} = \frac{48 \cdot 0.0417 \cdot 200 \cdot 0.212}{(0.444)^2} + \frac{6 \cdot 200 \cdot 28.5}{0.444} = 430 + 77\,027 = 77\,457 \, Pa = \underline{0.8 \, bar}$$

A large difference in result is observed in the two models. This is due to the fact that the Bingham model aims too high for the t_y. It is clearly seen in Figure 3-9 that at these low shear rates the Bingham model gives 3 times higher shear stress than the true readings. From the logarithmic plot of measured rheology data in Figure 3-9 it is seen that the 4 upper readings fall into a straight line, while the two lower ones do not. It is fair to conclude that the upper 4 points describe the Power law behavior of the mud, while the two lower ones point out the Binghamian nature of the fluid.

4.3   Turbulent pipe flow

When kinetic energy dominates over shear stress, the flow turns into turbulent flow. A dimensionless number called the Reynolds number, N_{Re}, is used for determining the flow regime;

$$N_{Re} = \rho \bar{v} d / \mu \tag{4.2}$$

Turbulent flow is chaotic flow and the velocity varies continuously both in the x and y direction, resulting in high energy consumption, and correspondingly high loss due to friction (head loss). Figure 4-10 demonstrates the higher loss rate at turbulent flow regime.
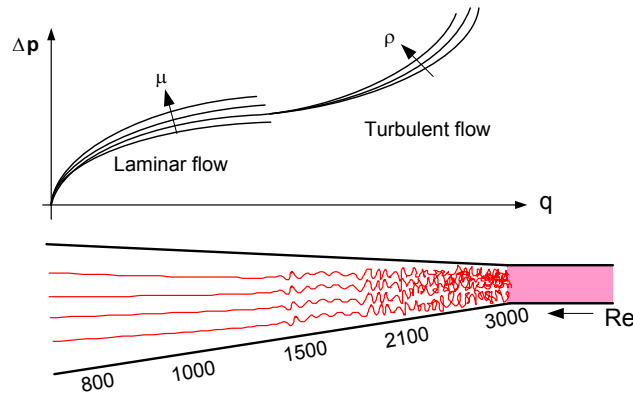
Figure 4-10: The Reynolds number is a function of flow rate, and friction increases exponentially with flow rate in the turbulent regime (upper Figure). Transition from laminar (parallel flow lines) to turbulent flow regime vs. pipe diameter (lower Figure).

Turbulent pressure loss relationships are based on experimentally determined friction factors (Fanning (f_F) or Moody (f_M)):

$$f_M = 4\tau_w \Big/ \frac{1}{2}\rho\bar{v}^2 = 4f_F \qquad\qquad (4.50a)$$

Example of data from such experiments is shown in Figure 4-11.
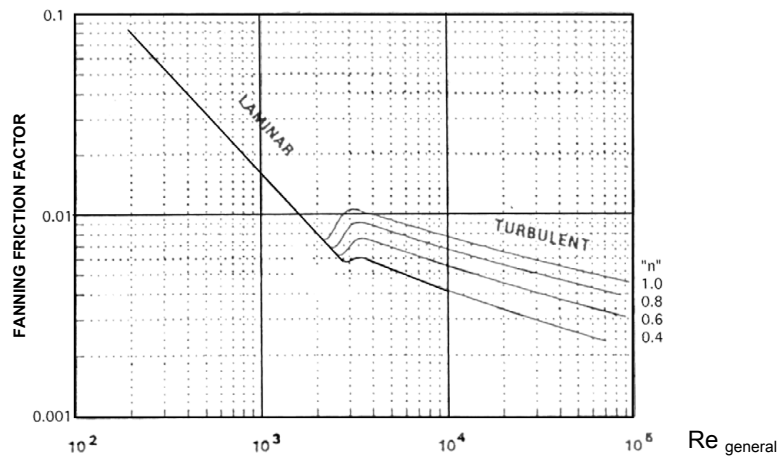
Figure 4-11: Friction factors for power-law fluids in smooth pipes.

Substituting the general (eqn (4.27)) pressure loss equation and the Power law fluids model into eqn (4.50) yields:

$$f_F = \frac{16 \cdot 8^{n-1} K \left(\dfrac{3n+1}{4n}\right)}{d^n \bar{v}^{2-n} \rho} = \frac{16}{N_{Re,gereral}} \qquad\qquad (4.51)$$

The general Reynolds number can now be defined as:

$$N_{Re,gereral} = \left(\frac{4n}{3n+1}\right)^n \frac{d^n \bar{v}^{2-n} \rho}{8^{n-1} K}$$

(4.52)

For n = 1 and K = μ, eqn (4.52) reduces to eqn (4.2), which is valid for Newtonian fluids. By curve fitting the experimental data in the turbulent region of Figure 4-10, several mathematical relationships have been suggested, and named after its author:

1. Blasius: Eqn (4.53) is valid for smooth pipes and for $10^3 <$ Re 10^5, and Newtonian fluids:

$$f_F = 0.0791 \cdot N_{Re}^{-0.25}$$

(4.53)

2. Moore: His equation is valid for drill pipes (smooth steel pipes) and for drilling fluids where the turbulent viscosity is equal to $\mu_{pl}/3.2$. This lowered effective viscosity provides pressure lost values that are more in agreement with field results.

$$f_F = 0.046 \cdot N_{Re}^{-0.2}$$

(4.54)

3. Metzner & Reed: This model is valid for power law fluids in smooth steel pipes;

$$f_F = a \cdot N_{Re,gereral}{}^{-b} \tag{4.55}$$

where a = [log(n) + 3.93]/50 and b = [1.75 – log(n)]/7

4. Prandtl: Eqn (4.56) is derived from the logarithmic law of the turbulent velocity profile.

$$\frac{1}{\sqrt{f_M}} = 2 \log \left(N_{Re}\sqrt{f_M} \right) \; - \; 0.8 \tag{4.56}$$

5. Nikuardse/Colebrook/Wood: Eqn (4.57) is developed for naturally rough pipes and for $10^4 < N_{re} < 10^5$

$$f_F = a + b * N_{Re}{}^{-c} \tag{4.57}$$

where a = 0.026 (e/d)$^{0.25}$ + 0.133 (e/d), b = 22 (e/d)$^{0.44}$ and c = 1.62 (e/d)$^{0.34}$.

Figure 4-12 is applied in conjunction with eqn (4.57). Absolute roughness, e, in a pipe in service will increase with time due to corrosion and scale build up.
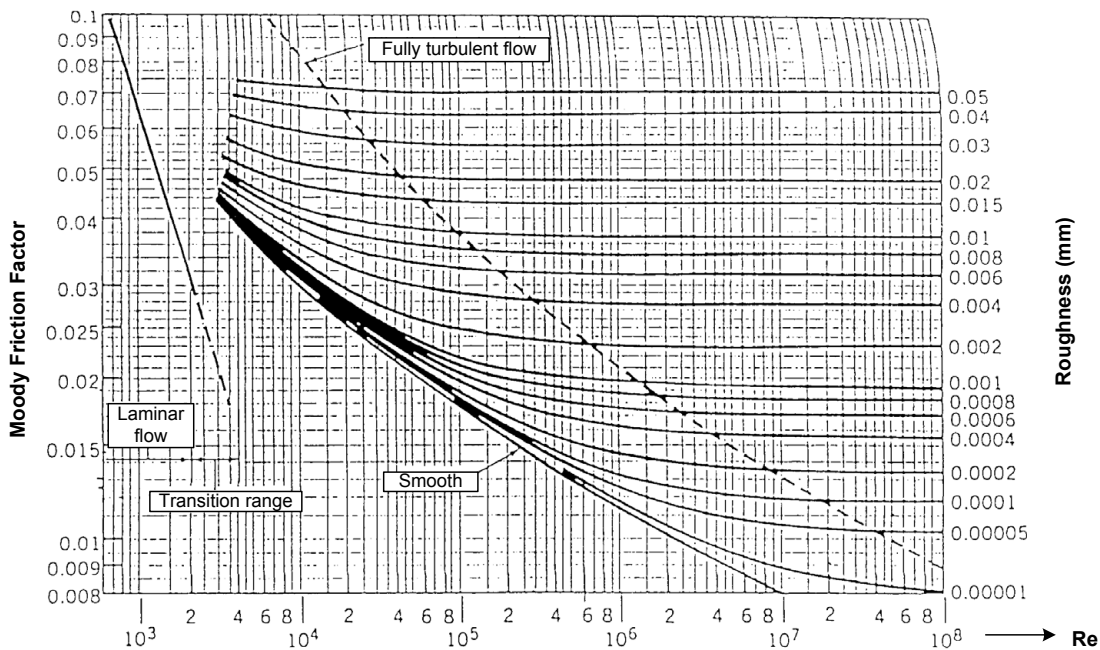
Figure 4-12: Moody friction factors vs. roughness.

Roughness for new pipe materials is shown in Table 4-1.

Material	Roughness e (mm)
Concrete	0.3–3.0
Wood	0.2–0.9
Cast Iron	0.26
Galvanized iron	0.15
Commercial steel	0.046
Drawn steel tubing	0.0015
Glass	0.00 (smooth)

Table 4-1: Equivalent roughness calculated on basis of experimental data. The uncertainty is +/- 50%.

6. Darcy-Weisbak: The Darcy-Weisbak equation is extensively applied for pressure loss estimation. It is valid both for laminar and turbulent flow. This equation is therefore added to the list of pressure loss equations. By solving eqn. (4.50a) with respect to pressure loss we obtain:

$$\Delta p = f_M \cdot \frac{1}{2} \rho v^2 \cdot \frac{L}{d_h} \tag{4.50b}$$

For non-Newtonian fluids the effective viscosity should be applied. It has been found that for Bingham fluids the transition to turbulent flow is insufficiently determined by the Reynolds number. The Hedstrom number is related to the critical Reynolds number, below which the flow pattern is laminar, as shown in Figure 4-13. The Hedstrom number is:

$$\text{He} = \rho \tau_y d^2 / \mu_{pl} \tag{4.59}$$
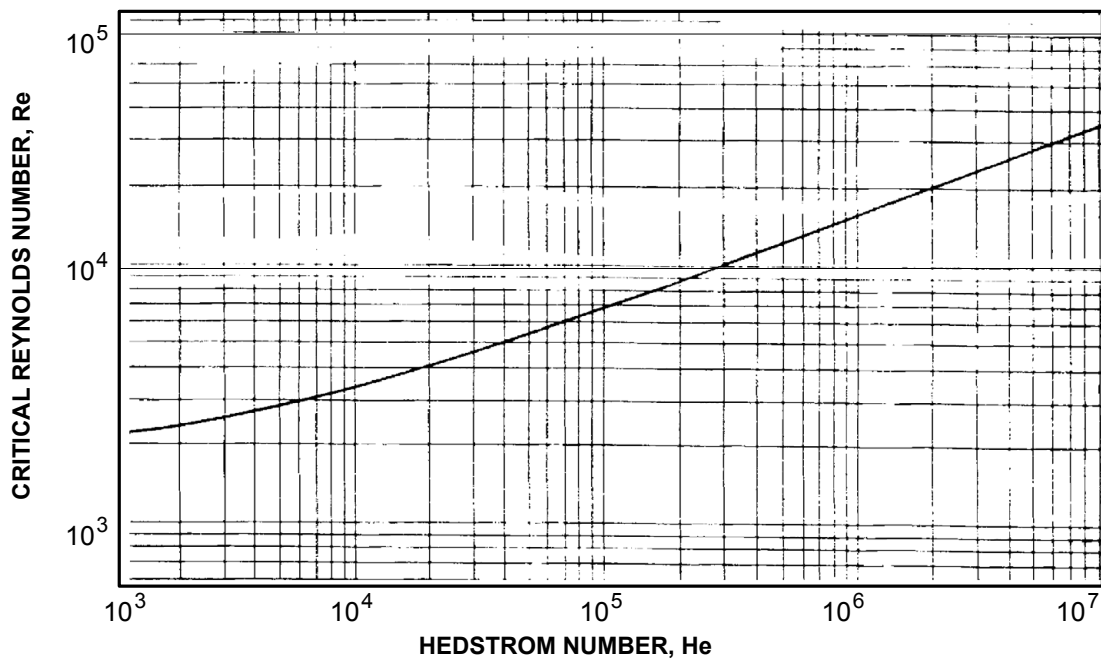
Figure 4-13: Critical Reynolds number for Bingham plastic fluids.

4.4   Singularity losses

Valves, bends, tees, pipe entrances, sudden expansions etc. have no length dimension and pressure loss through such restrictions are called singularity losses or minor losses. The losses are determined experimentally. The flow is always turbulent, and inertia effects will dominate over viscous effects. The loss coefficient, K_L, is therefore a comparison of how large a part of the dynamic pressure is lost:

$$K_L = \Delta p \,/\, (\frac{1}{2}\rho \bar{v}^2) \qquad\qquad (4.60)$$

The loss coefficient is a function of geometry. At the entrances or contractions the head loss is largely dependent on how well the entrance is rounded.

Table 4-2 presents loss coefficients for typical singularity loss geometries. In sudden contractions up to 50% of the kinetic energy change can be lost, while for sudden enlargements 100% of the change can be lost. K_L for pipes leading to a submerged tank is always equal to 1.0, independent of geometry. In a submerged exit all velocity head is lost due to viscous dissipation. This is in accordance with the second law of thermodynamics. Submerged exit losses are independent of geometry.

In sudden expansions, the loss coefficient can be determined by simple analysis. Conservation of mass, momentum and energy are summarized here:

$$mass: \qquad A_1 \bar{v}_i = \Delta_2 \bar{v}_2$$

$$momentum: \qquad p_1 A_2 - p_2 A_1 = \rho\, A_2 \bar{v}_2 (\bar{v}_2 - \bar{v}_1)$$

$$Bernoullis: \qquad \frac{p_1}{\rho g} + \frac{\bar{v}_1^2}{2g} = \frac{p_2}{\rho g} + \frac{\bar{v}_2^2}{2g} + \frac{\Delta p_{loss}}{\rho g}$$

A control volume analysis shows that the loss coefficient for sudden expansions becomes:

$$K_{L,\exp antion} = \left(1 - \frac{A_1}{A_2}\right)^2 \tag{4.61}$$

And for sudden contractions:

$$K_{L,contraction} = 0.5 \cdot K_{L,\exp ansion} \tag{4.62}$$
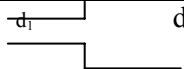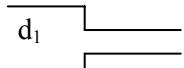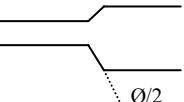
Sudden area enlargements	d_1 $\quad$ d_2	d_2/d_1:	1.5	2	2.5	10
		K_L:	0.3	0.6	0.7	1
Sudden area contraction	d_1 $\quad$ d_2	d_2/d_1:	1	0.8	0.6	0.4
		K_L:	0	0.2	0.3	0.4
Diffusor	Ø/2	Ø(°):	0	15	30	45
		K_L:	0	0.2	0.7	1
Bend	d	R:	d	4d		
		K_L:	0.4	0.2		

Table 4-2: Typical loss coefficients for restrictions vs. its geometry.

The most known singularity losses in the drilling fluid circulation system are summarized below.

Bit nozzle. Drilling mud is discharged at the bottom of the hole through the bit nozzles. In order to aid cuttings removal from the bottom, the nozzles have a relatively small cross-sectional area so that the mud is discharged at high velocities.

By applying the Bernoulli equation, flow of incompressible fluids through a nozzle is written:

$$p_1 + \frac{1}{2}\rho\, \bar{v}_1^2 = p_2 + \frac{1}{2} \cdot \rho\, \bar{v}_2^2 + \Delta p_{loss} \tag{4.63}$$

Eqn (4.63) is simplified in several ways. The loss of pressure head through the nozzles is composed of three parts: loss of kinetic pressure at the entrance of the nozzles, loss of kinetic pressure at the outlet of the nozzles to the annulus, and frictional pipe pressure loss through the 0.1–0.2 m long pipe leading to the nozzles. Since the nozzle velocity is much larger than the velocity at the entrance and at the outlet, the effect of ignoring entrance and end effect plus friction through the nozzle-pipe are compensated by including them in the loss coefficient, K_{bit}. The discharge coefficient K_{bit} for high-velocity jet bit nozzles is equal to 1.0 (the losses at the entrance are small due to the ellipsoidal shape of the entrance). By including the other loss effects, the coefficient becomes larger than 1.0. A typical value listed in the literature is 1.11. However, the uncertainty of estimating pressure loss through bit nozzles is high. When the coefficient is 1.11, the bit pressure loss becomes:

$$\Delta p_{bit} = 1.11 \cdot \frac{1}{2} \rho \overline{v}^2 \qquad (4.64)$$

Tool joint. Pressure loss across a tool joint restriction can be expressed in terms of the loss of dynamic energy when the mud is passing the tool joint;

$$p_1 - p_2 = K_L \cdot \frac{1}{2} \rho \left(\overline{v}^2 \right) \qquad (4.65)$$

Here $\overline{v}$ is the velocity across the tool joint and K_L is given by the sum of eqn (4.61) and (4.62).

PDM. Positive Displacement Motors (PDM) are characterized by a tortuous internal flow path, comprising by-pass valves, stator/rotor, transmission and shaft bearing. In addition an unknown percentage of the fluid flow (2–15%) is used for lubrication and passing through the axial bearing. The losses are a function of flow rates, WOB and resulting downhole torque. A general model is proposed:

$$\Delta p_{PDM} = \Delta p_{NL} + \left(\Delta p_{max} - \Delta p_{NL} \right) \cdot \frac{WOB}{WOB_{max}} \cdot \left(tool\ factor \right) \qquad (4.66)$$

Δp_{NL} = pressure loss measure at no load (NL) (WOB = 0), and Δp_{max} = pressure at maximum recommended WOB. The vendor specifies these numbers.

MWD. Pressure losses through MWD tools are simpler to model than losses through PDMs. Pressure loss data obtained from the vendor are used to construct a data base of tool-specific pressure loss polynomial coefficients. Pressure loss curves can be constructed as a function of flow rate for different mud weights and for different additional influencing parameters.

$$\Delta p_{MWD} = a + bq + cq^2 + dq^3 \qquad (4.67)$$

5   Removal of cuttings from under the bit

5.1   Cuttings removal process

In the rotary drilling process the rock surface is crushed by the drilling bit. In order to provide further crushing and progress, the cuttings must be removed instantly and efficiently from the rock surface. For this purposes, two forms of energy are brought from the surface to the rock surface, illustrated in Figure 5.1 (left).

- Mechanic energy
- Hydraulic energy

Once at the rock surface, the energy should be applied in an optimal manner: Mechanical energy is responsible for the rock crushing process, while hydraulic energy is applied for the purpose of cuttings removal. While drilling in soft and medium hard formations, both types of energy play an important part in rock crushing and rock removal. Several investigations have shown that drilling rate is increased significantly with increased hydraulic energy, expressed either as hydraulic horse-power, jet impact force or jet velocity through the bit nozzles. Opinions vary to which hydraulic quantity has the greatest effect on drilling rate.

Download free eBooks at bookboon.com

The methods of hydraulic program design can be divided into two groups:

1. Determining the level of bottom hole cleaning energy required in order to balance the mechanical energy level.
2. Maximise criterion of estimation, e.g. jet impact force.

Methods in group 1 require field tests. These tests are based on the theory that the drilling rate is proportional to bit weight if bottom hole cleaning is adequate. When this proportionality curve, shown in Figure 5-1, at some point starts deviating from its increasing trend, the minimum required bottom hole cleaning energy to avoid bit balling at that level of WOB is determined.
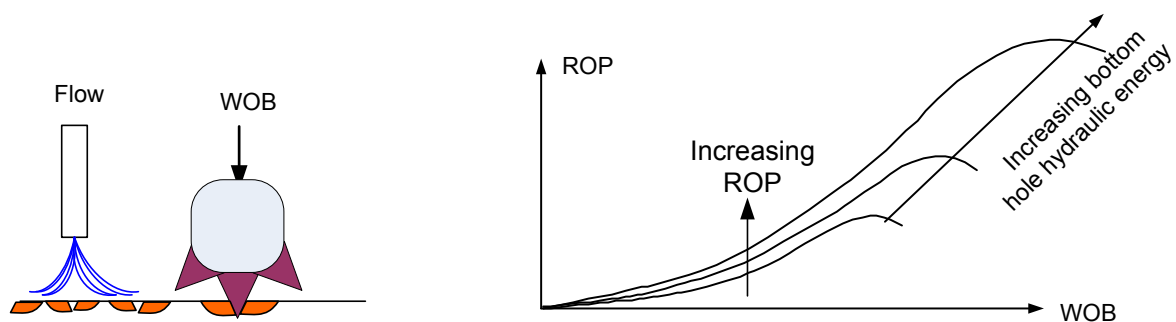
Figure 5-1: ROP vs. WOB for different bit hydraulic energy levels. The points where the curves are turning and pointing downwards are called the bit balling point.

For methods in group 2, optimum hydraulics is the proper balance of the hydraulic elements (flow rate, bit nozzles diameter) which satisfy some criterion of estimation (the objective function) e.g. maximizing the jet impact force. In this book we select the hydraulic quantity q/d_{nozzle} as a common quantity representing the above mentioned bit hydraulic objective function. From experiments and observations demonstrated through Figure 5-1, we suggest a mathematical model that relates ROP and the hydraulic objective function:

$$ROP = A \cdot \left(q / d_{nozzle}\right)^{a_8} \tag{5.1}$$

Figure 5-1 demonstrates rather clearly, that there is a general increasing trend of ROP when hydraulic energy is increased. Constant A in eqn (5.1) includes the effect of all other parameters (others than q, d_{nozzle}, and a_8) having an influence on ROP. All these parameters are assumed to be kept constant during the experimental phase and assumed to have little influence on the hydraulic parameters. Our task is to utilize the hydraulic energy of the drilling fluid to achieve the best possible cleaning below the bit so that ROP is maximized.

The performance of the pump and the flow system has several limitations or boundaries. These limitations are discussed next.

5.2   Boundary conditions of the drilling process

First, we have the limitations of the pump itself. Each pump is defined with a maximum recommended pressure, p_{max}, and a maximum flow rate. The characteristics of the pump is presented in Chapter 2, and repeated in Figure 5-2 below.

5.2.1   Friction loss increases with depth

Due to friction in the ever extending wellbore, the pump would at some stage reach its maximum available pressure during transmission of hydraulic effect through the circulation system. Previously it has been shown that the pump pressure is a mirror image of the pressure losses in the circulating system. For hydraulic optimization purposes, we now split the friction losses in two parts; bit pressure losses, Δp_{bit}, and remaining pressure losses in the circulation system, Δp_{loss}, also called parasitic pressure losses. This is expressed through eqn. (5.2):

$$p_{pump} = \Delta p_{bit} + \Delta p_{loss} \tag{5.2}$$

Figure 5-2 displays both mentioned pressure losses, when they are embedded on to the pump characteristics. When the flow rate increases, for a given well length, the pump pressure will be more and more consumed as friction, Dp_{loss}, and less and less is left for the bit.
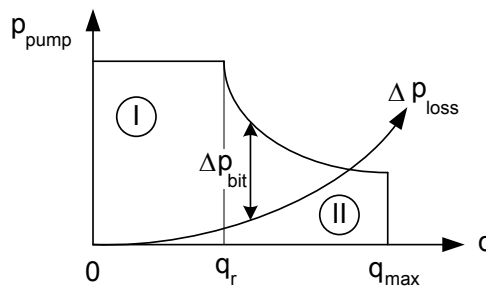
Figure 5-2: Hydraulic friction as a function of flow rate, superimposed on the pump characteristics.

The parasitic pressure loss can be estimated according to formulas presented in Chapter 3. For hydraulic optimization purposes, we apply a simpler expression, reduced to variables important for hydraulic optimization:

$$\Delta p_{loss} = K_1 \cdot D \cdot q^m \tag{5.3}$$

Parasitic pressure loss varies linearly with depth and is an exponential function of pump rate. The constants K_1 and m can be found by solving eqn. (5.3). Since there are two unknowns, two data sets are needed, at two different pump rates, rate 1 and rate 2. Taking the logarithm of eqn. (5.3) for two rates, we obtain:

$$m = \frac{\log\Delta p_{loss2} - \log\Delta p_{loss1}}{\log q_2 - \log q_1} \tag{5.4}$$

When m is known, K_1 is fond through:

$$K_1 = \frac{p_{loss2}}{D \cdot q_2^m} \tag{5.5}$$

Now a practical example of finding m and K_1 from simple rig experiments is summarized in Table 5.1:

Pump rate	Pump pressure	Estimated bit pressure loss
$q_1 = 0.0135 m^3/s$	$p_1 = 100 \cdot 10^5\, Pa$	$\Delta p_{bit_1} = 11 \cdot 10^5\, Pa$
$q_2 = 0.027\, m^3/s$	$p_2 = 320 \cdot 10^5\, Pa$	$\Delta p_{bit_2} = 44 \cdot 10^5\, Pa$

Table 5-1: Rig test for determining hydraulic parameters.

Observe that in Table 5-1 the bit pressure loss is estimated. For that purpose eqn. (4.63), was applied. Now Dp_{loss} can be found from eqn (5.2):

$$\Delta p_{loss1}=p_1-\Delta p_{bit_1}= 89 \cdot 10^5$$

$$\Delta p_{loss2}=p_2 - \Delta p_{bit_2}= 276 \cdot 10^5$$

m and K_1 are found from eqn (5.4) and (5.5) to be:

$$m = \frac{\log\left(\Delta p_{loss2}\;/\Delta p_{loss1_1}\right)}{\log\left(q_2/q_1\right)}=1.63$$

$$K_1 = \frac{p_{loss1}}{D\cdot q_1^{\,m}} =1.99*10^6$$

Table 5-2 presents some typical calculated values for m and K_1, based on the same field tests as described through Table 5-1.

Bit no.	d_b	Drilling depth	Nozzle dia.(3)	r_m	m_{pl}/Y_p	n	K	Dp_{bit}	Dp_{loss}	m	K_1
	in	m	32.in	kg/m³	cP/lb/100ft²		Pas⁻ⁿ	bar	bar		10⁶
9	12 1/4	950	14	1100	13 / 13	.58	.40	151.7	55.8	1.79	1.46
11	12 1/4	1700	16	1200	13 / 11	.62	.38	100.4	105.3	1.78	1.45
14	12 1/4	1840	14	1210	12 / 12	.58	.32	122.2	76.7	1.77	1.28
16	12 1/4	2100	13	1210	12 / 12	.58	.30	139.8	61.4	1.76	1.01
24	8 1/2	2560	11	1200	16 / 14	.62	.27	168.1	43.6	1.72	.78
28	8 1/2	2663	13	1320	15 / 10	.68	.18	132.1	73.2	1.76	1.08
44	8 1/2	2800	11	1290	18 / 9	.74	.13	150.7	55.6	1.68	.92
47	8 1/2	2916	12	1280	16 / 9	.71	.13	137.4	73.5	1.72	1.09
51	8 1/2	3014	12	1280	15 / 8	.72	.13	125.6	81.9	1.71	1.24
53	8 1/2	3060	12	1280	13 / 10	.65	.15	144.9	75.3	1.74	1.11

Table 5-2: Pressure loss constants in two well sections. Recorded data in left section, estimated to the right.

From Table 5-2 we see that this well consumed extremely many bits. The year was 1985, which was before the major improvement of steel quality selection, and in the 1990s they turned to frictional bearings. We also observe from Table 5-2 that bit nozzles were changed equally frequent. Today it may happen that they drill one full wellbore section with only one rock bit!

If flow is mainly turbulent in the drill string and the annulus, the exponent m will approach 2.0. When the flow is completely laminar in the complete flow system, m will approach the rheological power law exponent n. Figure 3-9 demonstrated this fact. Usually m is somewhere in between, although a bit closer to 2.0 since turbulent pressure drop (in drill string), dominates over laminar (in annulus).

5.2.2   Annular flow velocity limitations

Flow velocity in the annulus of vertical wells must be held within two boundaries. The upper one is normally designed so that turbulence is not developed around the drill collars. In horizontal wells, turbulent flow in the BHA-annulus is normally accepted; it helps largely in removing cuttings from this part of the annulus. ECD dictates if this can be accepted.

Cuttings concentration determines the lower boundary. It must be lower than 0.04, or 4 volume percent if it gets higher, problems related to accumulation of cuttings, like struck pipe, show an increasing trend. The lowest recommended flow rate is referred to as the required flow rate, and denoted q_r. In inclined wells the criteria concerning annular flow velocities are different and will result in a different hydraulic program compared to vertical wells. Optimal hydraulic parameter estimated for vertical wells can probably be used as a first approach for inclined wells. Summarized annular flow velocity limitations in vertical wells:

5.2.3   Limitations in vertical vs. horizontal wells

Due to cleaning requirements in horizontal wells the use of maximum available flow rate and RPM often precede pressure in importance. Therefore a large range is specified in Table 5-3. These numbers are also governed by the annular velocity boundaries:

$$v_{max} < v_{turb} \quad \text{(around drill collars)}$$
$$v_{min} \geq q_r \quad \text{(cuttings concentration in largest annulus} \leq 0.04)$$

It must be ensured that these parameters are not in conflict with limitations for top side equipment or downhole tools and also that they do not lead to formation fracture pressure.

	17½″ section	12¼″ section	8½″ section
Flow rate (lpm)	4 000–5 000	2 500–3 500	1 500–2 500
Drill string rotation (RPM)	140–180	130–175	120–170
Circulating Bottom Up	1–3	2–4	3–4

Table 5-3: Recommended hole cleaning parameters.

5.3   Optimizing ROP, liner by liner

As indicated by the heading, the hydraulic program is dependent on first selecting the most suitable liner of the piston pump, before optimizing. It is the annular flow rate limitation, q_r, which determines the selection of liners, as indicated in Figure 5-2. The smallest possible liner should be selected since this will result in the highest possible pressure available. The hydraulic variables are given by eqn (5.1). By requiring pump pressure in eqn (5.2) to be maximum and combining it and (4.63) with eqn (5.3) and multiplying by q^2 we obtain:

$$p_{\max} \cdot q^2 = K_1 D q^{m+2} + 1.1 \ \frac{1}{2}\rho \cdot \frac{q^2 \cdot q^2}{\left(\dfrac{\pi}{4} d_e^2\right)^2} \tag{5.6}$$

Here the equivalent single nozzle diameter d_e is defined through total nozzle area. Assuming there are three nozzles in the bit, the equivalent bit nozzle becomes:

$$d_e^2 = \left(d_1^2 + d_2^2 + d_3^2\right) \tag{5.7}$$

If the tree diameters are of identical size:

$$d_e = d_1\sqrt{3} \tag{5.8}$$

Rearranging eqn. (5.6) we obtain:

$$K_{bit}\left(\frac{q}{d_e}\right)^4 = p_{max} \cdot q^2 - K_1 \cdot Dq^{m+2} \tag{5.9}$$

The constant $K_{bit} = \cdot 1.1 \cdot \frac{1}{2}\rho \Big/ \left(\frac{\pi}{4}\right)^2$. Solving eqn. (5.9) with respect to q/d_e yields:

$$\frac{q}{d_e} = \left[\frac{1}{K_{bit}}\left(p_{max} \cdot q^2 - K_1 \cdot Dq^{m+2}\right)\right]^{1/4} \tag{5.10}$$

Combining eqn. (5.10) and eqn. (5.1) and deriving with respect to the two variables, flow rate and nozzle diameter, and equating it to zero, eqn. (5.11) defines the optimum of variable q:

$$\frac{\partial R_p}{\partial q} = \frac{\partial}{\partial q}A\left[\frac{1}{K_{bit}}\left(p_{max} \cdot q^2 - K_1 Dq^{m+2}\right)\right]^{\frac{a_8}{4}} = 0 \tag{5.11}$$

Deriving with respect to the variables d_e gives the following answer; minimize d_e. Moreover, since minimizing d_e is not feasible, only the q-derivation represents an applicable solution of eqn. (5.11). In eqn. (5.11) the constant p_{max} is the maximum recommended pressure for the selected liner. The only meaningful solution yields:

$$2p_{max} \cdot q - (m+2)\,K_1 D \cdot q^{m+1} = 0 \tag{5.12}$$

which, when solved for q results in the optimal solution:

$$q_{opt} = \left(\frac{2p_{max}}{(m+2)\,K_1 D}\right)^{\frac{1}{m}} \tag{5.13}$$

Combining eqn. (5.12) and eqn. (5.2), and solving for Δp_{bit} we obtain an additional optimal expression:

$$\Delta p_{bit,opt} = \frac{m}{m+2}\,p_{max} \tag{5.14}$$

The equivalent nozzle diameter d_e is sought, and can be found from eqn (4.63)):

$$d_e = \left[K_{bit} \cdot \frac{q^2}{(\Delta p_b)}\right]^{1/4} \tag{5.15}$$

Now the job is done, we have determined optimal parameters for a selected liner. The above procedure and solutions can also be solved graphically, as shown in Figure 5-3. Δp_{loss} from eqn (5.3) becomes a straight line in a log-log plot. Δp_{loss} represents the losses of the available pump pressure. When $\Delta p_{bit,\,opt}$ is secured, through the horizontal line, the sum of the two, $\Delta p_{loss} + \Delta p_{bit} = p_{pump}$, is given by the point where the two lines meet.
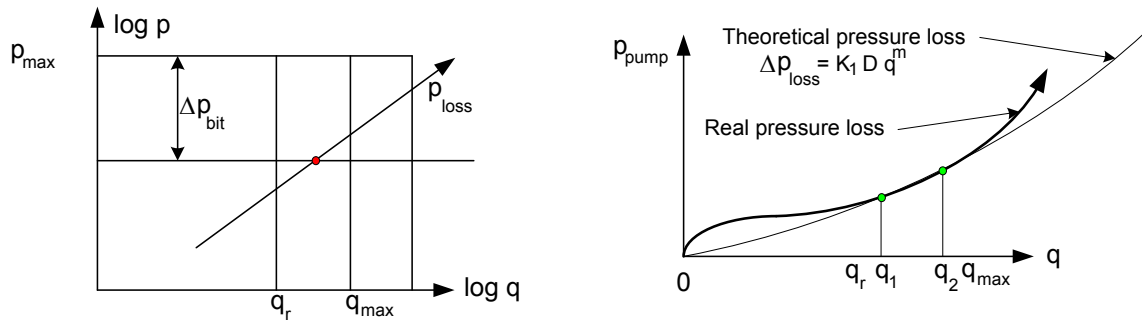
Figure 5-3: Graphical determination of optimal flow rate.

The technique presented in Chapter 5.3 represents the standard method of hydraulic optimization for vertical wells. A flow sheet of how to routinely determine the optimal bit nozzle and optimal flow rate is presented in Figure 5-4. Within a selected liner, the optimal flow rate will be a function of depth in accordance with eqn (5.13), while nozzle size will stay constant in accordance with eqn (5.14). With high quality drilling bits and pumps, it is probably sufficient to change liner and bit every time a new section is started. This program would suggest which liner, which nozzles and which flow rate is optimal at the selected depth.

Download free eBooks at bookboon.com
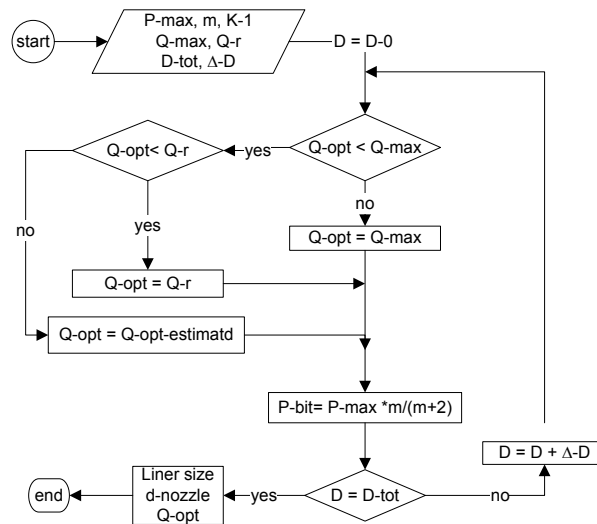
Figure 5-4: Flow diagram of how to compute optimal flow rates and nozzle diameter in a vertical well when pump liner has been selected.

5.4   Optimizing the complete well

To plan the complete well for all sections in one complete hydraulic program requires that the standard hydraulic program must be expanded. All the constants must be known before the well is drilled. One positive side effect obtained through this technique, is that it will be possible to suggest at what depth the pump liners can be changed. A complete hydraulic program would suggest which liner, which nozzles and which optimal flow rate should be chosen for every section.

First we need to define two pump operating ranges, as already suggested in Figure 5-2. In operating range I, defined by the smallest liner, the pump pressure can be held constant. In order to utilize the pumps full capability, and thereby optimizing ROP, the pump pressure is kept at its maximum pressure. In range II, defined by the remaining liners, the pump power, E_{pump}, can be held constant as seen in previous Figure 2-2 and from Table 2-3. Summarized we have:

> Range I: p_{max} = const
> Range II: E_{max} = const

The optimal solution in range II is found by combining eqn (5.1) and (5.10):

$$ROP = A\left(\frac{q}{d_e}\right)^{a_8} = \frac{1}{K_{bit}}\left(p_{max}q^2 - K_1 \cdot D \cdot q^{m+2}\right)^{a_8/4} \qquad (5.16)$$

By substituting $p_{max} \cdot q$ by E_{max} (which is constant over pump range II) in eqn (5.16) we obtain:

$$A\left(\frac{q}{d_e}\right)^{a_8} = \frac{1}{K_{bit}}\left(E_{max} \cdot q - K_1 D q^{m+2}\right)^{a_8/4} \qquad (5.17)$$

By differentiating eqn. (5.17) with respect to q, we obtain one meaningful solution:

$$\frac{\partial ROP}{\partial q} = E_{max} - (m+2)K_1 \cdot D \cdot q^{m+1} = 0 \tag{5.18}$$

which, when solved for q yields:

$$q_{opt_I} = \left[\frac{E_{max}}{K_1 \cdot D \, (m+2)} \right]^{\frac{1}{m+1}} \tag{5.19}$$

Combining the optimal solution in eqn. (5.18) with eqn. (5.2) and solving for Δp_{bit} we obtain

$$(\Delta p_{bit})_{opt_{II}} = \frac{m+1}{m+2} \cdot p_{max} \tag{5.20}$$

ROP, which is proportional to the cleaning function, can be plotted as a function of pump rate, as shown in Figure 5-5.
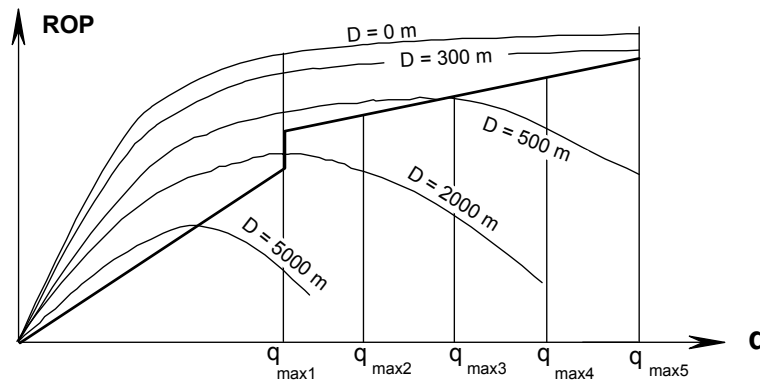
Figure 5-5: ROP (eqn. (5.10) in range I and eqn. (5.17) in range II) vs. pump rate and depth.

We are now able to decide when to change liner in order to fully utilize the mud pump. By studying Figure 5-5 we can find graphically at which depth the pump liner has to be changed. A pc-program to monitor pump range and respective optimal solution is suggested in Figure 5-6.
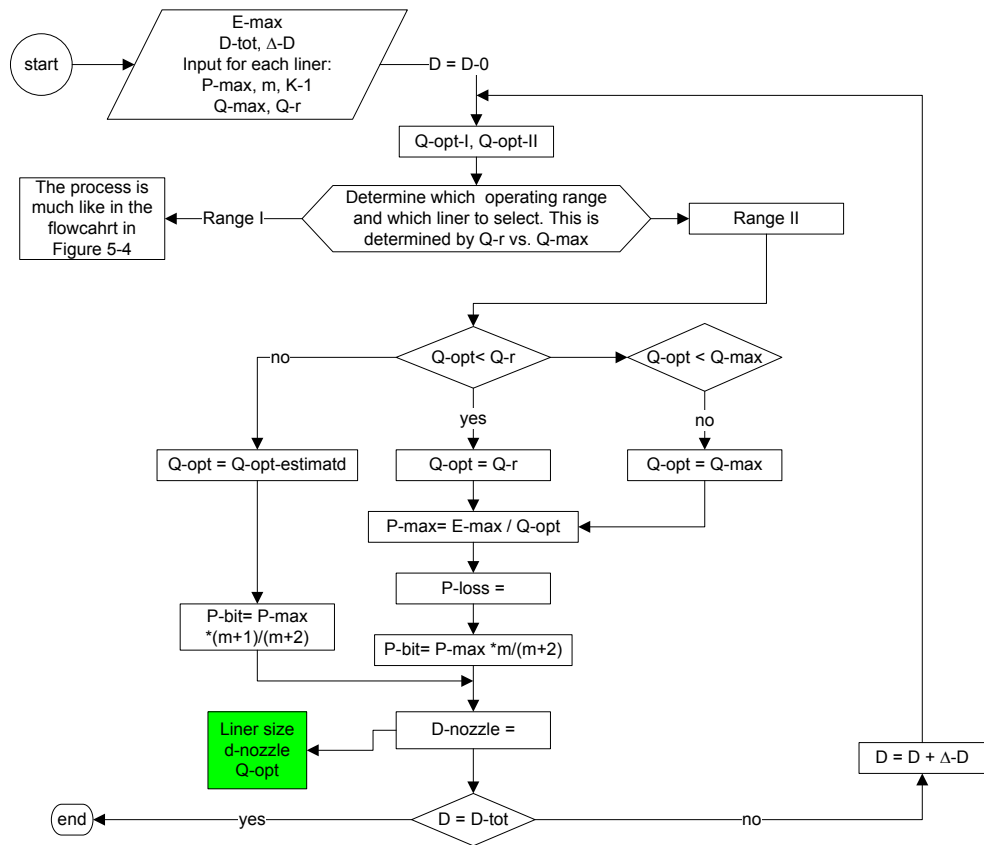
Figure 5-6: A simplified flow sheet to compute optimum hydraulic parameters in pump operating range II.

To optimize the complete well in one operation, the two programs indicated in Figure 5-4 and 5-6 have to be combined and expanded. Now let us exemplify the routine to prove its applicability:

Example:

Use mud pump specified in Table 2-3.

Effect $= 1441.7$ Hp $\cdot$ $745.7 = 1.075 \cdot 10^6$ (W) $= 322 \cdot 10^5 \cdot 0.0334$ $m^3/s = 4670$ psi $\cdot$ 529 GPM / 1714

Well and hydraulic data

D	=	2500 m	m	=	1.7
ρ	=	1200 kg/m³	$q_{required}$	=	0.018 m³/s (d_{bit} = 12 1/4")
K_1	=	$1.1 \cdot 10^6$	q_{max}	=	0.04 m³/s

    a.   Which liner should be used, and what is the optimal flow rate?
    b.   When should it be changed to a smaller liner dimension?
    c.   What is optimal nozzle size in 2500 meters depth?

a)

$$q_{opt,II} = \left[\frac{E_{max}}{K_1 \cdot D\,(m+2)}\right]^{\frac{1}{m+1}} = \left[\frac{1.075 \cdot 10^6}{1.1 \cdot 10^6 \cdot 2500(1.7+2)}\right]^{\frac{1}{1.7+1}} = 0.0337 \ m^3/s$$

    Liner: From Table 2.3, the necessary liner is 6 ¼" $\Rightarrow p_{6.25\ max} = 296.8 \cdot 10^5$ P

b)   When $q_{opt,II}$ reaches 0.0334 then change to the next liner, which is 6". At which depth to change, we can determine by solving the $q_{opt,II}$ eqn. with respect to Depth:

$$D = \frac{E_{max}}{K_1 \cdot (m+2) \cdot (0.0334)^{m+1}} = \frac{1441.7 \cdot 745.7}{1.1 \cdot 10^6 \cdot (3.7) \cdot (0.0334)^{2.7}} = \underline{2557.5 \ m}$$

c)   Solve the $\Delta p_{bit,opt}$ with respect to nozzle size:

$$d_e = \left[K_{bit} \cdot \frac{q^2_{opt_{II}}}{(\Delta p_{bit})_{opt_{II}}}\right]^{1/4} = \left[1.11 \cdot \frac{1200}{2\left(\frac{\pi}{4}\right)^2} \cdot \frac{.0337^2}{\frac{1.7+1}{1.7+2} \cdot 296.840^5}\right]^{1/4} = \underline{0.0154 \ m}$$

$d_e = \sqrt{3}d_1$, assuming they are all identical sized.

$$d_1 = \frac{d_e}{\sqrt{3}} = \frac{0.0154}{\sqrt{3}}\,[m] = 0.0154/\sqrt{3} = 0.0111$$

    Now meters must be translated into 32nds of inches:

$$\frac{0.0111}{\frac{2.54 \cdot 10^{-2}}{32}\,[m\,/\,32in\,]} = 11.2 \Rightarrow \frac{11}{32} + \frac{11}{32} + \frac{12}{32}$$

If $d_e > 11.3333$ we would have to increase nozzles size two 12/32nd in order on to take out less pressure across the nozzles than optimal (conservative).

---

6   Transport of cuttings to the surface

6.1   Hole cleaning in vertical wells

In vertical wells, hole cleaning is a question of pumping fast enough to counteract the vertical slipping of cuttings, thus causing its concentration to decrease. In horizontal wells it is different, the settling distance is short, cuttings will fall quickly to the bottom side of the well, and the particles will form beds and dunes.

The rate at which cuttings are generated by the drilling process is:

$$q_{cuttings} = \pi/4 \times d_{bit}^{2} \times ROP \tag{6.1}$$

During simultaneous pumping while drilling, the initial cuttings concentration at the bottom of the annulus becomes:

$$c_{cuttings,0} = q_{cuttings} / (q_{pump} + q_{cuttings} - q_{filling}) \cong q_{cuttings} / q_{pump} \tag{6.2}$$

In the next chapter, we will study important parameters for settling of particles in liquids.

6.1.1   Slip velocity of perfect spheres

As a first approach we will simplify the cuttings geometry to spheres. The slip velocity, v_{slip}, will be calculated for a single sphere with particle diameter d_p and density ρ_p, settling in a Newtonian fluid with viscosity μ and density ρ_{mud}. The settling of spheres in laminar conditions is shown and modelled in Figure 6-1:
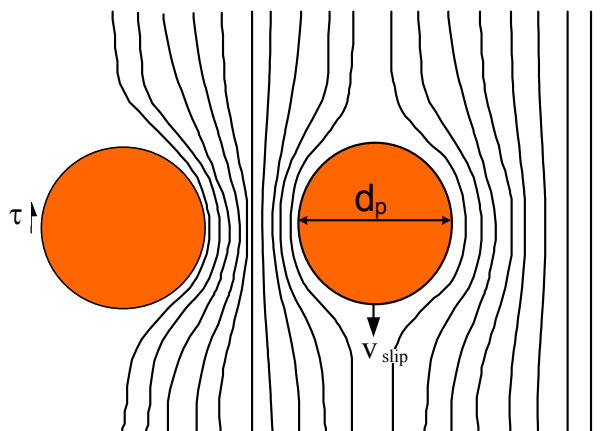
Figure 6-1: Two spheres settling in a fluid.

Only two forces are active at stationary, laminar flow; gravity and shear force:

$$\left(\rho_p - \rho_{mud} \right) V_{sphere} = \tau\, A_{shpere} \tag{6.3}$$

where:

$$V_{sphere} = \frac{4}{3}\,\pi\, r^3 = \frac{\pi}{6}\, d_p^3 \tag{6.4}$$

$$A_{sphere} = 4\pi\, r^2 = \pi\, d_p^{\,2} \tag{6.5}$$

The shear stress of a Newtonian fluid flowing in a pipe is given by:

$$\tau = \mu \cdot \frac{dv_x}{dr} \tag{6.6}$$

The axial velocity of the fluid, v_x, relative to the moving sphere is proportional to the distance the fluid must travel along the periphery of the sphere (see Figure 6-1):

$$\frac{v_x}{v_s} = \frac{v_{periphery}}{v_{center,\ sphere}} = \frac{l_{periphery}}{2r} = \frac{2\pi r / 2}{2r} = \frac{\pi}{2} \tag{6.7}$$

This results in:

$$v_x = \pi / 2 \cdot v_{slip}. \tag{6.8}$$

The shear rate in the fluid is the relative velocity change across the half sphere in the axial direction, $\frac{\pi}{2} \cdot v_{slip} - 0$, which results in:

$$\frac{dv_x}{dr} = \frac{\frac{\pi}{2} v_{slip}}{r} = \frac{\pi}{d_p} v_{slip} \tag{6.9}$$

Combining eqn (6.3), (6.4), (6.5), (6.8) and (6.9) we obtain:

$$\left(\rho_p - \rho_{mud}\right) g \cdot \frac{\pi}{6} d_p^3 = \mu \cdot \frac{\pi\, v_{slip}}{d_p} 4\pi \left(\frac{d_p}{2}\right)^2 \tag{6.10}$$

This reduces to Stokes law of a falling sphere:

$$v_{slip} = \frac{d_p^{\,2} \cdot g \left(\rho_p - \rho_{mud}\right)}{6\pi\mu} \tag{6.11}$$

Stokes law is only valid for infinite dilution (one sphere alone), small spheres (r < 0.1 mm) and laminar flow around the particle, $N_{Re,p} \leq 1$, which is found through:

$$N_{Re,p} = v_{slip}\, d_p\, \rho_{mud} / \mu_{eff} \tag{6.12}$$

When particle concentration, c, increases, the interaction between the particles and hence the shear rate will also increase, as illustrated in Figure 6.1 be two spheres. When two particles are present, the flow lines are closer (higher shear) compared to when only one is present (to the right of the right most particle). The flow resisting-function f(c) is related to the concentration as shown in Figure 6-2, resulting in a reduced settling velocity, $v_{slip,reduced}$:
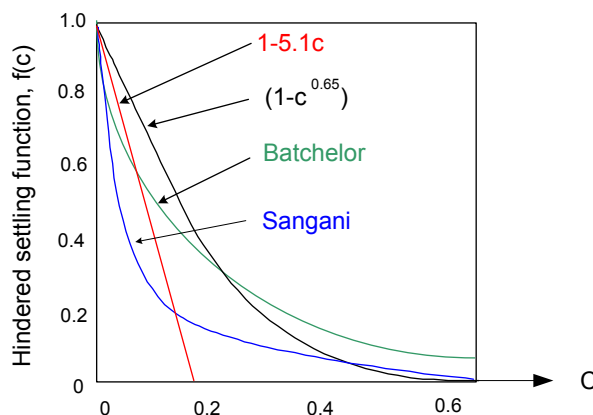
Figure 6-2: The hindered settling function f(c) vs. Particle concentration.

$$v_{slip,reduced} = v_{slip} \cdot f(c) \tag{6.13}$$

Cuttings volume concentration can be estimated through eqn (6.2) and exemplified through:

$q_{cuttings}$ = ROP · A_{bit} = 20 m/h ·π/4 · (12 1/4"· 0.0254)^2 = 0.00042 m^3/s

q = 1000 l/min = 0.0167 m^3/s

Under these conditions $c_{cuttings,0}$ = 0.025. A concentration of 2.5%, produces an f(c) = 1 − 5.1 ⋆ 0.025 = 0.87, reducing the settling velocity of a single particle by 13%. Other hindered settling functions in Figure 6-2 will give higher or lower results.

6.1.2   Slip velocity of imperfect spheres

Cuttings are non-spherical and perform strange settling motions. And when the flow regime is not laminar, empirical knowledge is necessary. The slip velocity must now be found through an empirical drag coefficient, C_{Drag}:

The two forces acting on slipping cuttings are still gravity, F_g, and shear, F_{Drag}, which at turbulent flow is:

$$F_{Drag} = C_{Drag}\, A_p \cdot 0.5\, \rho_{mud}\, v_{slip}{}^2 = \frac{4}{3}\pi d_p{}^3(\rho_p - \rho_{mid}) \cdot g \qquad (6.14)$$

At terminal (stationary) settling velocity the gravity and shear force will be equal, and the resulting particle slip velocity is found by combining eqn (6.13) and (6.14):

$$v_{slip} = \sqrt{4g(\rho_p - \rho_{mud})d_p / (3C_{Drag}\, \rho_{mud})}$$ (6.15)

C_{Drag} is a function of Reynolds number of the slipping particle. Figure 6-3 shows the inter relationship for different flow regimes, laminar, intermediate and turbulent.
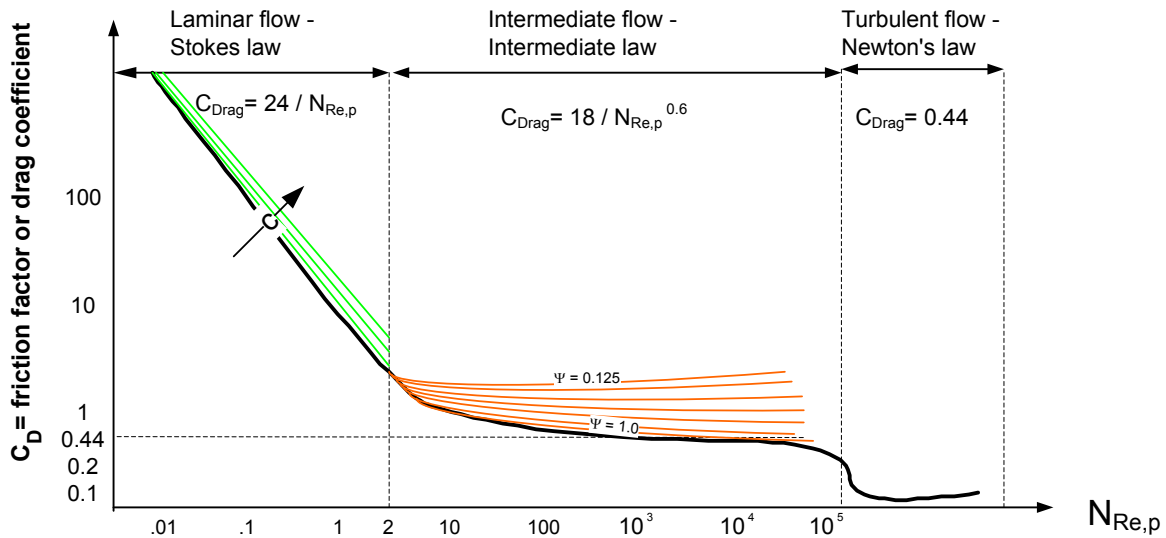
Figure 6-3: Relationship between CDrag and Reynolds Number for settling of real particles in Newtonian fluids.

In the intermediate flow regime C_{Drag} is a function also of the shape of the particle, given by the spherisity Y.

$$\Psi = \frac{area\ of\ a\ sphere\ of\ same\ volume\ as\ particle}{area\ of\ particle} = \frac{\pi^{1/3}\,(6V_p)^{2/3}}{A_p}$$ (6.16)

When the average mud velocity exceeds the resulting slip velocity, the particles will be transported out of the well at the resulting transport velocity;

$$v_{transport} = v_{ann} - v_{slip}$$ (6.17)

The differential speed can also be presented through a transport ratio:

$$R_{trasport} = v_{transport} / v_{ann} = 1 - v_{slip} / v_{ann}$$ (6.18)

The interdependency between the transport ratio and annular flow rate is determined through experiments as shown in Figure 6-4.
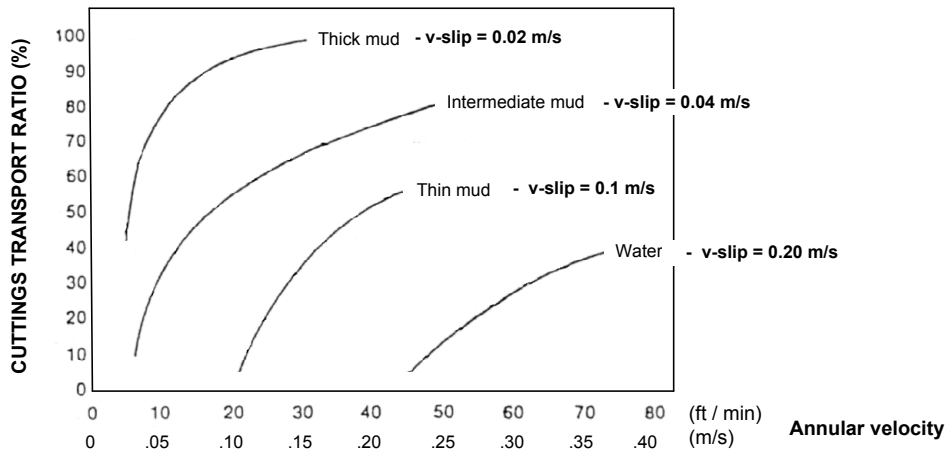
Figure 6-4: Annular velocity vs. transport ratio.

It is of interest to determine the minimum required annular velocity, below which problems related to accumulated cuttings become too serious. Practice has proven that this boundary velocity coincides with a cuttings concentration of 4 volume %. This realization is expressed through solving $R_{trasport}$ with respect to $c_{cuttings}$ and set it equal to 0.04. The result is shown in Figure 6-5. The required annular velocity is typically 30–60 ft/min.
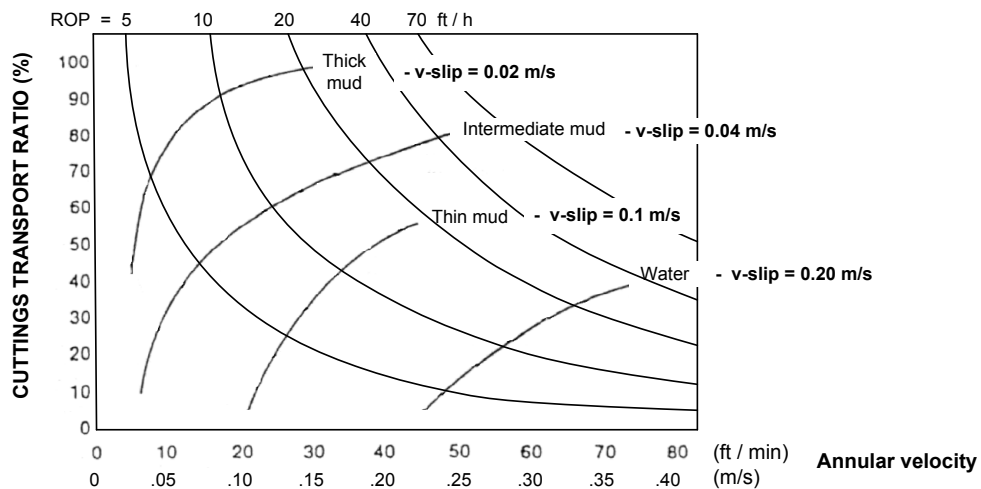
Figure 6-5: Annular velocity in a 5 * 12 ¼" annulus to keep cuttings concentration above 4 vol %.

At stationary settling conditions the cuttings concentration in the annulus becomes:

$$c_{cuttings} = c_{cuttings,0} / R_{transpor}$$

(6.19)

Cuttings size must be determined from samples taken at the shale shaker or from historical default values, related to lithology. As a first approach assume a cuttings diameter from the upper quarter of the size distribution profile.

6.2   Hole cleaning in medium inclined wells

A sub problem of directional drilling at depths where mud density is relatively high is barite segregation.

When $\rho_{mud} > \sim 1.5$ kg/l, the barite concentration is high. At still stand, most mud types quickly develop a yield point, and barite is suspended in the gelled mud. During pumping, at flow rates in laminar mode, any existing gel is broken, and barite will not be held in suspension as during still stand with gelled mud. However, the mud will under these conditions exhibit a high effective viscosity. Agglomeration may also effect the settling rate. Barite has a specific density of 4.2, and an average particle size of approximately 20 μm. In accordance with Stokes's law of settling, barite particles will settle, but as indicated above, very slowly. However, inclination will shorten the settling distance to only a few centimetres, and a stratified bed of barite and cuttings are formed. The stratified layers of solids of different densities will, when angle of repose is surpassed, slide downwards. Angle of repose is found mainly in the build-up section of the well, and here sliding takes place.

The phenomena described above are called sagging. Sagging takes place even at periods when mud is at rest, e.g. during tripping operations. Sliding may occur at any time, independent of stirring movements of the mud. But the avalanching barite will create eddies and stir the still standing mud and hence break the yield point, and initiate settling of barite and cuttings. There may be other effects also which maintain the disturbance of the settling; agglomerating of solids will enhance settling. A continuous, dynamic effect of sustainable settling and sliding has a dramatic effect on the operation. When the mud pump is started after a round trip, to drill further, and after barite sagging has taken place in the critical inclined part of the well, the mud density of this mud, when circulated to surface, can vary as much as 0.5 kg/l. This effect is shown in Figure 6-6, and can lead to kick, lost circulation and stuck drill string.
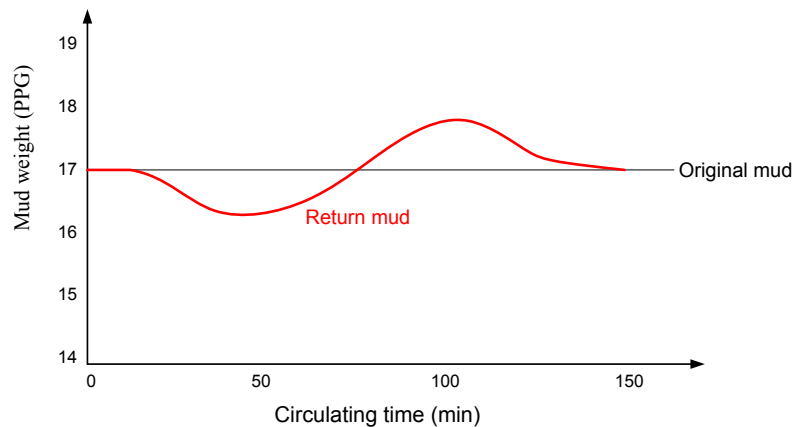
Figure 6-6: Density variation during circulation after a round trip caused by sagging in stillstanding mud.

Best Practice to avoid Barite sagging

- Apply micro barite or equivalent. Such systems have an average particle size of 2 μm.
- Use top drive rigs to allow for pipe rotation and redistribution of settling barite and cuttings while tripping and drilling (also with downhole motor).
- Maximize fluid velocity during drilling and reaming by increasing pumping power and/or use large diameter drill string. This improves hydraulic and agitation of cuttings.
- Design mud rheology so that it enhances turbulence in the annulus (if ECD allows). Turbulent flow will bring the cuttings and barite back into the flow stream if max fluid velocity is insufficient.
- Use various hole cleaning monitoring techniques including monitoring of drilled cuttings retrieval rate, drilled cuttings physical appearance, pressure while drilling, comparison of pick-up weight and slack-off weight (drag resistance) etc.
- Perform frequent wiper trips.
- Design well path so that if critical angles (with respect to optimization of mechanical stability) are avoided

6.3   Hole cleaning in highly inclined wells

The economic advantage of drilling directional wells is firmly established and for offshore operations only exploratory wells are vertical. The direction of cuttings settling is still vertical, but for inclined wells the fluid velocity has a reduced vertical component. This decreases the mud's capability of suspending drilled cuttings, and it results in an increased tendency for particles to settle out of suspension, more so with increasing hole inclination. Once reached the borehole floor, the particle has little chance of re-entering the fluid, because local fluid velocities near the wall are small and insufficient (no slip effect). Consequently, particle resident time in the annular space increases significantly, resulting in higher concentration of cuttings in the well bore, and, alas, cuttings beds are created. Because of the complexity, experimental knowledge is necessary for determination of cuttings movement.

The most common drilling problems related to insufficient hole cleaning occurs during tripping and reaming operation. Such problems manifest themselves as small and large restriction. However, when not cleared, the situation may worsen and end up in creating stuck pipe, lost circulation and serious hindrances during casing running.

The main objective of cuttings transport predictions is to avoid such operational problems and to operate with the most optimum; safe and economical cuttings transport option. High flow rate will always remove cuttings. However, in narrow wells like 12¼" and smaller, high ECD will limit the flow rate.

Mechanisms of particle transport in inclined wells are complex, and there are many mechanisms involved in transportation of cuttings. There are two main schools of modelling the complex system of cuttings transport:

1. Mechanistic models
2. Empirical models

6.3.1   Mechanistic model

The mechanistic model explains the physics and defines all forces involved basing the analysis of the balance between hydraulic and mechanical forces for a given particle in the bed made up of solids. According to this model, two mechanisms are considered responsible for removing protruding cuttings; rolling and lifting. The forces required to activate a single cuttings particle determines also the mechanisms that dominate the process of removal. Figure 6-7 shows the forces involved in cutting transportation.
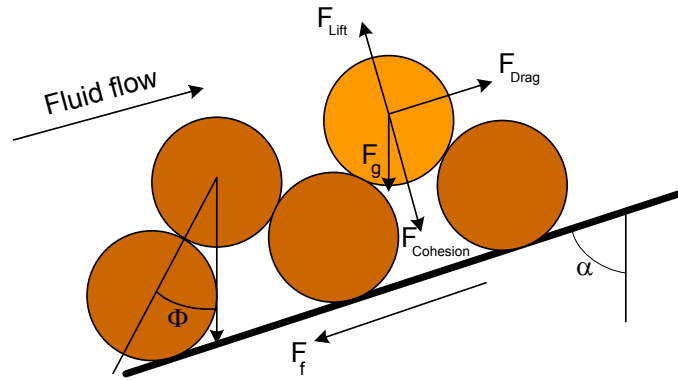
Figure 6-7: Forces acting on particle at an active erosion site of a cuttings bed. F is the angle of repose.

Of the five forces defined in Figure 6-7, friction forces are not included in cuttings transport. Friction is involved only during avalanching of cuttings bed, initiated when inclination is higher than the angle of repose.

Drag force. Drag can be estimated using the drag coefficient C_{Drag} as follows:

$$F_{Drag} = C_{Drag}\frac{\pi\, d_p^2}{8}\rho\, v_x^{\;2}$$

(6.20)

where v_x is the local relative velocity between the local fluid velocity and that at the center of the particle. When the particle is at stationary condition the drag force attains its maximum value.

Figure 6-8 shows how the local fluid velocity changes with distance from the particle bed.
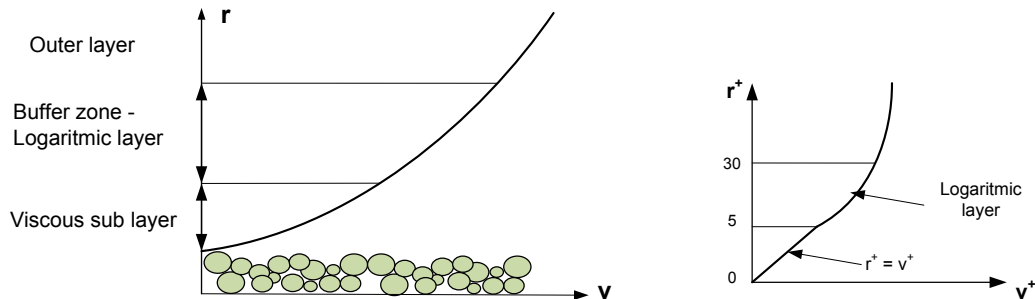
Figure 6-8: Near-bed velocity profile. Increased roughness will lead to increased drag due to increased local velocity. In the viscous sub layer dv^+/dr^+ is assumed to be 1. $dr^+ = r/R$, $v^+ = v/v_{max}$.

The drag coefficient for slipping particles is presented in Figure 6-3. Also for stationary particles the drag coefficient is a function of shape (see Figure 6-9), size, fluid properties and surface roughness of the bed. An empirical correlation for spherical and smooth particles is:

$$C_{Drag} = 24/N_{Re,p} + 6/(1 + N_{Re,p}) + 0.4 \qquad (6.21)$$

By taking $N_{Rep} = v_x^2 * \rho_p / \tau$, eqn. 6-21 is valid also for non-Newtonian fluids.
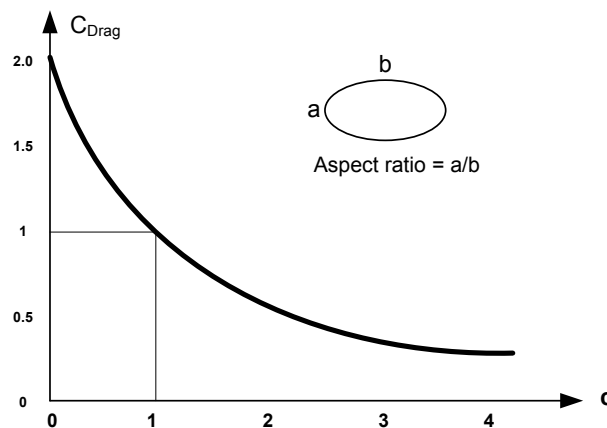
Figure 6-9: Drag coefficient for an ellipse vs. its aspect ratio for Rep = 10^5. Values < 1 indicate a 90^0 re-orientation of the ellipse.

Lift force. Drag force is present in all types of flow around a solid particle. However, lift acting on a spherical particle is present only if there is asymmetry in the flow field, which is the case for velocity profiles in pipe flow due to no slip velocity at the wall. The lift force can be estimated through eqn. (6.23) when the lift coefficient is known:

$$F_{Lift} = C_{Lift} \frac{\pi \, d_p^{\,2}}{8} \rho \, v_x^{\,2} \qquad (6.22)$$

Einstein found that the lift force acting on protruding particles in a sedimentary bed could be estimated by using a lift coefficient of 0.09 for bed particles. Another lift coefficient suggested for uneven horizontal surfaces is:

$$C_{Lift} = 5.82 \left[\frac{d_p}{2 v_x N_{Re,p}} \cdot \frac{dv_x}{dr} \right]^2 \qquad (6.23)$$

Here dv_x/dr is the local velocity gradient or the shear rate.

Cohesive force. Cohesive force is a force of attraction between particles in the mud and the bed and is classified as:

- Attraction forces without contact consist of van der Waals forces and electrostatic forces
- Attraction forces with contact consist of viscous bridges or solid bridges

One way of estimating cohesive forces is based on the slip-line theory, the start of avalanche, and is given by eqn. (6.24) and illustrated in Figure 6-10:

$$F_{cohesive} = \frac{\pi \, d_p^{\,2} \tau_y}{4} \cdot f_y \qquad (6.24)$$

where $f_y = 2 \left(\varphi + (\pi / 2 - \varphi) \sin^2 \varphi - \cos \varphi \sin \varphi \right)$

ϕ is the angle of repose, and τ_y is the yield strength of the drilling fluid.
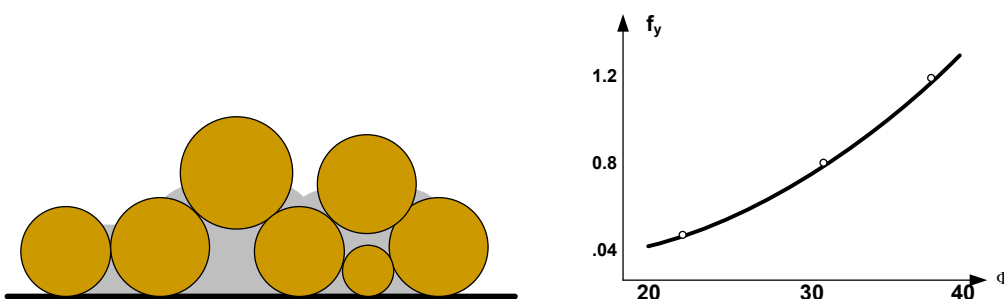
Figure 6-10: Stagnant fluid surrounding a bed-particle (left). Stagnant factor f_y vs. angle of repose (right).

Force of gravity. The weight of the particle in the fluid minus buoyancy force is given by:

$$F_g = g\, \frac{\pi\, d_p^3}{6}\left(\rho_s - \rho_{fluid}\right) = W \qquad\qquad (6.25)$$

Gravity will bring particles down onto the bed.

Critical velocity of lifting and rolling. When the annular mud velocity is high enough, cuttings in the particle bed will start to roll or to be lifted up to join the flowing mud. Generally, the annular mud flow velocity needs only to exceed a given critical value, known as the critical mud velocity, to reach the condition sufficient to initiate lifting/rolling of cuttings. For a given flow rate, the concept of critical velocity leads therefore to the existence of an equilibrium bed height. This height corresponds to the incipient condition of cuttings transportation.

If we now consider a drilling fluid with some amount of cuttings at a given flow rate at sub-critical velocity, a cuttings bed will start to build. As it builds up, the mud velocity over the bed increases accordingly (assuming constant pump rate), until the mud velocity eventually reaches the critical value. At this condition, the bed height remains unchanged. If additional cuttings are deposited on the bed, the mud velocity in the neighbourhood of that region exceeds the critical velocity. Consequently, the flow will dislodge the cuttings from the surface of the bed. After these extra cuttings are moved downstream, the local equilibrium bed height is maintained.

A force balance for a single bed particle in the direction normal to the bed, will increase the local critical velocity sufficiently to lift the particles from the surface of the bed.

$$F_{net,lift} = F_L - F_{cohesive} - W \cdot \sin \alpha \; > \; 0$$
(6.26)

The local critical velocity is the undisturbed velocity, i.e. the axial velocity acting above the cuttings bed at a point that corresponds to the protruding cuttings centre at the start of lifting.

The other mechanism involved in cuttings transportation is rolling. Rolling of the particles commence when the rolling torque resulting from the drag and lift force is able to overcome the counteracting torque from gravity and cohesion forces. Rolling can be obtained under this condition:

$$F_{net,rolling} = \frac{d_p}{2}\left[F_D \cdot \sin \Phi + (F_L - F_{cohesive})\cos \Phi + W \sin(-\alpha - \Phi)\right] \; > \; 0$$
(6.27)

Usually, these two calculated values of local velocities are different. In such cases, the lower has to be taken to estimate the bed shear stress and the critical velocity.

Estimation of two critical velocities has here been exemplified. However, a through presentation f this complex are where deeper knowledge of many interacting processes are necessary is not feasible in this book.

When the roll torque exceeds the static torque of cohesive and gravity forces, the cuttings tend to roll along the bed. This is the most dominant and important transport mechanism in stratified solid liquid flow. The roll torque increases with mud velocity. Rolling is somehow related to the formation of ripples. Ripples are formed when particles at a given point are rolled over the stationary part of the bed. The formation of ripple changes the drag and lift forces acting on the particles. Here we have to note that the random nature of lifting and rolling mechanisms originate from the stochastic behaviour of particle size, shape, density, rearrangement and the hydrodynamic forces of lift and drag. Therefore, it is ideal to assume a uniform process of cutting transportation over the bed and the formation of ripple has to be understood in this sense. Hence, we can say that during cutting transportation both erosion and deposition are simultaneously involved. Since only rolling and lifting are involved in the mechanistic model, no friction is involved. Dragging of a particle is less likely than rolling.

Since the fluid velocity decreases inside a washout of the wellbore, it can be assumed that the most probable cause of restriction during tripping (up or down) is when the BHA is passing a washout as illustrated in Figure 6-11.
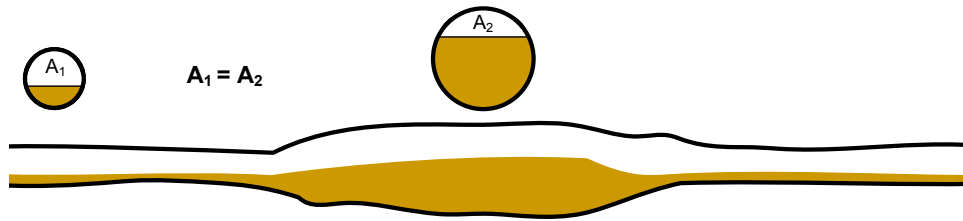
Figure 6-11: Cuttings are being filled into a washout. After long periods of circulation during drilling, the hydrodynamic equilibrium will dictate a thicker bed inside the washout. When the BHA is shovelling a large quantity of cuttings into the normal part of the wellbore, the drill string will experience severe Overpull here.

6.3.2   Empirical model

When it comes to empirical transport models, particle transport can be classified with respect to cuttings bed behaviour as illustrated in Figure 6-12. The models are classified into two layer models or, three layer models. In the two and three layer models the modelling approach is based on mass, momentum and energy balance of each layer. And bed behaviour is to a large part determined by particle size:

1. Particles less than 40 μ: Homogeneous suspension
2. Particles from 40 to 150 μ: Heterogeneous suspension maintained by turbulence
3. Particles between 150 and 1 500 μ (1.5 mm): Increased rheology will lead to an increase of which sizes can be transported in a heterogeneous suspension
4. Particles larger than 2 500 μ transported by saltation. Otherwise stationary bed.
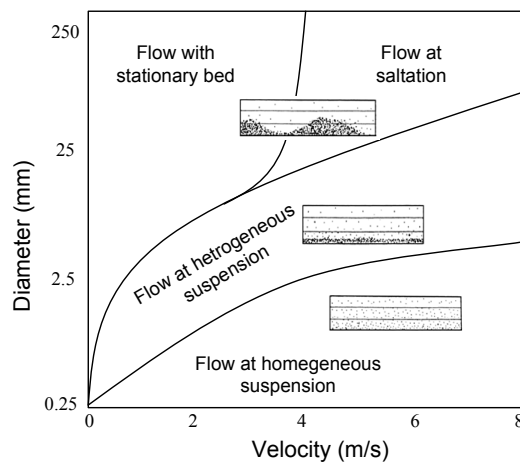
Figure 6-12: Three flow patterns for cuttings transport in deviated wells.

According to Figure 6-12, decreased cutting size leads to increased shear area available to move the cutting along the wellbore. And increasing flow rate increases available energy for saltation and maintains turbulent cross flow. Higher viscosity reduces the slip velocity and increases the distance traversed during one cycle of saltation. Pipe rotation serves a dual purpose in horizontal hole cleaning. The pipe can mechanically crush cuttings to reduce cutting size; rig experience has shown that cutting size on the shale shaker is often smaller with pipe rotation. Pipe rotation tends to induce cross flow in laminar flow profiles. Tools, such as stabilizers, act to break up cutting beds.

Lag time in inclined wells. Through experiments of cuttings transport in inclined wells, performed at U of Tulsa, it was found that the lag time is, as expected, much lower than in vertical wells. In fact, during pumping a moving bed was formed, and its velocity increased with increasing flow rate.

Bed velocity	1.7	1.4	1.1
Input velocity	4	3.2	2.4
Ratio	.43	.44	.46

In average the bed velocity was 45% of the average mud velocity at all velocities (above critical moving – bed velocity). Simultaneous rotation increased the moving – bed velocity by typically 15%.

6.3.3   Field observed transport mechanism

Much of the observations reported here are based on the work of K & M (2002). In Figure 6-13 the drill string will drag the drilling fluid along due to no-slip conditions at the fluid-drill string interface. The dragged-along fluid is referred to as the viscous coupling, since the viscous fluid is dragging particles along.
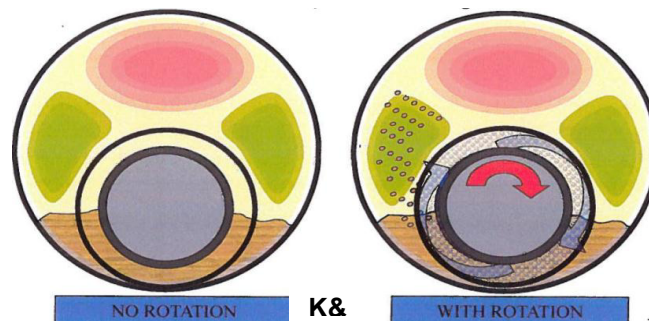
Figure 6-13: The drill string is lifting cuttings from the bed and into the main stream (the red ellipse).

K & M (2002) discovered through their investigations that the cuttings transport theory did not fit well with observations. This drill string is described in Figure 6-14. Here it is shown that cuttings transport becomes efficient first when a drill string rotary speed of 110–120 RPM has been reached. The explanation behind this behavior is presented in Figure 6-15. There are actually two effects taking place:

a) The drill string walk up the hole making the transport up-hill more efficient
b) The diameter of the viscous film, and thus the diameter of how far the cuttings will reach, will at some RPM become higher than the tool joint diameter
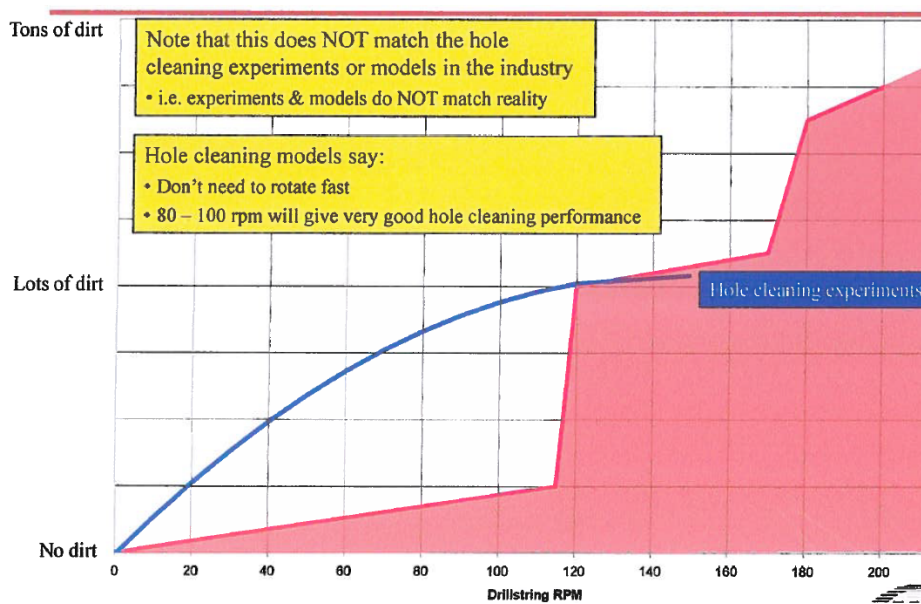
Figure 6-14: Cuttings cleaning effect vs. RPM. Red color represents observations. Blue line represents theory.

After the particles have been brought up into the main stream, the particles will slowly drop out due to gravity, according to Stokes law. This is true since the flow is normally limited to laminar flow due to ECD requirements. A particle will typically move one stand in a horizontal wellbore, and longer in inclined ones. Wells are thus cleaned from the rear as indicated in Figure 6-16. The finest particles will be picked up first and will move quicker and longer. A sorting process is thus always involved. At a certain flow rate a stationary bed will be established during drilling. To clean better, the flow rate must be increased or the drilling rate decreased.

2. At medium RPM (say, 100 rpm)
- Pipe begins to walk up the hole a little
- Viscous coupling film gets thicker, but still "thinner" than tooljoint upset
  - Still laminar flow at bottom of the hole

1. At low RPM:
- Viscous coupling film is thin
- Not much energy in the system

3. At 120 rpm
- Pipe walks further up the hole
- Viscous coupling film thickness reaches height of tooljoint upset …
  - Fluid now unable to pass through the gap in laminar flow
  - Vortices (turbulence) break off, stirring the bed

Figure 6-15: Efficiency of bringing cuttings up into the main stream is a function of drill string RPM.
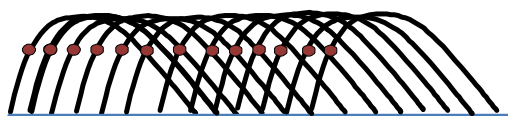
Figure 6-16: The behavior of cuttings entering the flow stream in horizontal wellbores.

In accordance with Figure 6-14 one could argue that flow rate and string-RPM belong together. Figure 6-17 indicates this relationship. In horizontal wells the ideal flow velocity for cuttings transport is typically 1 m/s while in vertical wells typically 0.2 m/s.

Wellbore	Ideal RPM	Ideal flow rate (lpm)
17.5	180	5 000
12.25	150	3 000
8.5	120	2 000
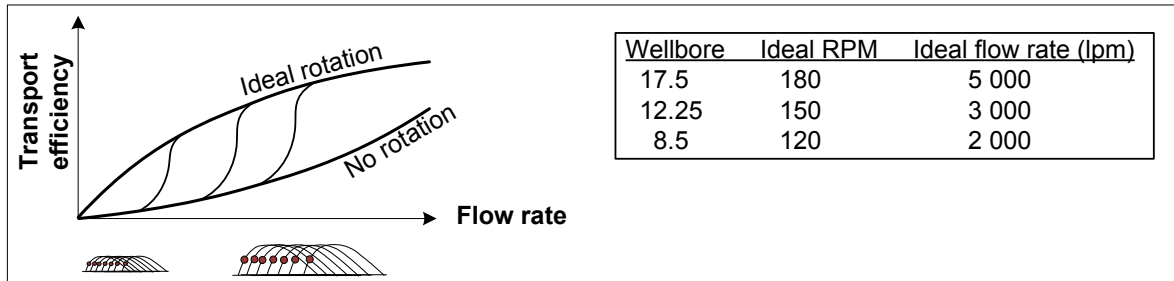
Figure 6-17: Transport efficiency is a function of flow rate, hole size and string RPM. Assume laminar flow.

Another finding in the literature is the importance of the low-end rheology. The 3 and the 6 RPM rheological readings are especially important for cuttings transport in horizontal wells, as indicated in Figure 6-18.
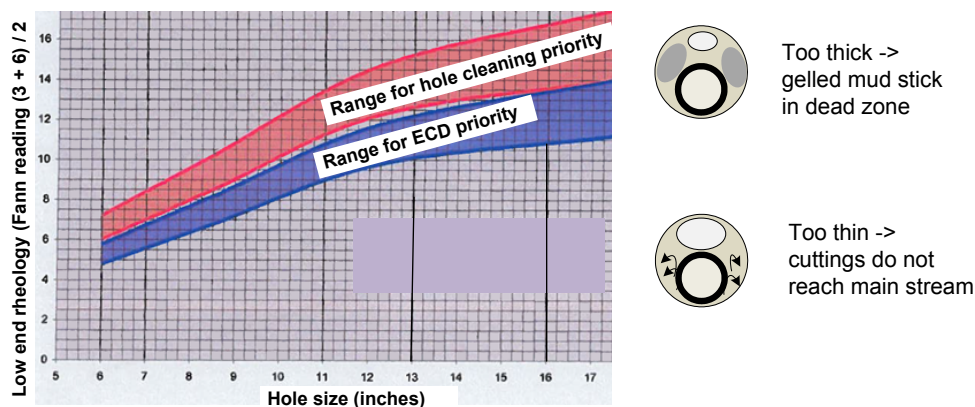
Figure 6-18: The low-end rheology must be kept within strict ranges.

6.3.4   Sweeps/bottoms up/backreaming

Drilling is easy, while backreaming is difficult. Once started the process cannot be stopped because only the rear is fully cleaned. At the surface the cuttings and debris comes in a wave as shown in Figure 8-19. After a difficult trip out, including reaming etc., the trip in is easy. The sweeps and backreaming operations cause the following problems:

- Higher viscosity and higher ECD
- Difficult to interpret the PWD
- Dunes are formed if the operation is not completed
- Difficult to trip-in
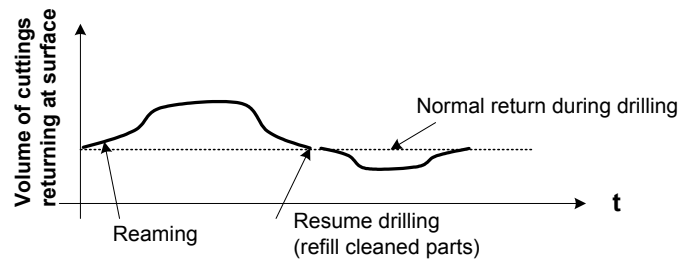
Figure 8-19: Cuttings return vs. operation

On the other hand it is necessary to clean the well before tripping and casing running as indicated in Figure 8-20. And the way to do it is to keep a steady, high flow rate and high string-RPM. In the old days a viscous sweep consisted of a high viscous pill, where the objective was to glue the particles together. Today the solution is as suggested above or to send in a low viscous pill to create local turbulence.

Drilling:
"Dirtier" hole can be tolerated as the drillpipe moving through the cuttings bed

Tripping:
Hole needs to be cleaner as drill collars, stabilizers and bits have to be pulled through the cuttings bed.

Running Pipe:
Hole needs to be as clean as possible in order to ensure "plowed" cuttings do not prevent casing / liner from reaching TD
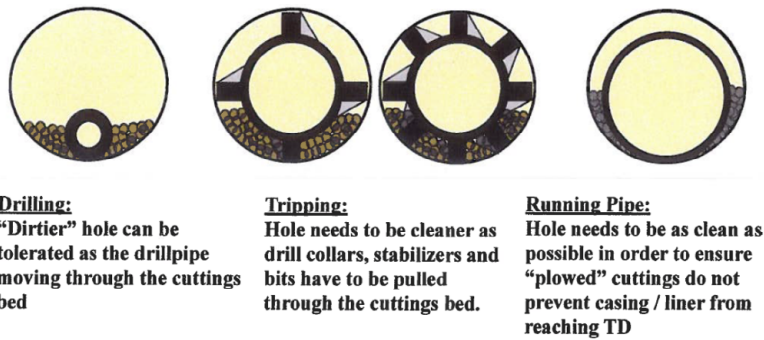
Figure 8-20: The importance of hole cleaning vs. tubular in the well.

7 Keeping wellbore within maximum and minimum pressure; ECD-control

Equivalent Circulating Density (ECD) represents the total actual bottom hole pressure exerted on the formation being penetrated and is usually presented in terms of equivalent density. ECD is the sum of the static density, the additional density increment due to the weight of drill cuttings contained in the annulus and the effect of pressure drop along the annulus. ECD effects are shown graphically in Figure 7-1, a figure that will increase the understanding of the phenomenon.
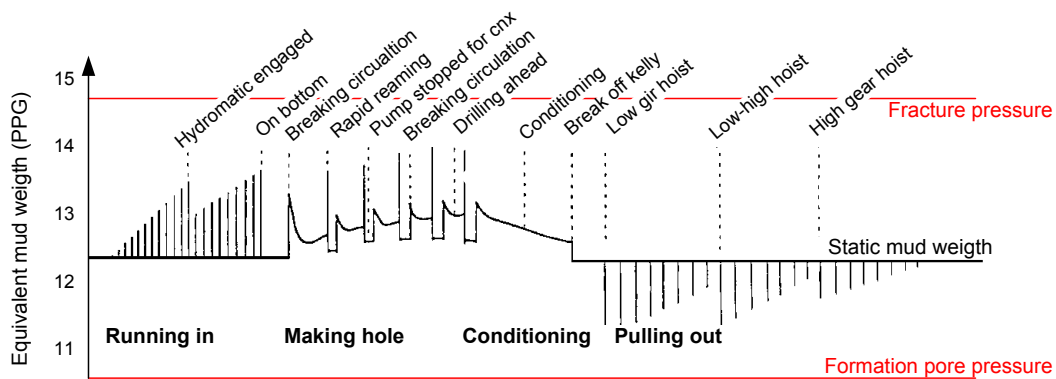
Figure 7-1: Graphical view of pressure variation during tripping and drilling.

The additional "weight" obtained as a result of the annular pressure drop may be of considerable importance when drilling through long and narrow well bores. In equation form, ECD can be expressed as:

$$ECD = \rho_{mud} + \frac{\Delta p_{annular\ friction} + \Delta p_{cuttings} + \Delta p_{surge\&swab} + \Delta p_{rotation} + \Delta p_{acceleration}}{gz} \qquad (7.1)$$

ECD becomes more important in deeper wells as illustrated in Figure 7-2. Here the pressure window becomes narrower.
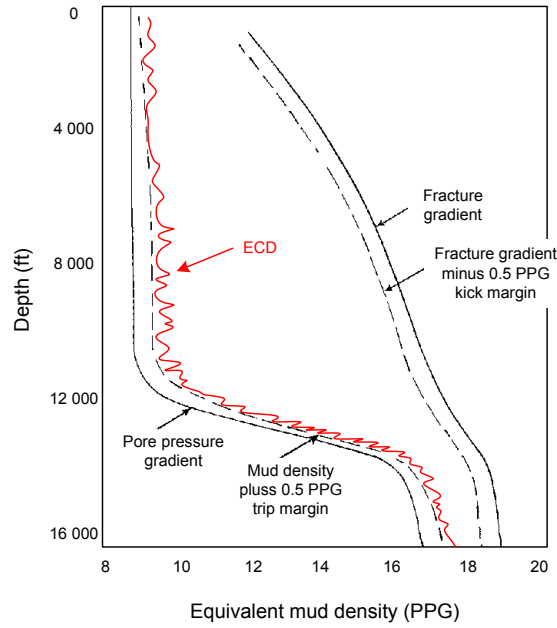
Figure 7-2: Equivalent pore- and fracture-density versus depth. Prevention of kicks, and loss of circulation, requires that down hole ECD remains within the given boundaries.

Before discussing the pressure variation in a well, we need to introduce how to produce a specific mud density.

7.1 Density control

There are two basic ways of increasing the density of water or oil; by adding weight material or salt.

Calcium carbonate: Calcium carbonate (CaCO3) is widely applied as weighting agents in non-damaging drilling fluids. Its main advantage comes from its ability to react and dissolve in hydrochloric acid. Hence any filter cake formed in productive zones can be easily removed and thereby enhancing production. It has a specific gravity of 2.60–2.80 which limits the maximum density of the mud to about 12.0 ppg. Calcium carbonate is readily available as ground limestone, marble or oyster shells.

Table 7-1 gives a list of the most common used weight material.

Material Name	Chemical formula	Density (kg/l)	Soluble in acid
Carbonate	$CaCo_3$	2.7	yes
Barite	$BaSO_4$	4.3	no
Hematite	Fc_2O_3	5.1	partly
Galena	$Pb \cdot S$	7.5	no

Table 7-1: Selected materials for densification of mud

Barite: The mineral barite can appear as an insolvable sediment (evaporites) Barium Sulphate, $BaSO_4$, with a specific density of typically 4.2 kg/l. The commercial product Barite is a fine powder with a medium particle size of 25 mm, but sieved to an upper particle size of 74 mm. Barite is insolvable in water and therefore said to be inert, unlike clay, polymer and salt, and carbonate which all react with water.

Salt: When salt is added to water, its density is altered, and volume conversion tables must be consulted. Brines can be formulated over a range of densities as shown in Figure 7-3.

Contain impurities like quartz, chert, calcite, and an hydrates while lower its density.
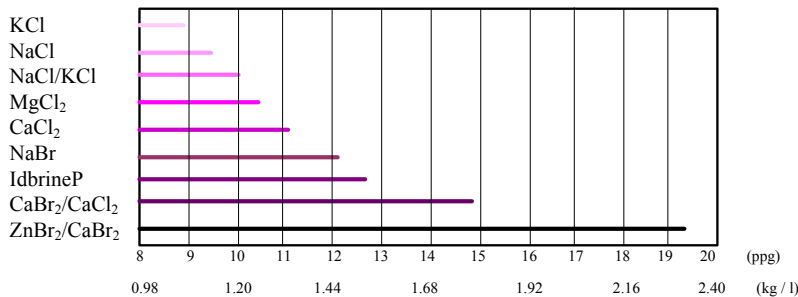
Figure 7-3: Different salts used to obtain brine density (in ppg and kg/l) when saturated at ambient conditions (15^0C and 1 bar$_a$).

When inert components are added to the mud, they maintain their original volume, and are thus additive. For such components we can write a mass and volume balance:

$$m_1 + m_2 + \text{.........} = \sum_{i=1}^{n} m_i \tag{7.2}$$

$$V_1 + V_2 + \text{.........} = \sum_{i=1}^{n} V_i \tag{7.3}$$

Mass and volume of a substance are interrelated through its density:

$$\rho = \frac{\sum m}{\sum V} \tag{7.4}$$

Increasing or decreasing the density from ρ_1 to ρ_2 by means of an additive of density ρ_{add}, can be estimated through eqn (7.5):

$$\frac{V_{add}}{V_1} = \frac{\rho_2 - \rho_1}{\rho_{add} - \rho_2} \tag{7.5}$$

V_1 is the original volume of a fluid with density ρ_1.

7.2 ECD factors

7.2.1 Mud density vs. temperature and pressure

Mud density is exposed to several effects:

- Increasing temperature, especially with increasing well depth
- Increasing hydrostatic pressure with increasing well depth
- Formation gas will expand substantially when approaching the surface and lower mud density. But the effect is negligible further down in the well since gas here is highly compressed

These density effects are all small and can for practical purposes be ignored. Pressure and temperature effects will normally neutralize each other.

Mud and especially OBM is very responsive to changes in pressure and temperature. This may affect the bottom hole pressure in cases whenever the two parameters change independently. Such situations do arise when the pump is shut off. Then a general increase in mud temperature will take place (more heating in lower part of the well than cooling in the upper part) leading to a decrease in the hydrostatic pressure. In static OBM columns, the complete heat transfer from the formation may take as much as a day. During tripping such slow density decrease combined with swabbing effects could cause kicks. Pressure testing or pressurizing the well during BOP tests or kick circulation cause compressible OBM to increase its density.

The following paragraph presents models for determining the effects of pressure and temperature on mud density.

Water and base oil (Clairsol) have been tested at a wide spectre of temperatures and pressures. The two fluids were curve fitted with respect to its individual dependency to temperature and pressure. The resulting linear curve fit to the measured data gave

$$\rho_w = 8.5 - 2.6 *10^{-3}T + 2.5 *10^{-5}p \quad (7.11)$$
$$\rho_o = 7.0 - 3.0 *10^{-3}T + 4.4 *10^{-5}p \quad (7.12)$$

Here T is in °F, p in psi and ρ in PPG. When increasing viscosity and solids concentration the constants increase by up to 50%.

Oil based fluids are in general twice as compressible as water. The thermal expansion of OBM and WBM are less different. Another large difference between the two fluid types is the reaction time to temperature changes (due to difference in heat capacity); water reacts slower.

7.2.2 Annular friction

There is a dispute on which of the following rheological models that best describe the fluid viscosity; Newtonian, Bingham, Power law or Herschel Buckley. For the purpose of ECD estimation, we suggest simplifying by selecting only one rheological model (the best fitted) and base the estimation of constants on the SI approach. This suggestion will increase accuracy.

7.2.3 Effect of cuttings

It is an almost impossible task to find the exact effect of cuttings on pressure. How is it possible to guess the amount of cuttings in suspension at any given time in an inclined wellbore? A rough guess is here suggested: We know how much cuttings is generated:

$$q_{\text{cuttings}} = \pi/4 \cdot d_{bit}{}^2 \cdot ROP \tag{7.13}$$

Most of it will settle out from time to time, some of it will be re-injected into the mud stream due to the rotation of the drill pipe; some will be lifted by the lift fore created by the mud flow. But how much? The following assumptions will bring us closer to the truth:

Cuttings beds occupy typically around 2–6% of the cross sectional area in inclined wellbores. A rough assumption is therefore that 97% of the generated cuttings come out at different times, the rest is deposited. When more cuttings is deposited, the flow area becomes smaller, mud velocity increases and bed erosion increases. There will be an equilibrium bed height (at least locally) for a given pump flow rate.

The original cuttings concentration at the bottom is a function of the flow rate:

$$c_{cuttings,o} = q_{cuttings} / (q_{pump} + q_{cuttings}) \approx q_{cuttings} / q_{pump} \tag{7.14}$$

In the vertical section (I < 60°) the cuttings concentration increases due to slip, expressed through a Transport Ratio R_t:

$$R_t = v_{transport} / v_{ann} = (v_{ann} - v_{slip})/ v_{ann} = 1 - v_{slip} / v_{ann} \tag{7.15}$$

In the vertical section the average cuttings concentration becomes:

$$c_{cuttings,average} = c_{cuttings\ from\ the\ horizontal\ section} / R_t \tag{7.16}$$

And the slip velocity is estimated through Stokes law from Chapter 6:

$$v_{slip} = d_p{}^2 \cdot g\ (\rho_p - \rho_{mud}) / (6\pi\ \mu_{eff}) \cdot f_{cuttings} \tag{7.17}$$

Eqn. (7.17) includes the effect of concentration of cuttings through the factor $f_{cuttings}$. At high concentration there will be a hydraulic resistance to flow expressed in a satisfactory manner for our concentration range through eqn. (7.18):

$$f_{cuttings} = 1\text{-}5 \ c_{cuttings,average} \tag{7.18}$$

In the inclined section ($I > 60^o$) we simplify and assume that the average concentration in the mud fluctuates around the initial concentration as shown in Figure 7-4.
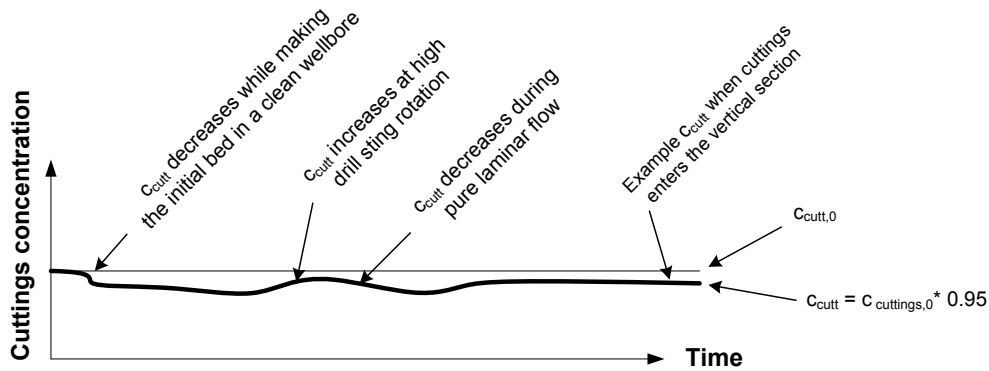
Figure 7-4: Example of how cuttings concentration varies in the deviated part of the wellbore.

If the proposed concentration function becomes too complex, it is better to forget it and rely only on measured ECD. However, if measured ECD is not available, then you have to model it.

After constructing an average cuttings concentration function, the effect on well pressure is found by assuming that the density of cuttings is 2.3 kg/l. This is a good assumption: At shallow depths, the local sediment density may be as low as 2.0 kg/l, due to low compaction and accordingly high porosity. At large depths (> 5000 mTVD) porosity approaches zero, at which the matrix density is 2.8 kg/l for most sedimentary rocks.

Additional ECD effect in the vertical part of the well then becomes:

$$\Delta p_{cuttings} = \rho_{mud,average} \cdot g \cdot TVD \tag{7.19}$$

where

$$\rho_{mud,average} = \rho_{mud}\left(1\text{-} c_{cuttings,\ average}\right) + \rho_{cuttings} \cdot c_{cuttings,average} \tag{7.20}$$

7.2.4   Surge & swab

When the drill string is hoisted up or lowered down, mud will flow in the annular space, as indicated in Figure 7-5, flow that results in pressure loss. Before applying pressure loss formulas developed in the previous sub chapter, the resulting flow rate needs to be determined.

Pipe velocity, v_{pipe}, is the same as the speed of the travelling block with closed pipe-end. The resulting annular volume rate becomes in downward motion pr. time
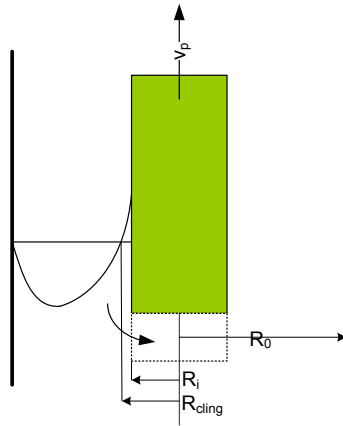
Figure 7-5: Upwards pipe movement causes downwards annular fluid flow.

$$q_{ann} = rate\ of\ volume\ displaced\ \ = v_{pipe} \cdot A_{pipe} \qquad\qquad (7.21)$$

As indicated in Figure 7-5, the flow volume down is different from the removed volume, and must be adjusted. For this purpose we make simplifying assumptions.

1. Closed pipe end: Assume the drill string is closed at the bottom. Displaced volume when running-in-hole (RIH) becomes larger than the theoretical one.
2. Clinging factor: The no-slip conditions on the pipe surface will cause some of the mud to cling to the drill string and move along with it as indicated in Figure 7-5. The effective pipe diameter increases.

The first task is to derive the velocity profile. For that purpose we assume Newtonian fluid later we introduces the μ_{eff}

From the velocity profile we obtain an expression of r_{cling}, and can find the

$$V_{cling} = \int_{R_{cling}}^{R_i} v(r)\ rdr$$

Now we define the cling factor as

$$c_{cling} = \frac{V_{cling}}{V_{ann}}$$

Now estimate the pressure loss along BHA in accordance with procedures in Chapter 4. The surge pressure will largely depend on the narrowness of the annulus. If the mud pump is turned on during tripping operations, which is rather unusual, v_{ann} must be adjusted accordingly.

Common drilling practice to avoid swabbing is:

- Make connection higher up to avoid pulling out 1 m, or pump when pulling up into/out of slips
- Pump while POOH in suspicious wellbores

7.2.5   Other effects

Effect of rotation: It is known that drill string rotation may have a significant impact on pressure drops in the annulus during fluid transport. During laminar flow, pipe rotation will induce an additional shear velocity component. And since drilling fluid is normally shear thinning, pipe rotation will increase total shear, reduce viscosity and thereby reduce the pressure drop.

If we solve for the rotational component in addition to the axial we may include the main features of these effects in a fundamental way. The transport equation for the rotational velocity for steady-state flow becomes:

$$0 = \frac{1}{r^2} \frac{\partial}{\partial r} \left(r^3 \, \mu_{eff} \, \frac{\partial}{\partial r} \left(\frac{v_\theta}{r} \right) \right)$$ (7.24)

The consequence of the solution of eqn (7.24) is that the effective strain rate (see Chapter 3) is increased and the effective viscosities are reduced. Hence, rotation will reduce the axial pressure drops. However, for laminar developed flows of Newtonian liquids, such effects do not exist, since viscosity is independent of shear rate.

Experience indicates that in real drilling operations the opposite often takes place; pump pressure increases with increasing pipe rotation. One explanation for this is the development of instabilities. A number of vortices develop in the radial-axial plane. Hence, rotation leads to axial-radial mixing which will have the same effect on momentum transport as turbulent mixing. Turbulent flow is shear thickening.

Effect of acceleration: Acceleration is experienced during tripping operations during pump rate manipulation, and also when a gas kick reaches the surface where expansion accelerates. High acceleration of the pipe should be avoided in critical situation, because of the acceleration pressure it creates in the corresponding fluid mass. Acceleration pressure caused by accelerating pipes, a_{pipe}, is estimated from eqn. (7.25). Figure 7-5 indicates the importance of the effect of cross sectional area. The clinging effect is not included in eqn. (7.25).

$$\Delta p_{accelleration} = ma/A = \rho \, L \, a_{pipe} \cdot \frac{A_{pipe}}{A_{ann}}$$ (7.25)

Its magnitude is exemplified through the running of a 13⅜" casing into a 17½" hole. Let the pipe, at the depth 1000 m, accelerate 0.2 m/s². Drilling fluid density is 1200 kg/m³. Pressure increase will then become:

$$\Delta p = 1200 \cdot 1000 \cdot 0.2 \cdot (\frac{13 \ 3/8}{17.5})^2 = 3 \cdot 10^5 \ Pa$$

Effect of gelling: One more effect caused by pipe movement or pump start needs to be considered as a part of the ECD: Most mud types are time dependent and tend to build up a gelled structure when quiescent. By moving the drill sting axially, extra pressure is needed to break the gel that has formed on the pipe surface. The surface shear stress relates to pressure:

$$\Delta p_{gel} = \frac{4\tau_w \cdot L}{D_{pipe}}$$ (7.26)

It becomes much worse if the mud pump is used to break the gel. Then it must be broken first inside the drill string and then in the annulus along two surfaces; one surface is the drill string and the other is the wellbore. A 1000 m long 5″ × 4.27″ drill pipe (= 0.127 m × 0.108 m) has been at rest in a 12½″ (0.216 m) wellbore. The 10 minute gel strength = 50 lb/100 ft^2 = 50 · 0.4788 = 23.94 Pa. From eqn (7.26) we obtain: Δp_{gel} = 19.6 ·10^5 Pa. This answer assumes that the fluid is completely incompressible and that the shear stress is broken simultaneously over the whole length.

However, in practice the drilling fluid is compressible, and compression and the resulting deformation of the long mud column would break the gel over a much shorter distance than the complete well length. Compressing a mud volume of 1000 l by one bar would compress it typically 0.1 liters. Such a small shrinkage would result in a deformation sufficiently large to break the gel locally. The effective length over which the gel is breaking simultaneously is shorter the higher the initial pressure. The gel breaking pressure is probably small and hidden in the acceleration pressure. Another effective method to break the gel structure in the annulus is simply to rotate the drill string.

The same reasoning must be applied when figuring out how high the drill string must be hoisted Dh before gravity force overcomes the gelled shear stress inside the drill string. Theory would show a high value, in accordance with eqn. (7.27), where L is length of well:

$$\rho g \Delta h = \frac{4\tau_w \cdot L}{D_{pipe}} \tag{7.27}$$

7.3   Temperature variation

7.3.1   Ocean and wellbore temperature profile

In order to estimate factors such as expansion of drilling fluids, change of fluid viscosity or variation in other fluid properties as a function of temperature, we need a model of the temperature variation in the well. A steady-state analytical model for computing circulating mud temperature profiles has been suggested through the API-model, a model that has gained general acceptance by the industry. Nevertheless, the model is not good enough for deep-water wells. The main reason is the cooling effect in the riser section in deep water wells as indicated in Figure 7-6.
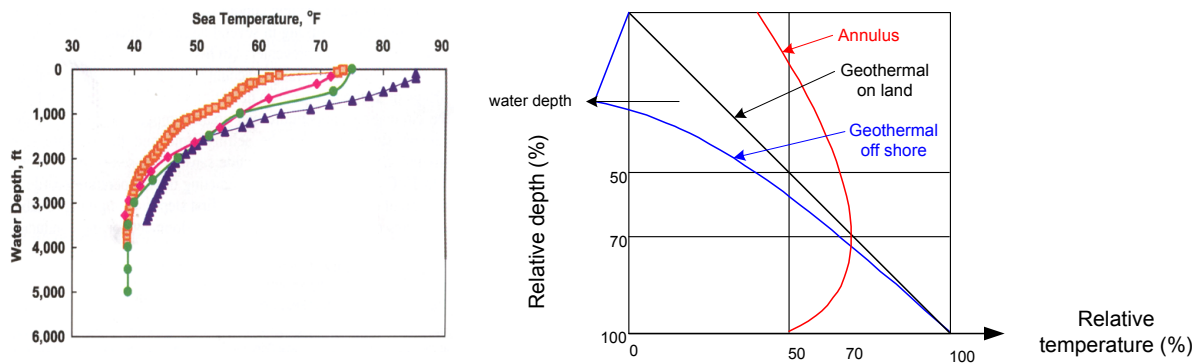
Figure 7-6: Sea temperature (left), principal wellbore temperature profile after long pumping period (right).

The heat capacity of water is high, and after shutting the pump off it may take a day, until the geothermal temperature profile is established.

When a drill string is lowered into a well and exposed to a temperature gradient, the resulting temperature distribution after pumping is initiated, assuming constant density and heat capacity, the resulting temperature is a result of convection and conduction of heat:

$$\rho\, c_p \cdot \frac{\partial T}{\partial t} = -\rho\, c_p u \frac{\partial T}{\partial z} - k\nabla^2 T \qquad (7.28)$$

The first term in eqn (7.28) expresses the resulting rate or change of internal heat flux pr. unit area (W/m²). The second term expresses rate of change of convective flux (in the fluid), while the latter term expresses radially conducted heat from the material in contact with the fluid. The minus signs indicate positive flow towards a negative temperature gradient. In pipe flow both convection and conduction is involved in heat exchange on the interface between the pipe and the fluid. Our engineering task is now to find a heat transfer coefficient that is acceptable for both type of heat transfer

The geometry of the drill pipe and the parameters involved are presented in Figure 7-7:
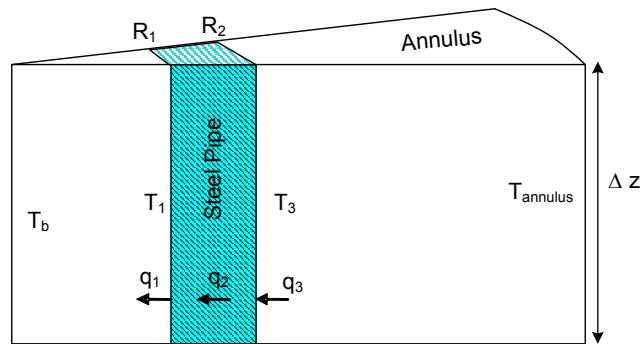
Figure 7-7: Heat transfer along and across the drill pipe steel wall (drill pipe centre to the left in the
figure) from the annulus into the flowing liquid in the drill pipe:

q1 = convection (on surface)   q2 = conduction   q3 = convection (on surface)

In pipe flow heat is convected mainly through mass transport since water has a certain heat capacity.
The two terms in eqn (7.1) will be discussed separately below:

7.3.2   Conduction

A simplified solution of the conductive heat transfer equation for steady state conditions, simplifies to
(in Cartesian coordinates), expressed in terms of finite differences:

$$k\nabla^2 T = \frac{\partial}{\partial r} \cdot k \frac{\partial T}{\partial x} = k(\frac{\partial T}{\partial x} + r \frac{\partial^2 T}{\partial x^2}) \Rightarrow k \frac{\partial T}{\partial x} = k \frac{dT}{dx} \tag{7.29}$$

In cylindrical coordinates:

$$k\nabla^2 T = k\left(\frac{d^2 T}{dr^2} + \frac{1}{r} \frac{dT}{dr} \right) \Rightarrow \frac{k}{r} \frac{dT}{dr} \tag{7.30}$$

The final terms of eqn. (7.29) and (7.30), where second order terms are neglected, represent steady state
1D conditions with constant k.

For estimation purposes we need to include the area. Annuli with small gaps can be assumed to be a
flat wall of thickness r and length Δz:

$$q = -k A \cdot \frac{dT}{dr} = -2\pi r k \Delta z \frac{dT}{dr} \tag{7.31}$$

For small concentric pipes with large wall thickness, heat transfer becomes a function of the curvature.
For a pipe wall, as in Figure 7-7, integrating from R_i to R_o yields:

$$q = -\frac{2\pi k \Delta z \Delta T}{\ln\left(R_2 / R_1\right)} \tag{7.32}$$

For most materials and liquids k varies 10–20% for temperature ranges between 0 and 200 °C. Multilayer
insulation will reduce conductivity by a factor of decades:

7.3.3 Convection

In Figure 7-8 heat is transferred from a flat plate of solid material into a flowing fluid. Temperature gradient (∇T) depends on how quickly heat is carried away by the fluid.
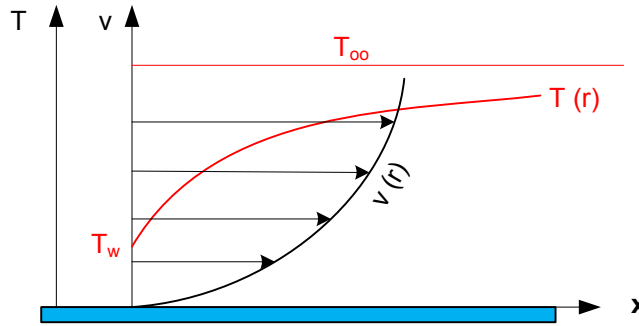
Figure 7-8: Velocity and temperature profile above a flat, cold plate.

Heat exchange (heating or cooling) of the liquid adjacent to the wall is expressed through Newton's law of convective cooling;

$$q = h\, A\!\left(T_w - T_\infty\right) \tag{7.33}$$

The convective heat transfer coefficient, h, must be determined experimentally. Holman (2001) shows how the heat coefficient can be arranged into a Nusselt Number for laminar pipe flow:

$$Nu = \frac{hd}{k} = 4.364 \tag{7.34}$$

For turbulent flow in smooth pipes, evaluated for bulk temperature, T_∞, and valid for 0.6 < Pr < 100 (i.e. liquids), the Nusselt Number becomes;

$$Nu = \frac{hd}{k} = 0.023 \cdot \mathrm{Re}^{0.8} \cdot \mathrm{Pr}^{1/3} \tag{7.35}$$

Eqn. (7.34) and (7.35) are empirical. Errors are in the order of ± 25%. Roughness (caused by tool joints etc.) must be corrected for through a higher Re-number.

If the convective heat transfer coefficient is unknown the approach is to eliminate T_2 and T_3 (the wall temperature in Figure 7-7) through the equations:

$$q_{1 =} q_{2 =} q_3 \tag{7.36}$$

7.3.4   Numerical solution

When simultaneous heat conduction and convection is taking place inside a control volume, it can be expressed on differential form:

$$\frac{\partial}{\partial t} \rho\, c_p T = -\frac{\partial}{\partial z} \rho\, u\, c_p T - \frac{k}{r} \cdot \frac{\partial T}{\partial r} \tag{7.37}$$

The explicit approach of finite differences is characterized by estimating the next time step on bases of information in the previous time step. If the time steps are sufficiently small a satisfactory accuracy will be maintained. Taking now the cylindrical volume ΔV *as* $2\pi r \cdot \Delta r\, \Delta z$, and assuming ρ and c_p are constants, an approximated integration of eqn. (7.37) yields;

$$2\pi r \Delta r \Delta z \left(\rho c_p\right)\frac{T(i,j,t+1)-T(i,j,t)}{\Delta t} = -2\pi r \Delta r \Delta z \cdot \rho U c_p \cdot \frac{T(i+1,j,t)-T(i,j,t)}{\Delta z} - 2\pi r \Delta r \Delta z \cdot \frac{k}{r} \cdot \frac{T(i,j+1,t)-T(i,j,t)}{\Delta r} \tag{7.38}$$

Solving eqn. (7.38) with respect to T(i,j,t+1), you are on the track.

Conductivities and heat capacities for steel and water are presented in Table 7-2.

Material		ρ (kg/l)	c_p (kJ/kg °C)	k (W/m °C)	Pr
Steel	20 °C	7.87	0.46	61	
Cement slurry	20 °C	2.5		0.29	
Granite	20 °C	2.64	0.82	1.7–4.0	
Cork	20 °C	0.05	1.88		
	40 °C	0.12		0.045	
Glass wool	40 °C	0.024	0.7	0.038	
Engine oil	20 °C	0.89	1.88	0.145	10400
	100 °C	0.84	2.22	0.137	
Water	20 °C	1.0	4.180	0.602	6.80
	100 °C	0.96	4.208	0.682	1.70

Table 7-2: Material constants relevant for heat transfer.

In liquid and solids we observe from Table 7-1 that the denser the material the higher the thermal conductivity.

7.4 Mathematical model of pressure surge & swab

Mathematical models give more precise statements of the nature than models formulated in words, and they make quantitative predictions (simulations) possible. Mathematical models can be used to describe, to explain and to interpret physical systems. Mathematical modeling is an art and the skill must be developed through persistent attempts of learning-by-doing. A stepwise approach follows, based on the work of Basmadjian (2003). We will exemplify the approach on the problem of surge/swab during drilling operations.

In most wells the magnitude of pressure surges is not critical because proper casing design and mud programs leave large enough margins between the fracture pressure and the formation fluid pore pressure. A certain fraction of wells, however, cannot be designed with large surge-pressure margins. In these critical wells, pressure surges, especially while running of low-clearance liners in deep wells, must be maintained within narrow limits.

Different approaches to surge and swab pressure are presented in the literature. Three approaches of how to treat the friction loss caused by the resulting flow are exemplified below:

1. Analytic approach for laminar flow regime, including the effect of fluid cling to the moving drill string
2. Standard hydraulic friction models
3. Advanced approach taking elasticity of fluid and steel pipe into consideration

Approach 1 is the selected method which will be presented here. Approach 3 will be discussed in step 2 in conjunction with boundary conditions and simplifying limitations. In method 2, which is the most straight forward approach, the standard friction factor we already known. It is based on the Darcy-Weisbak equation:

$$\Delta p_{surge} \cdot 0.5 \; \Delta D/\Delta L = 4 \, f_{M} \cdot 0.5 \rho v_{DS}{}^{2} \qquad\qquad (7.39)$$

Pressure loss in the gap geometry, 0.5 ΔD over the length dl is studied experimentally, and the friction factor is adjusted on basis of measured pressure loss during surge/swab tests.

But now to the analytical approach.

Step1. Understand the underlying physical system

The major factors contributing to swab and surge pressures in a wellbore are usually the frictional pressure drop resulting from flow of drilling fluid. The equation of laminar, steady-state flow in an annular geometry is applied. Only laminar flow of Power Law fluids is considered. The flow is caused by the axial movement of an inner, concentric pipe, which has a closed end. Pipe movement is causing displacement of fluid as indicated in Figure 7-9. Due to no-slip conditions along the pipe wall, part of the fluid is accompanying the downward pipe movement. Fluid is being dragged along by the pipe.
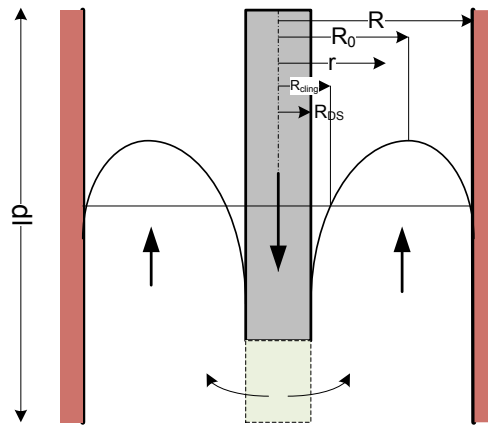
Figure 7-9: Annular flow caused by downwards pipe movement. Closed pipe end. Relative parameters are seen to the left of the pipe.

Step 2. In order to reduce the complexity, apply as many as possible of all simplifying assumptions.

In Figure 7-9 many simplifying assumptions have already been introduced. They are included in the extensive list below:

- Concentric inner pipe
- Smooth cylinders define annular wall and pipe wall
- Closed end pipe. With open pipe an iterative process is needed aiming at satisfying the requirement: $\Delta p_{inside\ DP} = \Delta p_{ann}$. A float valve or flapper valve assure no-flow through the pipe during surge movements.
- Swab / surge pressure are significantly reduced due to eccentricity, up to around 40% for certain geometries
- A clinging factor is often either ignored or just assumed, typically 0.5 (the clinging volume exhibits up to 50% of the downward flowing volume, depending on relative slot size). In our model it is not ignored
- Steady-state process. No fluid acceleration or compressibility is included
- Simplified rheology (only Newtonian and Power law fluids are included)
- Fluids are both elastic and compressible. A negative pressure surge is often observed at the surface when the downward movement of the drill string is brought to rest. At the bottom the pressure is increased. This is a water hammer affect
- Both pipe elasticity and fluid viscous force are participating in determining pipe displacement during tripping, as well as formation and cement elasticity. They all influence pressure surge. These issues are discussed by Mitchell (1988).

Balance of mass includes three effects.

Expansion of hole (dA) + compressibility of fluid + influx/outflux of fluid

$$\frac{1}{A} \cdot \frac{dA}{dp} \qquad + \qquad \frac{1}{K} \cdot \frac{dp}{dt} \qquad + \qquad \frac{\partial v}{\partial z} \qquad = 0 \qquad\qquad (7.40)$$

To balance the fluid's momentum four terms are needed.

Inertia = p. grad + viscous force + gravitational force

$$\rho \frac{dv}{dt} \qquad = \qquad -\frac{\partial p}{\partial t} \qquad + \qquad \Delta p(v) \qquad + \qquad \rho g \cdot \cos q \qquad\qquad (7.41)$$

Balancing of elastic pipe momentum includes three terms:

Longitudinal elasticity + pipe pressure + viscous pipe drag

$$E \cdot \frac{\partial p}{\partial t} v_{pipe} \qquad + \qquad fp \quad \frac{\partial}{\partial z} \cdot \frac{\partial}{\partial t} p_{pipe} \qquad + \qquad f_{drag} \cdot \frac{d}{dt} \cdot v \qquad\qquad (7.42)$$

All three equations require one for the inside of the drill string and one for annular conditions. Figure 7-10 comparers a surge situation where inertia effects are present.
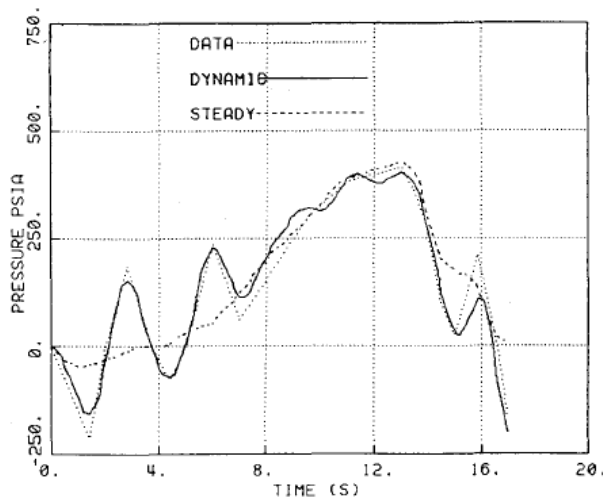
Figure 7-10: Surge pressure vs. time during tripping-in one drill pipe length

Step 1   Understand the underlying physical system.

Step 2. In order to reduce the complexity, apply as many as possible of all simplifying assumptions.

Step 3. Start with the simplest possible system. Make a sketch. Which forces must be incorporated? Insert possible variables, how they attack, and their desired result.

In the most simplified evaluation of surge/swab pressure we assume steady-state flow. The geometry is defined in Figure 7-9. Only two forces are involved; frictional pressure pr. length unit and shear forces over the same length.

Step 4. List the laws that govern the system's processes and draw an envelope with ingoing and exiting quantities

This problem is relatively simple. In Figure 7-11 the envelope is presented. We have already determined that only two forces define the system. At steady state they are in equilibrium with each other:

$$dp \cdot A_{\text{cross section}} = \tau \cdot A_{\text{shear}} \tag{7.43}$$

$$dp \cdot \pi r^2 = \tau \cdot 2\pi r \cdot dl \tag{7.44}$$

$$dp \cdot r = \tau \cdot 2dl \tag{7.45}$$
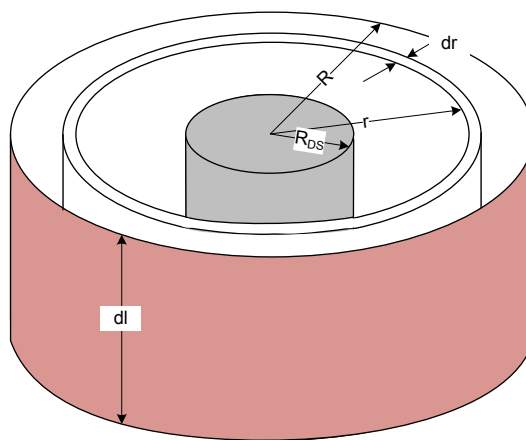
Figure 7-11: The envelope of acting forces is defined by the annular geometry.

Integrating axially, and discretizing

$$1/2 \cdot \Delta p/(\Delta L) \cdot dr = d\tau \tag{7.46}$$

Step 5. *Solution.*

For laminar flow it is possible to make a purely analytical solution. Alternatives are finite element and other numerical methods, or empirical solutions. In present case it seems rather straight forward. We start by integrating radially, after differentiating r to dr, from $r = R_0$, where $\tau = 0$, to $r = r$ (any r):

$$1/2 \cdot \Delta p/(\Delta L) \cdot \int_{R_0}^{r} dr = \int_{0}^{r\tau} d\tau \tag{7.47}$$

$$1/2 \cdot \Delta p/(\Delta L) \cdot (r - R_0) = \tau \tag{7.48}$$

$$\tau = 1/2 \cdot \Delta p/(\Delta L) \cdot (r - R_0) \tag{7.49}$$

Shear stress for a Power Law fluid is:

$$\tau = K \cdot \gamma^{\,n} \tag{7.50}$$

$$\gamma = (\tau/K)^{1/n} \tag{7.51}$$

Shear rate in eqn. (7.51) is positive for $R_{DS} < r < R_0$ and negative for $R_0 < r < R$. Shear rate is defined by:

$$\gamma = dv(r) \,/\, dr \tag{7.52}$$

Substituting eqn. (7.51) in (7.52)

$$dv(r) = (\tau/K)^{1/n} \, dr \tag{7.53}$$

Substituting eqn. (7.49) in (7.53) and integrating

$$dv(r) = [1/2 \cdot \Delta p/(\Delta L) \cdot (r - R_0)/K]^{1/n} \, dr$$

$$\int_{v_{DS}}^{v(r)} dr = v(r) - v_{DS} = [\Delta p \,/(\Delta L \cdot 2K)]^{1/n} \int_{R_{DS}}^{r} (r - R_0)^{1/n} \, dr \tag{7.54}$$

Similarly for the negative shear rate (to the right of max velocity):

$$v(r) = C_x \int_r^R (r - R_0)^{1/n} \, dr \tag{7.55}$$

For r = r eqn. (7.54) and (7.55) are equal, yielding

$$v_{DS} = C_x \int_{R_{DS}}^r (r - R_0)^{1/n} \, dr - C_x \int_r^R (r - R_0)^{1/n} \, dr \tag{7.56}$$

Bulk flow is resulting from the integral velocity across the annulus

$$q_{tot} = A \cdot v(r) \tag{7.57}$$

Knowing that dA = 2prdr, we obtain

$$q_{tot} = \pi R^2 \cdot v(r) \, 2\pi \, rdr \tag{7.58}$$

Substituting (7.39) into (7.58) and integrating we obtain and expression of the flow rate

$$q_{tot} = \pi R^2 \cdot \int_{R_{DS}}^R \{v_{DS} + C_x \int_{R_{DS}}^r (r - R_0)^{1/n} \, dr + C_x \int_r^R (r - R_0)^{1/n} \, dr\} \cdot 2\pi \, rd \tag{7.59}$$

Bulk flow rate can be expressed in terms of

$$q_{tot} = q_{pump} + q_{DS} = q_{tot} + v_{DS} \cdot A_{DS} \tag{7.60}$$

Knowing that the solution to the integral of type

$$\int (ax + b)^n \, dx = \frac{(ax + b)^{n+1}}{(n+1)^a} \tag{7.61}$$

We have now reached the end of the derivation. Further it can be worked out the exact solutions of the integrals in eqns. (7.59) and (7.60), but only for three integers of 1/n; n = 1, n = ½, n = 1/3

Equivalent Clinging Constant: It has become customary to represent flow of this nature in terms of a clinging constant, which describes the apparent contribution of pipe velocity towards pressure drop. The clinging constant may be expressed as:

$$K_c = q_{cling} / q_{tot} \tag{7.62}$$

where q_{cling} is the flow rate corresponding to the clinging part in Figure 1. q_{cling} may be obtained by rearranging and solving equations (7.59). It must then be integrated from r = R_{DS} to R_{cling}. Here v(r) = 0.

When an acceptable simple system, like the one above, has been defined, a more complex system is a natural follow-up.

8   Keeping the wellbore stable

Many of the problems are related to wellbore stability. It is therefore valuable to first present an overview of wellbore stability, mechanical and chemical, as an introduction.

8.1   Introduction

After drilling a hole in the formation, the previous balance between the rock strength and the in-situ stresses is disturbed, and likewise, the equilibrium between pore fluid and the sediments will be affected. Wellbore instability problems take many forms, and the most frequent ones are pointed out in Figure 8-1.

Fracture, balooning

Breakout, weakened formation and washout

Creeping (slow plastic flow)

Sloughing, elevated localized pressure, spalling, caving

Figure 8-1: Possible wellbore instability problem during drilling.

Wellbore instability is experienced mainly in shale sections, induced by either high stress concentration or physical-chemical interactions of the drilling fluid with the shale, or a combination of both;

1. Mechanical stress-induced wellbore stability
2. Chemical related instability
   a) Time-dependent water interaction with shale
   b) Time dependent water interaction with chalk, limestone, anhydrite, gypsum etc

Mechanical related stability problems are, besides minor erosion from turbulent flow and drill string interaction with the wall, governed by wellbore stresses. It is related to the tangential stress, radial stress and vertical stress. The tangential and radial stresses are governed by mud pressure while vertical stress is created by the overburden. The overburden results in vertical compression/deformation, which create compressional stresses in the horizontal direction. Mechanical wellbore instability is a topic covered in courses of rock physics. In this book, mechanical wellbore instability will merely be pointed at, since it is inter-related to its chemical counterpart; water interaction with the sediments will have a negative influence on mechanical stability.

Chemical stability of the wellbore is related to water and its complex interaction with shale. The time dependency is related to the time it takes for water to be transported into the shale.

Reaction with chalk/limestone/anhydrite is related to dissolution of dissolvable material. Chalk, limestone and salt are all ionic compounds. Dissolution of them can lead to several problems:

- Flocculation of the colloidal phase of drilling fluid like clay or polymers lead to increasing viscosity, while aggregation of clay after ion-exchange leads to decreased viscosity
- High solids content (disintegration of weakened cuttings)
- Hole enlargement (washout of weakened wall)

8.2   Mechanical stability

Shear and tensile failure mechanisms are the two largest concerns that can lead to mechanical instability when drilling in shale. These problems are time-consuming and expensive to fix, especially offshore where rig costs are high. In the worst case, mechanical borehole instabilities can annihilate both the drilling rig and its personnel. Despite great efforts to reduce borehole instabilities, they remain a serious concern. Mechanical instability can be classified into two groups;

- Stress related instability
  - Mobile formations or Plastic formations or Creep: Wellbores that stays open for a long time (weeks), exhibiting a slow "flow", tending to close the wellbore. It is especially claystone and Halite (NaCl) which deform under stress. The Halite in the Zechstein Fm in the southern North Sea is found under the Sulphates and the Carbonates: Anhydrite on the other hand, is strong and immobile.
  - Tensile failure occurs at too high ρ_{mud}: Fractures are detected at the surface as lost circulation. The losses will evolve with increasing mud pressure from minor losses to total loss.
  - Compression failure occur at too low MW: The compressed and crushed wellbore wall will evolve with decreasing pressure from cavings, breakouts to total wellbore collapse.

- Weakness in the formation
  - Faults and stress zones crossing the wellbore. Pre-existing fracture and cracks especially observed in limestone, chalk and in brittle shale.
  - Inter-bedded formations (between lithology changes, bedding angle close to wellbore angle, anisotropy, heterogeneity, and strength anisotropy).
  - Naturally weak formations (coal beds, conglomerate).
  - Unconsolidated formation (loose sand, gravel, silt).

To evaluate these types of instabilities we are dependent on information that can indicates what type of weakness has been encountered. Weakness in the formation, like sand and gravel often lack cementation material and are referred to as an unconsolidated formation, a problem that occurs mainly at shallow depths. The problem with unconsolidated formations is that they cannot be supported by hydrostatic overbalance from the drilling fluid alone. For example, unconsolidated sand and pea gravel often fall into the hole and pack off around the drill string. Problems also occur if insufficient filter cake is deposited on loose, unconsolidated sand to prevent it from "flowing" into the wellbore and packing off the hole. Solids-control equipment will be overloaded with large quantities of solids that do not correspond to the rate of penetration.

To drill such weak formations, the mud should provide a good-quality filter cake to help consolidate the formation so that hydrostatic pressure can "push against" and stabilize the annular wall. It is important to control the filtrate loss of the mud so that the water will not destabilize the formation. To minimize erosion, avoid any unnecessary reaming or turbulent flow opposite unconsolidated formations.

When drilling deeper one have to consider three types of mechanical stress:

1. In-situ vertical (overburden) and resulting horizontal stresses
2. Pore pressure (resulting from previous geological and resent chemical processes)
3. Forces acting at inter granular contact or at cementation points; cohesive force

In Figure 8-2 a model of all there forces are presented.
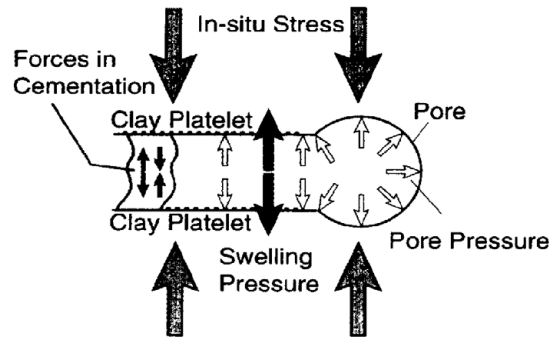
Figure 8-2: Forces acting within shale, depicting a single set of clay platelets connected to a pore (van Oort, 1997).

In Figure 8-3 the three types of forces are repeated (from earlier chapters). It is the shear force which governs when the rock will fail. As shown in Figure 8-3 this may happen when the cohesive strength decreases, the pore pressure increases, or when the shear angel decreases. A change in the pore pressure is controlled the pore water flow (discussed in next chapter). If a shale yields, its permeability will increase, and water will flow easier; a self-accelerating process.
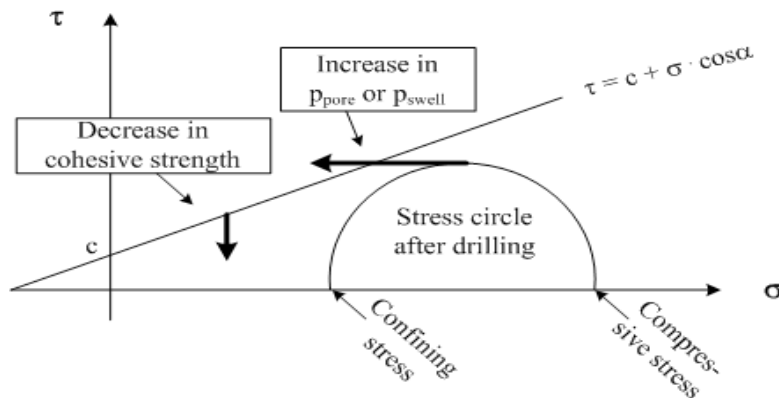
Figure 8-3: Three mechanical forces which may lead to destabilization of the sedimentary rock.

Stress related instability is related to the rock strength, weak bedding plane, pore pressure and the hydrostatic pressure in the wellbore. It is also related to extraordinary in-situ stresses in the formation; historical tectonic activity in the area. Normally stressed basins are characterized by stresses in the vertical direction being the largest one. But under tectonic stress regime, stress orientation is valuable information to evaluate failure direction. Too high wellbore pressure leads to fracture at the casing shoe, since the weakest point in the formation is located here.

By lowering the formation pressure below its collapse pressure, the formation will experience shear failure in the borehole wall resulting from high tangential stress. In older consolidated clay, which is hard and brittle, the wall will splinter under compressional stress and cave or slump into the hole. This leads to hole enlargement and possibly bridging when combined with inadequate hole cleaning. As the wellbore pressure drops further below the collapse pressure during the final stages of a gas blowout, the well will collapse and become packed with crushed wall material, and the blowout will eventually come to a stop.

Instability caused by high tangential stresses around the wellbore while drilling is a function of formations pressures /stresses and the geometry of the wellbore and its beds. This can be expressed through a linear and plane strain failure criterion, like Mohr-Coulomb's.

During the initial stage of collapse, the cavings eventually arriving at the shale shaker can indicate what is causing the problem. The information that potentially can be gained from cavings is pointed out in Figure 8-4:

Splintery cavings from underbalanced drilling in shale

Angular cavings, shear failure due to excessive horizontal stress

Tubular cavings with parallel, smooth, flat surfaces indicating pre-existing, natural fractures
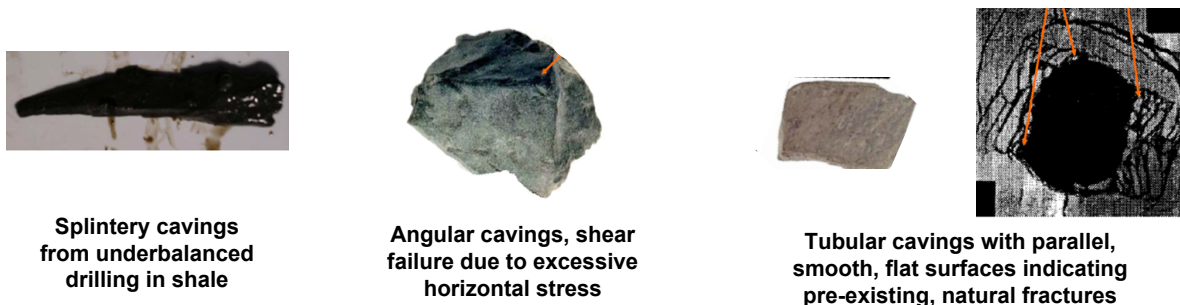
Figure 8-4: Surface symptoms of sub-surface mechanical stress-problems, revealed from the geometry of the cavings. Cavings are always larger than cuttings, typically 3 cm.

8.3   Chemical stability

Shale makes up for more than 75% of the drilled formations, and more than 70% of the borehole problems are caused by shale instability (including mechanical related). Shale properties range from very soft to hard, and from very laminated to very compact. Shale destabilize when drilling fluid penetrate existing fissures, fractures and weak bedding planes. In addition to shale fluid interaction, fluid invasion will also alter the pore pressure or effective stress state.

The term shale is used for an entire class of fine-grained sedimentary rocks that contain substantial amounts of clay minerals. The amount and type of clay content determine the shale's affinity for water. The Smectite shale type called Montmorilonite reacts strongly with water for one main reason; shale contains negatively charged clay minerals, and polar water is attracted to the mineral. Shale containing Smectite has a greater affinity for water than shale containing Illite, Mica, Chlorite, Zeonites or Kaolinite.

Drilling overbalanced through shale formations with WBM allows drilling-fluid pressure to penetrate the formation. Because of the saturation and low permeability of the formation, the penetration of a small volume of mud filtrate into the formation causes a considerable increase in pore-fluid pressure near the wellbore wall. The increase in pore-fluid pressure may break the cohesive bonds in shale. According to Moody and Hale (1993), there are three important chemical factors that affect wellbore stability.

- Relative salinity of the drilling mud in relation to the formation pore fluid. This is expressed as the water activity A_w which is inversely proportional to salinity.
- Change in pore pressure is limited by the membrane efficiency, which describes how easily ions can pass from the drilling mud into the formation.
- Ion exchange capacity of the shale is important as the replacement of cations such as K^+, Mg^{++}, Ca^{++} and Na^+, in that order, weakens the shale.

There are three chemical forces in general

- van der Waal forces between clay platelets
- Electrostatic repulsive forces between clay platelets
- Forces (repulsive/attractive) resulting from hydration/solvation of clay surfaces from ions present in interlayer spacing (adsorbed or free)
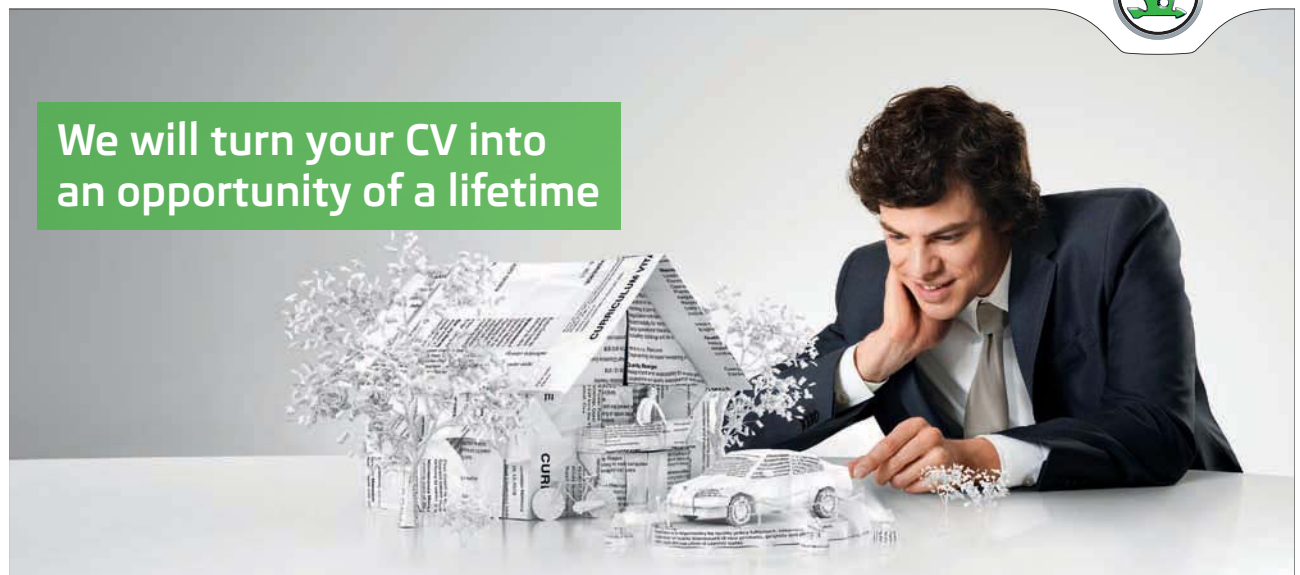
Latter two forces are usually lumped together to form the hydration or swelling pressure. To better understand the topic of chemical stability we introduce two related processes:

- Water transport
- Swelling pressure

8.3.1   Transport mechanisms

In Table 8-1 the type of transport and its driving forces are introduced, several of them are discussed in detail by Hale at al. (1993).

Flowing material	Dp/Dl	Δ(chem.pot)/Dl
Water	Convection (direct transmission)	Osmoses
Solution / ions	Advection (indirect transmission)	Diffusion

Table 8-1: Four types of driving forces leading to two types of material flow.

The four driving forces are:

1. Convection or Hydraulic pressure: During overbalanced drilling, flow of water into the formation is governed by Darcy's law.
2. Advective pressure diffusion:
3. Osmotic pressure: Water is transferred from regions of low salinity to regions of high salinity to reach equal concentration. The activity of the pore water, $A_{w,pore}$, must be equal to that of the mud, $A_{w,mud}$, achieved through adding the correct amount and type of electrolytes (salt).
4. Chemical diffusion: Transfer of specific ions from regions of high concentration to regions of low concentration (the opposite of osmotic flow direction).

The resulting flow from the four driving forces can be expressed mathematically. The four most useful equations are:

1. Convection flow of water driven by hydraulic pressure:

$$dV/dt = kA/\mu_f \cdot dp/dr \qquad (8.1)$$

2. Advective pressure diffusion ahead of the water front:

$$dp/dt = k/(\mu_f \cdot \varnothing_{eff}) \, [d^2p/dr^2 + 1/r \cdot dp/dr] \qquad (8.2)$$

$$\varnothing_{eff} = \varnothing + 1/b_l \cdot (\beta_{fm} - \beta_{grain} \, (\varnothing)) \qquad (8.3)$$

3. Diffusion (Fick's law):

$$dc/dt = D\ [d^2c/dr^2 + 1/r \cdot dc/dr. \tag{8.4}$$

Diffusion of ions moves in the opposite direction of water flow

4. Osmotic pressure: Activity of pore water, $A_w = A_w$, is proportional to the vapor pressure, and is controlled through salt concentration:

$$p_{swell} = RT/V \cdot ln\ (p_{vapor,mud}\ /\ p_{vapor,fm}) \tag{8.5}$$

In chemically inactive material the Capillary pressure will dominate and take the place of the convective induced flow. Capillary pressure is expressed through: Only OBM can change the capillary pressure sufficiently to avoid this type of water entrance. Usually, in shale capillary threshold pressure is very high due to very small pore throat.

$$p_c = 2\ \sigma_c \cdot cos\ \theta\ /\ r \tag{8.6}$$

In the following paragraphs the transport of materials through shale has been exemplified and illustrated by van Oort (2010)

Assuming

- Drilling at high hydraulic overbalance (mechanical stability is taken care of)
- Drilling fluid ion concentration > pore fluid ion concentration, but just slightly, sufficient for diffusion of ions to take place.
- Assume no coupled flow between the different driving forces

How will the 3 processes (water content, pore pressure and swelling pressure) look like after some time?

Van Oort (1997) applied the flow-equations at an engineering level. Pressure penetration and ion diffusion in shale, obtained by applying expanded solution of the three transport equations and material constants for typical shale ($k_{shale} = 10^{-21}$ m²). The governing equations predicted the development of three fronts around a wellbore in shale vs. time as presented in Figure 8-5.
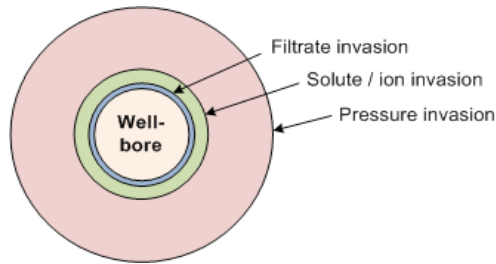
Figure 8-5: Extention of three different material fronts flowing into the wellbore wall while drilling in overbalance and with balanced salt contetration (van Oort, 1997).

The estimation revealed that pressure would precede ion-diffusion at 1-2 order of magnitudes higher. Shale is so tight it cannot dissipate water fast enough.

8.3.2   Swelling of shale

Swelling is a complex process and osmotic swelling is a too simplistic model. Results from a laboratory experiment are presented in Figure 8-6. Here swelling pressure in Na-Montmorillonite as a function of inter platelet distance was studied. Stable states are indicated by arrows in Figure 8-6 and are characterized by odd numbers of water layers. Density distribution of water – oxygen is a function of the distance from the sheet surface. Results are shown for the stable states of 4 different spacing. Osmosis is a powerful force and can be compared to congelifraction.
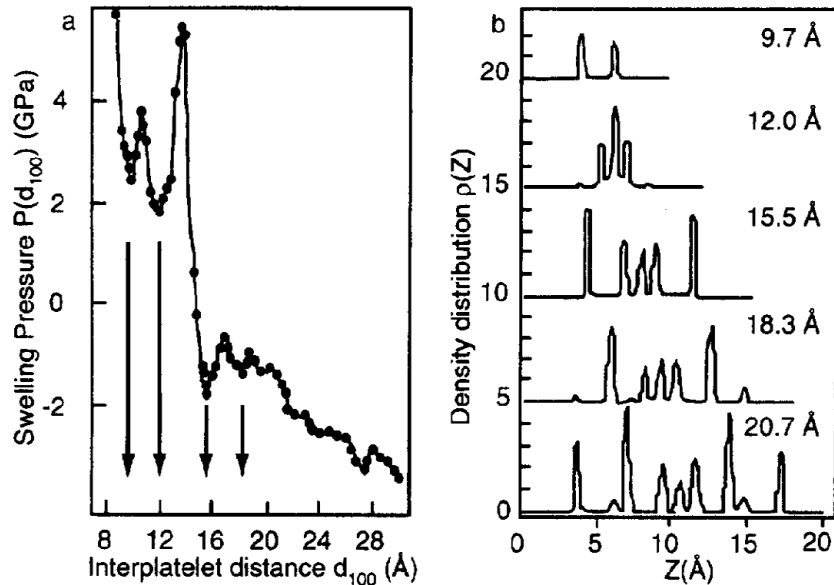
Figure 8-6: Swelling pressure vs. interplatlet distance (left), and number of water molecular layers vs. interplatelet distance (right), obtained through Atomic Adsorption Scanning (van Oort, 1997).

Since osmotic pressure is being the most important one in clay, some more details are appropriate: Argillaceous rocks experience significant swelling, alteration, and degradation by adsorption of polar molecules (such as water) or ions (such as Na^+) onto weakly charged clay sites. Water is attracted to the surface of the mineral but also enters the opening between unit layers and may cause the distance between them to increase, a phenomenon called swelling. Swelling pressure can be predicted through the knowledge of the water activity in the shale and basic thermodynamic relationships. Swelling stress can be predicted by equation 8.7:

$$p_{swell} = -\frac{RT}{V} \ln\left(\frac{p}{p_o}\right)$$

(8.7)

R is the universal gas constant, V the partial molar volume of pure water, p the aqueous vapour pressure of the formation fluid, p_o the aqueous vapour pressure of pure water. The quotient p/p_o is very close to the value of the water activity of pore water.

New swelling tests were performed on shale containing 65% Montmorillonite. The swelling index does not go to zero, i.e. there is always residual swelling as seen in Figure 8-7.
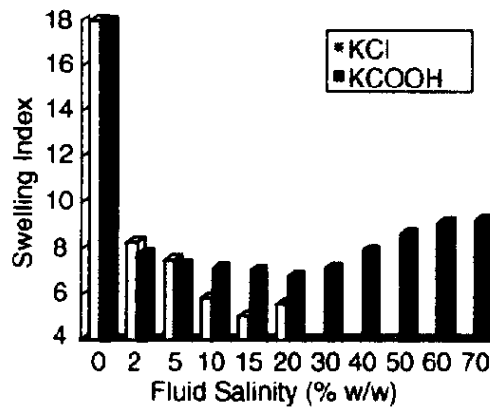
Figure 8-7: Swelling vs. fluid salinity (van Oort, 1997).

KCl minimizes swelling due to small degree of hydration of K^+. But it is more complex: At high c, swelling increases again. K^+ replaces less inhibitive ions. Also anions are introduced in the interplatal spacing. In the field K^+ never occur at such high concentration alone. This cation exchange effect takes place slowly (diffusion is slow). p_{swell} can never reach zero. However, swelling (expansion) can be zero due to cementation bonds. Potassium is generally regarded as the most effective in making the clays less hydratable. And the geometry of Potassium ions is well suited for entering the space between Montmorillonite unit layers as indicated by Table 8-2.

Molecule	Not hydrated	Hydrated
H	1,6	1,6
O	1,3	1,3
H_2O	2,9	2,9
K^+	2,1	7,6
Na^+	1,8	11,2
Ca^{++}	3,0	19,2
Na SiO_2	6,1	6,1
Clay pore throat	10-100	

Table 8-2: Diameter of some molecules (in A).

But the swelling is also clay type dependent: K^+ does not inhibit Illite, and may increase swelling of Kaolinites.

8.4   Inhibitive muds

In the drilling fluids service industry the term "inhibition" has come to mean the suppression of hydration of clay, which means inhibit the water to transform the shale into swelled, soft, sticky shale, while her ewe mean the inhibition of swelling pressure. After this knowledge it is acceptable to define inhibition as Reduction of swelling pressure

Before tending to inhibitive muds we would like to introduce some basic issues concerning swelling pressure and hydraulic pressure

Swelling pressure vs. hydraulic pressure: Inhibitors cannot prevent pore pressure increase induced shale problems because the inhibitors (in the diffusion front) will always lag behind the pressure front. Swelling pressure can therefore not be reduced down to zero. An effective tensile force is remaining supporting the shale. When the net tensile forces overcome the shale's tensile strength (low in shale), yielding will occur at the weakest sites, which will trigger subsequent full-scale failure. Pressure fluctuations (from S&S) will change hydraulic support, and may deliver the "final blow" to already weakened shale.

This time-lag in inhibitor transport is regarded as the main reason behind inhibitors shortcomings as shale-stabilizers. When inhibitors are arriving together with water they may lead to very small to low p_{swell} (as opposed to large p_{swell} if no inhibitor was present).

Under these circumstances something more than inhibition is needed. The answer is: Prevent water flow to suppress pressure penetration. This is how to achieve it:

0. Apply radial support through proper MW (prerequisite)
1. Maintain support by reducing filtrate invasion
2. Use inhibitive mud

Pressure inside the cuttings: Cuttings are exposed to the same mechanisms as the wellbore, except that

• Geometry and stress condition are different
• Timing is different. Exposure is typically only 1 hour

In Figure 8-8 the forces action on a shale cuttings is presented.
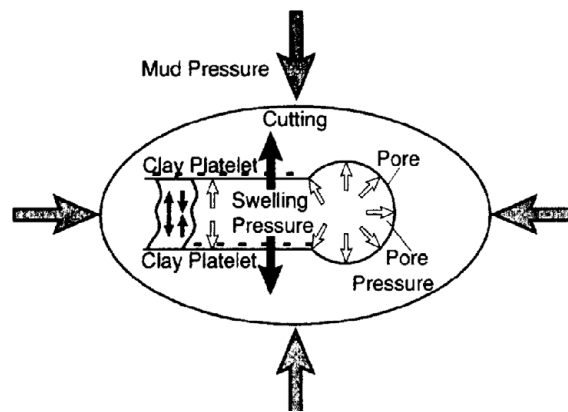
Figure 8-8: In-situ stresses are suddenly relieved and replaced by mud pressure (phydr) when cuttings are generated (van Oort, 1997).

The resulting radial forces can be expressed as:

$$\sigma_r = p_{hydr} - p_{pore} - p_{swell} \tag{8.8}$$

and will be in tension if $p_{hydr} < p_{pore} + p_{swell}$ and disintegrate if $p_{cohesion}$ is overcome

The following will take place:

1. p_{hydr} will lead to slow invasion and equalize p_{pore}, but normally not within 1 h
2. A bigger problem is the p_{hydr} reduction as cuttings are transported up the wellbore, combined with slow increase of p_{swell}, probably the most detrimental effect

Counter measures:

1. Encapsulation
2. Shut off water by enhancing viscosity of filtrate
3. Use inhibitive mud (see later)

Inhibitive muds can be grouped into three types. We will now compare their pressure transmission-ability through shale, and present the most common representative mud for each mud type.

8.4.1   Conventional inhibitive WBM: KCl/PHPA

Reducing p_{swell} in Smectite clay – young reactive gumbo type shale. KCl exhibits the highest inhibitive effect of all salts. This is indicated in Table 8-2 above.

Cations exchange place with Na^+ ions. But have some shortcomings:

1. No filtrate prevention due to low base fluid viscosity, as shown in Figure 8-9.
2. Only moderate osmotic pressure due to low membrane effect (1–2%) due to high mobility of KCl in shale $\rightarrow$ unsuitable in older, less reactive shale like Illite and Kaolinite. These shale types contain too low p_{swell} –potential for KCl to act upon. The older shale types will fail due to mud pressure penetration at prolonged exposure caused by KCl filtrate invasion.
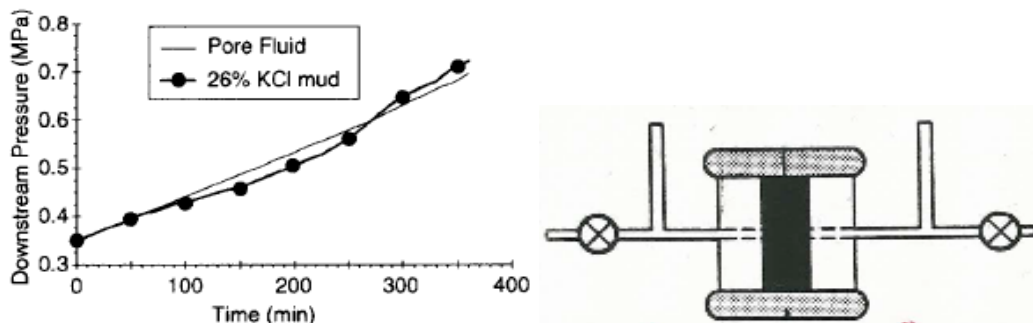
Figure 8-9: Shale's ability to transmit pressure in the base fluid of conventional inhibitive WBM (van Oort, 1997).

Polymers, like PHPA, with functional groups of positive polarity absorbs onto clay surfaces at multiple sites à they are more difficult to exchange/remove. Good inhibitors when low-molecular (< 10 000); penetrate pores of the shale. High molecular polymers, like PHPA, latches on to the outer surface of shale in a web-like pattern and combat disintegration of shale. Pore blocking is minimal as shown in Figure 8-10. Ideal additive for cuttings stabilization.
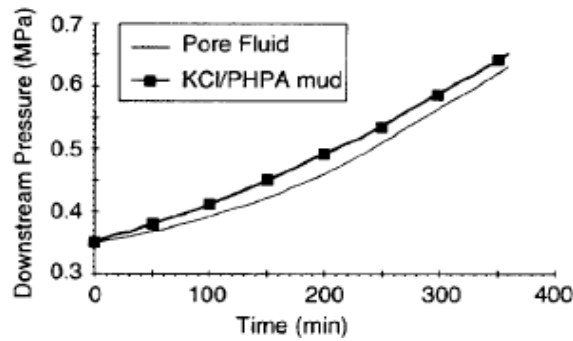
Figure 8-10: Shale's ability to transmit pressure in conventional mud (van Oort, 1997).

Figure 8-11 shows changes relative to the properties in the native shale and to non-inhibitive WBM. It shows that pore pressure will be enhanced in all three invasion zones, but the water content and swelling pressure is reduced. However, both ingredients (KCl + PHPA) fall short when older, less reactive shale are drilled.
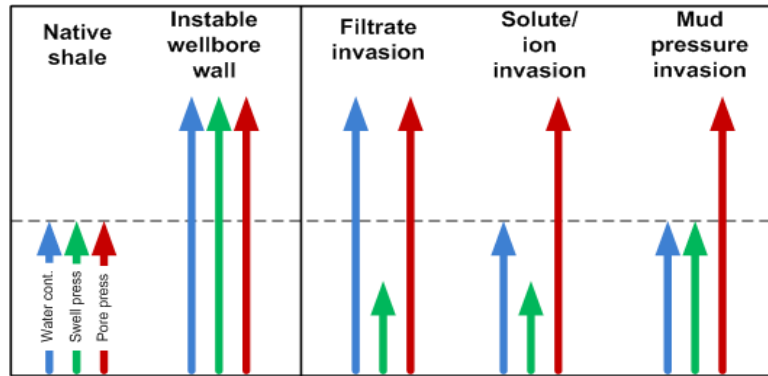
Figure 8-11: Native shale and shale with no inhibition (left). Estimated behavior of conventional Inhibitive WBM (right) (van Oort, 1997).

8.4.2   Osmotic WBM: CaCl$_2$ + methyl-glucose

CaCl$_2$, CaBr$_2$ are highly soluble à high density. Their ad- and disadvantages are:

- High osmotic pressure (but due to low membrane efficiency (1–10%) the osmotic pressure is limited to 1/10–1/100), can be applied to partially offset the hydraulic overbalance
- High filtrate viscosity
- Leaky membrane $\rightarrow$ ion diffusion into shale, against the back-flowing water $\rightarrow$ Na$^+$ exchange K$^+$ $\rightarrow$ p$_{swell}$ will again increase

Poly-glycerol and – glycols are saccharides of low molecular size (< 10 000). They viscosify the filtrate / build an internal filter and retard filtrate invasion as shown in Figure 8-12.
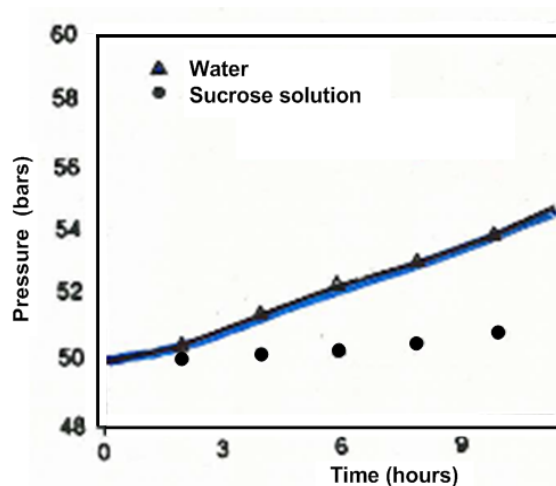
Figure 8-12: Shale's ability to transmit pressure in a sucrose solution.

Resulting mud type behavior is shown in Figure 8-13. We see that the water content and the pore pressure are expected to be reduced. But swelling pressure is elevated in the filtrate- and the SI-zone due to unfavorable exchange of cations (Na^+).
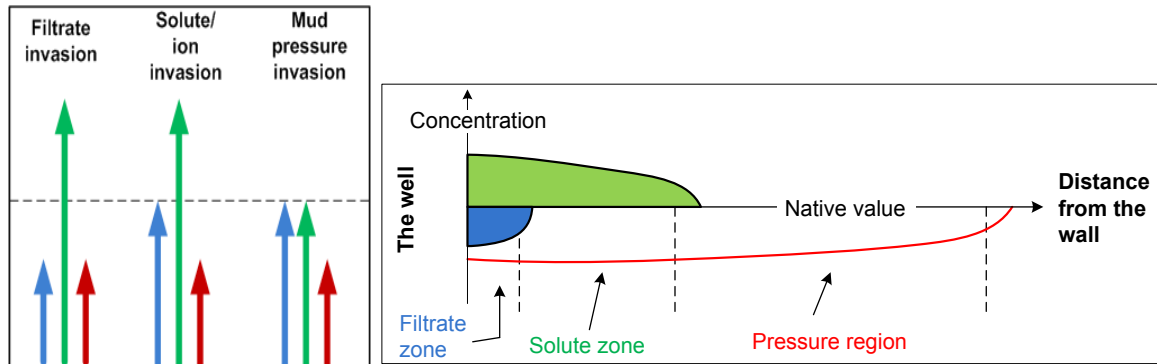
Figure 8-13: Estimated behavior of shale in an osmotic WBM and interpreted wellbore behavior (right) (free after van Oort, 1997).

WBM allow water and thereby well pressure to penetrate into wellbore shale. Near wellbore pressure increases and thereby reducing the true overbalance. Without it, shear failure may occur. A perfect drilling fluid should create a high-osmotic-efficient membrane.

Although shale is almost impermeable, the osmotic flow is determined by chemical potential or water activity A_w in the mud and in the pore water. A_w is a measure of water's salinity

A_w, distilled water   = 1.00
A_w, saturated NaCl   = 0.755
A_w, saturated $CaCl_2$ = 0.295

When $A_w = 1$, the water has the highest possible potential.

It is the difference in salinity that causes osmotic water flow, ΔA_w = chemical potential. When $\Delta A_w = 0$ between pore water and mud, there will be no osmotic flow of water, hence no swelling and accordingly no problems during drilling. Whenever there is a difference in A_w between clay and mud, the swelling pressure is defined as:

$$p_{swell} = - \frac{RT}{V_w} \cdot \ln \frac{A_{w,clay}}{A_{w,mud}} \tag{8.9}$$

Salt water muds are able to restrain the flow of water from the mud to the shale. This is accomplishing by decreasing the concentration of free water molecules in the drilling fluid. In salt water muds, large quantities of NaCl or KCl are added to the mud system, and the water activity is largely reduced. When $A_{w,\,clay} = A_{w,\,mud}$, the formation will become stable. It has later become evident that also salt type must match pore water salt type to completely eliminate swelling. For limestone and salt formations this theory holds true.

Below follows a method of how to determine $A_{w, pore}$. We will use eqn. (8.10) to determine p_{swell}.

$$p_{swell} = \frac{RT}{V} \ln \left(\frac{p_{vapor,mud}}{p_{vapor,porewater}} \right)$$
(8.10)

By comparing this eqn. with eqn. (8.9) we see that vapour pressure is synonymous with water activity. The apparatus presented in Figure 8-14 is used for this purpose. The figure and the procedure below demonstrate how.
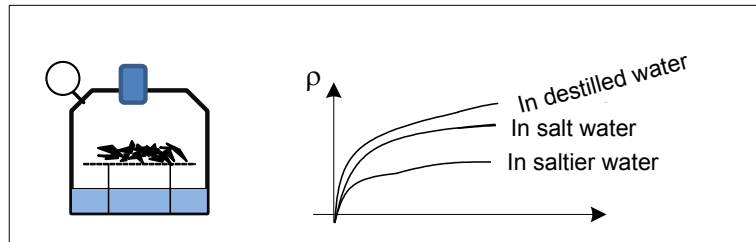
Figure 8-14: The density of dried and crushed shale is measured after water has been absorbed in the shale inside the desiccator.

1. Collect clay from upper Jura. Dry and crush
2. Measure ρ vs. A_w
3. Make a plot
4. Collect preserved clay. Measure $\rho_{original} = 2.13$
5. Find original A_w from plot

Download free eBooks at bookboon.com

Figure 8-15 demonstrates how shale from upper Jura, which had an in-situ density of 2.13 kg/l, is determined to have an in-situ pore water activity of 0.60.
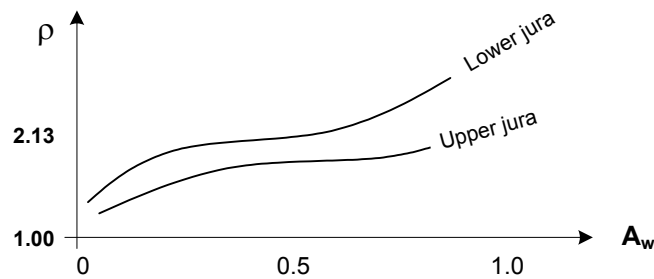
Figure 8-15: Through the original density of shale its pore water activity can be determined.

Typical WBM have activities between 0.85 and 0.95. Typical shale in places like the Gulf of Mexico have pore fluid activities between 0.75 and 0.85, based on extrapolations from laboratory measurements. Hence, the use of typical muds in typical sales is expected to cause an increase in the pore pressure within the shale, leading to shale swelling, weakening, and the development of washouts. Membrane efficiency describes shale affinity to WBM and OBM. The membrane efficiency is affected by the mud chemistry, solute concentrations and other properties; oil- based mud has nearly perfect efficiency, whereas water-based mud generally has very low efficiency. Thus, oil-based mud is good for drilling in shale to mitigate swelling or contraction problems due to its perfect membrane efficiency, but it can be very expensive to implement or precluded by regulatory restriction.

When exposed to pure water, eqn. (8.9) or (8.10) suggests that tremendous swelling pressures can be developed in relatively saline shale. Rupture tests have shown that shale sections exposed to water in a borehole can fracture if critical stress conditions exist.

8.4.3   Type 3: Non invading WBM / OBM

For both of the non-invading fluids water is hindered to flow into the shale, but hindered by two different techniques. The WBM, shown in Figure 8-16, is applying filter building techniques. Either poly-glycols or silicates will hinder filtrate influx. The OBM, shown in Figure 8-17, create a high negative capillary entry pressure. Both mud types constitute a highly efficient osmotic membrane. Osmotic membrane hinders hydraulic flow of water, ions and particles, but not osmotic transfer of water.
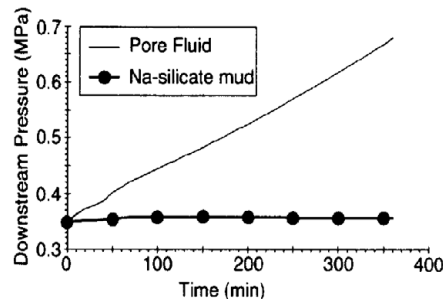
Figure 8-16: Shale's ability to transmit pressure in a NA-silicate WBM.
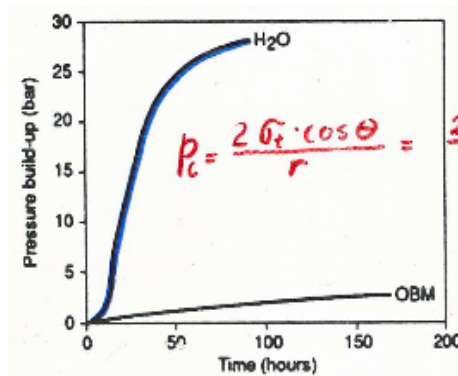
Figure 8-17: Shale ability to transfer pressure in OBM.

The resulting evaluation of the two fluids of non-invading character, one with balanced water activity (will neither lead to change in the shale) and one with lower water activity (will neitherlead to any change in the shale) is presented in Figure 8-18.
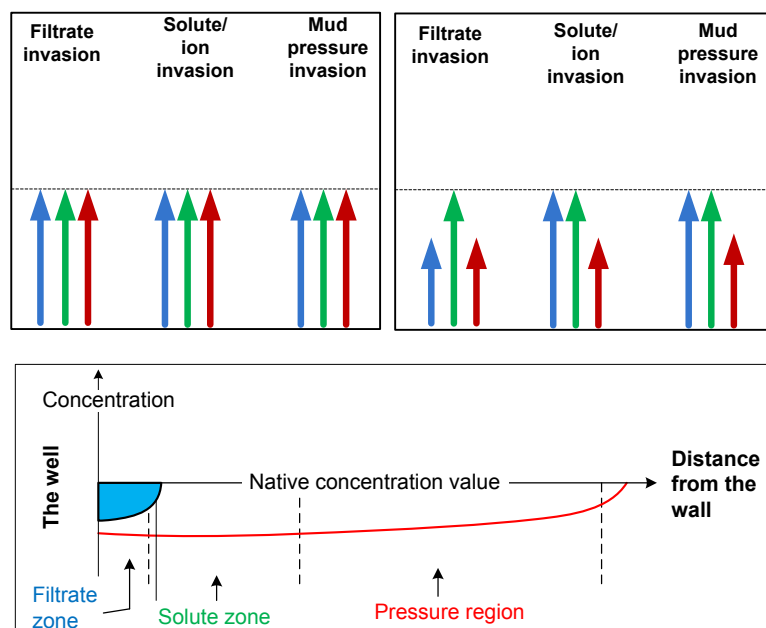
Figure 8-18: Estimated behaviour of shale in non-penetrating inhibitive muds with balanced water activity (upper left) and lower water activity (upper right). The lower water activity results in the invasion shown at the bottom (free after van Oort, 1997).

In the paragraphs below we would like to present some further knowledge about oil based mud. In spite of the environmental related restrictions there are still many occasions when oil based mud of some kind is necessary. As yet, water based muds do not provide the levels of shale inhibition and lubrication offered by oil based muds. The viability of many offshore field developments depends on the ability to drill wells from a single central platform, with high lateral displacement. For many such wells, oil based muds are viewed as the only effective mud types to allow the targets to be safely and economically reached.

Oil based mud consists of these components:

1. Base oil   – the continuous phase
2. Water   – viscosifying droplets
3. Emulsifier   – emulsify water in oil
4. Wetting agent   – makes the wellbore oil wet
5. Viscosifyer   – like in WBM
6. Weighting material – like in WBM

The three first items on the list make up the basic emulsion. When mixed together the result becomes like shown in Figure 8-19. Besides of lowering the interfacial tension, the emulsifier stabilizes the emulsion, because its molecules are adsorbed at the oil/water interface, forming a skin around the droplets. This skin acts as a physical barrier, preventing the droplets from coalescing when they collide with each other. The size of the droplets is in the colloidal size range. In order to create oil droplets in water or vice versa the surface tension between the two phases must be lowered, so that the droplet curvature increases and smaller droplets are formed. Two methods of measuring surface tension are presented next.
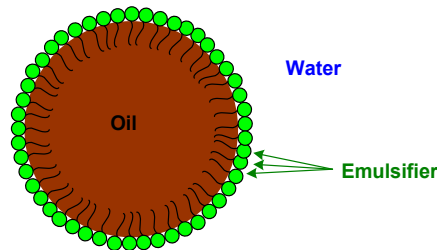
Figure 8-19: Protective skin of surfactants molecules around the surface of an oil droplet.

Figure 8-20 shows a capillary tube, where the height a liquid will spontaneously rise to is measured. At equilibrium, the contractile force of the meniscus is balanced by the hydrostatic head of the column of liquid, expressed through:

$$F = p \cdot A = \pi r^2 h \cdot \rho_{liquid} \cdot g \ = \ 2\pi r \cdot \cos\theta \cdot \sigma \qquad (8.11)$$
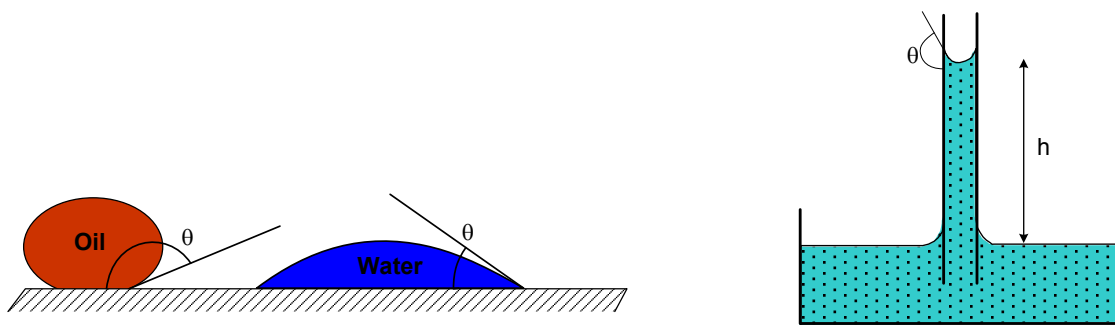
Figure 8-20: Contact angle (left) and capillary tube. When angle $= \theta \leq 90^o$ the solid is water wet.

σ is the surface tension, θ the contact angle, and r the radius of the capillary tube. The surface tension between the liquid and the contacting substance above the liquid is found by solving eqn (8.11):

$$\sigma = \frac{g\ h\ \rho_{liquid}\ r}{2\cos\theta} \qquad (8.12)$$

Solved for pressure (p = ρ g h), eqn. (8.12) takes the form:

$$p = 2\sigma\cos\theta / r \qquad (8.13)$$

If two immiscible liquids are juxtaposed on a surface, one liquid has preference over the other in wetting the surface, depending on the relative tension between the liquids and the solid, and on the interfacial tension. The angle θ indicates the preferential wettability. The interfacial tension between oil and water is very high, θ ≈ 0º, so if the liquids are mixed together mechanically they separate soon after the agitation ceased, to maximize the interfacial area. Lowering the interfacial tension with a surfactant enables one of the two liquid to form very small droplets. The interfacial tension between mineral oil and water is about 50 dynes/cm, and a good emulsifier will lower it to about 10 dynes/cm.

To avoid water wetted solids or steel surfaces, add oil-wetting agents to the mud. Figure 8-21 presents the resulting condition in the wellbore.

The emulsion stability is tested with an Emulsion Stability Tester. The working principle is to determine at which voltage the currency will be short cut when immersed into the emulsion. As a rule of thumb, it is necessary with around 3 volume % of the emulsified phase to reach a maximum voltage. The stability of an emulsion increases with increasing viscosity (of the continuous phase) because the number of collisions between the droplets is decreased. Similarly, the stability decreases with increasing temperature because the number of collisions increases. The lower the interfacial tension can be made, the smaller the droplets become, and the more stable the emulsion.

Water (blue) is emulsified (yellow)
but wetting shale and cuttings (gray)   Wetting agent (red) is added
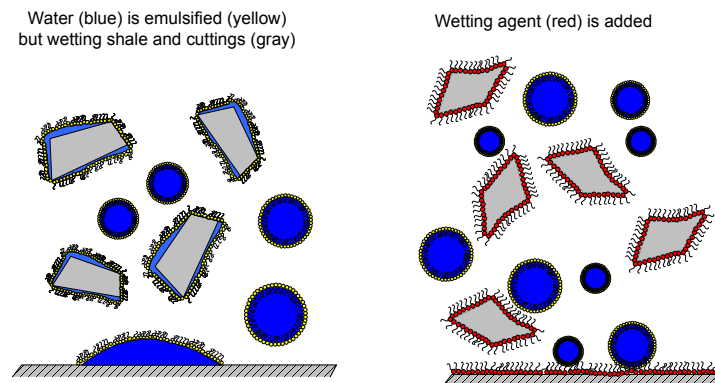
Figure 8-21: Water wetted solids (left) and oil wetted (right).

Pseudo oil based mud (POBM): The restrictions on the discharge of cuttings contaminated with mineral oil, led to the development of synthetic or natural derivative fluids which allowed synthetic oil based muds to be formulated with enhanced biodegradability and reduced bioaccumulation and toxicity, but which still possessed the high performance of mineral oil based muds. Pseudo-oil-based muds are made from:

Ester, ether, olefin and other extracts from plants and animals.

All the synthetic mud types have similar properties as mineral oil; they make emulsions (up to 50% water in oil) by means of optimal emulsifiers, thus reducing cost and environmental impact; make wide ranges of densities and rheologies; tolerate contaminants; provide lubrication properties similar to mineral oil; similar compressibility/expansion ability as mineral oil; excellent return permeability; are thermally stable and are biodegradable.

8.5 Hole problems

Failures are defined as serious incidents, so serious that it becomes necessary to make repair actions. The operator is spending non-productive time (NPT) to restore the situation back to normal. As an introduction to hole-problems we have decided to group all failures in accordance to where the problem is located, and summarized them in Table 8-3:

Location of failures	Failure	Failure Sub Class
In the formation	**Lost Circulation**	Induced Fracture LC Natural Fracture
	Kick	High Pore Pressure Kick Operational Related Kick
	Inefficient ROP	Formation Related Low ROP Operational Related Low ROP
In the wellbore	**Stuck Pipe**	Differential Stuck Mechanical Stuck
	Poor Hole Cleaning	Accumulated Cuttings Accumulated Cavings Wellbore Wash Out Chunk In Hole
In drilling equipment	**Drill String Wash Out**	

Table 8-3: Classification of downhole failures with respect to where they are located.

We differentiate between failures and errors. By errors in this context is meant deviation from normal expected behaviour. Errors may heal themselves or be healed, but may lead to a failure if not taken seriously enough. The errors are presented in Figure 8-22 can be applied as indicative symptoms to the failures.
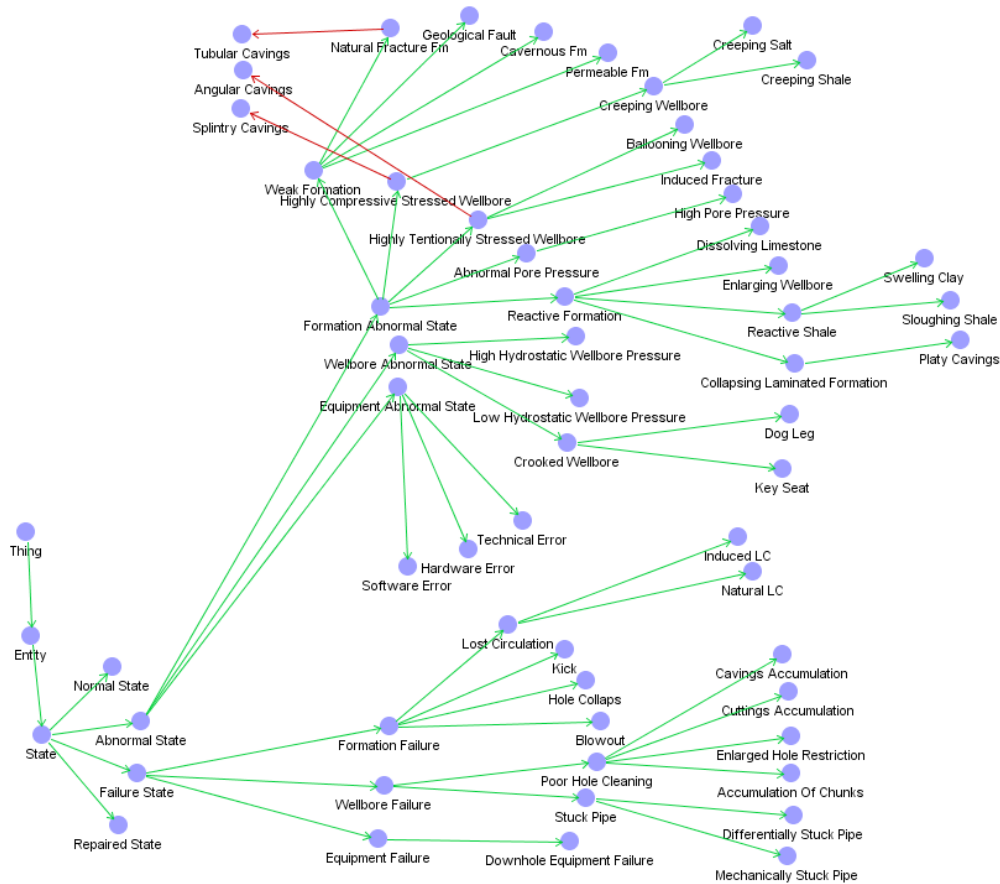
Figure 8-22: Errors during oil well drilling, grouped with respect to location of where they emerge. If these errors are detected at the surface location we call them indicative symptoms of failures.

In the following paragraphs we have selected four errors to discuss in somewhat more details. Can errors be used as symptoms to avoid failures as indicated in Figure 8-23.
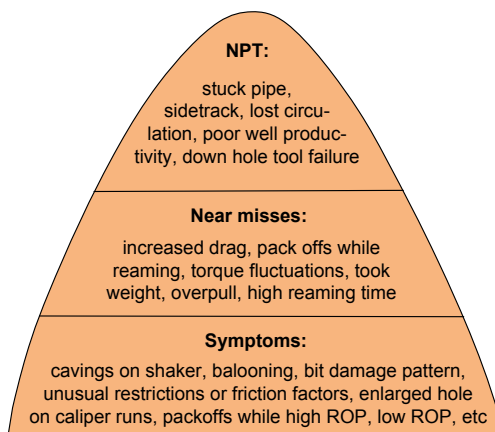
Figure 8-23: Symptoms and near misses can be used to adjust performance to avoid failures. In addition they can trigger re-design of the operation, to even avoid the ever-repeating symptoms!

Here follows a few selected errors and their symptoms.

Bit balling: Attractive forces exist between two solid surfaces but the two surfaces do not normally adhere when pressed together, because the attractive forces are extremely short ranged (Angstroms), and the area of intimate contact is very small. Even two smooth, highly polished surfaces have microscopic irregularities, and contact is obtained only between highs, as shown in Figure 8-24. Two plates of polished glass will stick together. It is the attractive van der Waal forces that are activated through the closeness of the two plates. And to separate the two plates a wedge must be forced in between them.
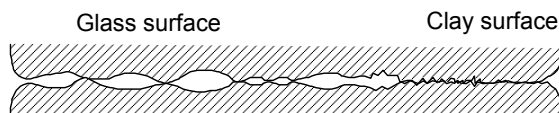
Figure 8-24: Microscopic view of two polished solid surfaces showing surprisingly small area of contact (left). Two clay surfaces have more intimate contact (right).

Solids can bond tighter together if they are ductile enough to be forced into intimate contact. For instance, the old-time blacksmith welded two steel bars together by heating them white-hot, and hammering them together. For the same reason, shale, consisting of colloidal particles, has the ability of coming in intimate contact with the rock bit or the drill collars. Swellable, soft clay stick easily to steel surfaces since it is ductile and deformable, thus increasing the contact. One method of dealing with sticky gumbo is therefore to use inhibitive mud. Symptoms of bit balling are:

- Reduced ROP
- Increased SPP – due to reduced d_{ann}
- Blocked shaker screen (soft clay)
- Overpull on tripping-out

Swelling shale: Hydratable shale usually occurs at shallow depths (< 2 500 mTVD). However, swelling shale may also be found at larger depth where the diagenesis process has been inhibited (in high pressured formations). A typical problem in upper formation is: Shale swelling → weakened wellbore → erosion → expansion of the hole. Due to low permeability water penetrate the shale very slowly. The driving force behind water transport in shale is, as stated above, either hydraulic pressure or osmosis. Hydraulic pressure can often be excluded; the transport rate is extremely slow in shale. Only osmosis, through a salinity difference between pore water and mud, can explain water invasion leading to swelling. Swelled shale becomes soft and sticky. During tripping operations the expanded wellbore could possibly be scraped off by stabilizers and the bit. Material accumulated on the BHA during tripping may be observed in surface parameters as overpull and pack off (pack off is seen only when the pumps are on).

At shallow and medium depths: Typical problems at medium depths are weakening of the wellbore – erosion of the hole: The swelling process is a slow process. When one layer of shale has swelled, it is weakened, and therefore prone to erosion. The erosion could be both of hydraulic and mechanical nature. The longer the hole stays open, the higher the probability is that the wellbore has weakened. As soon as the wellbore has swelled, the erosion starts on the weakened layers, exposing new layers. Symptoms of swelling shale are:

- Soft, hydrated cuttings coming over the shaker
- Clay balls. Shaker is blocked off
- Torque fluctuations
- Increased LGSC
- Increase of the following mud parameters: filter loss, MBT, PV, YP
- Pack off, overpull, took weight on trips
- These problems increase with increasing open hole time
- Probably not seen in vertical holes!

Enlarged wellbore: The combination of enlarged wellbore and cuttings accumulation leads to many of the problems related to poor wellbore cleaning like overpull, took weight, pack off and stuck pipe. This problem need therefor especial attention, and is illustrated in Figure 8-25.
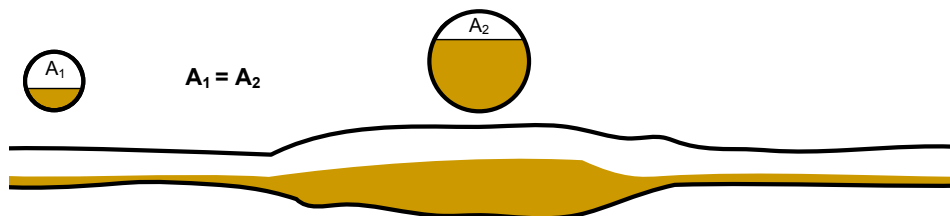
Figure 8-25: Cuttings accumulation in hole enlargement.

Enlargements are developing due to mechanical and hydraulic erosion of weakened formations. Enlarged holes are also referred to as wash out, and can either be caused by caving production or by erosion of weak or weakened wellbore, leading to overpull and took weight during tripping operations, poor control of wellbore directions, inefficient hole cleaning, casing running and cementing problems. The borehole wall usually varies in hardness. In laminated formations, the hard stringers are composed of calcite quartzite, whereas the layers in between may be composed of soft, reactive shale. Softer shale will react with the mud and become weakened and gradually hydraulically and/or mechanically eroded, leaving an enlarged hole behind. The hard stringers form sharp shoulders and ledges. These enlarged holes are eventually filled with cuttings.

8.6 Countermeasures to hole-problems

In order to do something about the problems they need to be detected and recognized. For this purpose we start the chapter by discussing surveillance and interpretation of observed deviations from normal operations

8.6.1 Surveillance

Most common is it to have access to surface recorded real-time data. In Figure 8-26 we have manually drawn some typical variations of the most meaningful data.

Figure 8-26: Variation of surface data vs. time. In presented example we can observe soft stringer, wiper tip and off-bottom test.

8.6.2   Best Practice – Drilling Limit

Every oil company/service company develops their own Best Practice. The following summary of Best Practical guidelines involves the Drilling Limit. This is an approach where the well is drilled as fast as possible, simultaneously ensuring a clean and a stable wellbore. Use best-in-class technology to eliminate/ minimize NPT to make a perfect hole. This principle is based on field experiences and on laboratory investigations.

- Keep rate of penetration (ROP) to a maximum
- High cleaning performance
    - High flow rate and high RPM of the drill string
    - Learn to drill the dirties holes possible
- Ream/circulate only 1–2 minutes prior to cnx (it does not help to do more)
- Low mud viscosity will enhance local turbulence
- Use mechanical cleaning device

The Drilling Limit is achieved through 5 consecutive steps:

Step 1:   Review relevant offset wells

Reveal typical problems. Find offset wells

Step 2:   Analyze formation properties

Determine the most time-consuming problem. Collect formation data and properties and identify operational problems vs. formation. See example of step 2 in Figure 8-27

Step 3:   Wellbore stability model

Wellbore stability is probably the most important premise for obtaining trouble free wells. Understand and apply the proper procedures.

Step 4:   Focus on additional prioritized areas, three models are needed.

- ECD
- Swab & Surge
- Cuttings transport

| Daily Drilling Report | Lithology | Formation | Well Section |

Packed off with 20 bar. Worked pipe down, lost 2 m3.

Worked tight spot and continued pooh. Worked pipe down. Torque dropped. Rotated with 10 rpm. Full return.

POOH to 20" casing shoe. Circulate BU. Established circulation. Backreamed. Observed pack off tendency

Backreamed observed pack off tendency of 10 bar. Large amount of cuttings /gumbo over shakers. Flowline plugged up with gumbo

RIH with casing. Hole packed off. Flowcheck. POOH. Tight spot at 4700 m, 15 ton overpull

Ream and log from casing shoe to TD with LWD. string stalled out.

Unable to free string by rotation. Pulled string free with 45 Ton overpull. Slided string to pass restriction

Sandy claystone — Tight spot
claystone
Pack-off
Shale
Tight spot
Sandstone
Marl

36"
26"
17 1/2"
12 1/4"
8 1/2"

Figure 8-27: Transforming the Daily Drilling Report into focused problems vs. lithology

Step 5. Summary

Some final integrated issues:

- Will ECD cross the pressure window? → Change well path or strengthen fm, change rheology, change mud type (WBM has a better fracture healing ability due to swelling of clay
- High T&D? → Add lubricity
- Long openhole time? → Higher MW is necessary to maintain stability (due to slowly climbing p_{pore})
- Nearby well? → Increase fracture propagation resistance

Only long experience and good insight can enable avoiding the problem and tight surveillance:

- Days vs. depth against a Technical Limit (# of drilling days spent when no hole problems).
- Use latest available techniques at all time. Keep yourself updated
  - Accurate simulators / models, including most realistic assumptions
  - Integrate all models and assumptions if possible
- Plot the roadmap (torque & drag up/down vs. depth).
- Make a cavings log
- Log ECD and ESD (equivalent static density)
- Watch for pack off, took weight, overpull etc.

When deviations or suspicions signs are seen during surveillance, stop and fix problem in accordance with best practice.

9   References

Bourgoyne, A.T., Jr., Chenevert, M.E., Millheim, K.K. & Young, F.S., Jr.: "Applied Drilling Engineering", SPE Textbook Series, Vol. 2, 3rd edition, Society of Petroleum Engineers, Richardson (1991).

Basmadjian, D.: Mathematical Modeling of Physical System. Oxford University Press, New York, 2003

Casson, N.: "A Flow Equation for Pigment-Oil Suspensions of the Printing Ink Type", Rheology of Disperse Systems, Pergamon Press, New York, N.Y. (1959).

Chilingarian, G.V. and Vorabutr, P.: Drilling and Drilling Fluids, Elsevier Science Publishers, Amsterdam, Updated first edition (1983).

Classifications of fluids systems, World Oil (June, any year)

Darley, H.C.H. and Gray, G.R.: "Composition and properties of drilling and completion fluids", Gulf publishing company, Pittsburgh," fifth edition, second printing (1991).

Drilling fluid engineering manual, Magcobar Division of Dresser Industries Inc., Houston (1982).

Drilling service companies:

> Geosevices http://www.geoservices.com/
> Halliburton http://www.halliburton.com/
> M-I Swaco – http://www.miswaco.com/ MI-Drilling Fluid Manual
> Schlumberger – http://www.slb.com/

Google as dictionary; http://www.google.no/language-tool/

Govier, G.W. and Aziz, K.: "The Flow of Complex Mixtures in Pipes", E. Krieger Publishing Co., Malabar, Florida (1972).

Hale, A.H., Moody, F.K. and Salisbury, D. P.: The influence of chemical potential on wellbore stability. SPEDC; Sep., 1993.

Holman, J.P.: Heat Transfer. Eight SI Metric Edition, McGraw Hill, Printed in Singapore, 2001.

Kutasov, I.M.: "Correlation simplifies obtaining downhole brine density", Oil & Gas J. (Aug. 5, 1991) 48–49.

Mitchell, R.F.: Dynamic surge/swab pressure predictions. SPEDE September 1988, 325–333.

van Oort, E.: Physico-chemical stabilization of shale. SPE paper 37 263, presented at the SPE International Symp. on Oilfield Chem., Houston, 18–21 Feb. 1997.

White, F.M.: Fluid Mechanics. International Edition, WCB/McGraw-Hill, Singapore, 1999.

Wikipedia as encyclopaedia in 250 languages; http://en.wikipedia.org/

Aadnøy, B., Cooper, I., Miska, S., Mitchell, R.F. and Payne, M.L.: Advanced Drilling and Well technology, SPE, Richardson, 2009.

10 Supportive information

10.1   Nomenclature

Latin:

A	cross sectional area	m²
A	Angstrom, 1A = 10^{-10}	m
c	concentration of volume fraction of particles	-
$c_{p,water}$	= 4184 = specific heat, reasonably const. [f(T)]	*J/kg/ºK*
d	diameter	m
E	energy or work	W
F_R	reactive torque factor	-
f	fraction	-
G	gradient	
g	acceleration due to gravity	m/s²
h	height	m
h_e	specific enthalpy = $c_p \cdot T$	J / kg
h	convective heat transfer coefficient = film conduction	*W/m²/ºK*
I	inclination of the well	º
K	power law consistency index	Pasⁿ
K_L	coefficient for bit	-
k	specific thermal conductivity, k varies with p and T	
	in similar manner as viscosity	*W/m/ºK*
	$k/(\rho c_p)$ thermal diffusivity	m²s
L	length	m
m	mass	kg
m	exponent in Δp_d expression	-
M	momentum	Nm
N	number	-
n	exponent in power law (flow behaviour index)	-
Nu	Nusselt number = $h \cdot Dl/k$	-
Pr	Prantl`s number = $\mu c_p / k = \dfrac{\nu}{\alpha}$	-
p	pressure	Pa
Δp	pressure change	Pa
P	power or effect	J (W/s)
q	flow rate	m³/s
mQ	heat flow = q"A	W
q"	heat flux pr. unit area = -k $\partial T/\partial x$	W/m²

Q	heat	J
r	radial position	m
R	resistivity	-
R	radius of pipe	m
R	the gas constant = 8.31447	J/(°K · mol)
St	Nu / (N$_{Re}$ · Pr) = $h/(\rho c_p u_\infty)$ = Stranton's number	-
T	temperature	°K
V	volume	m^3
v	fluid velocity	m/s
x,y,z	Cartesian coordinates	m
$\bar{v}$	average fluid velocity	m/s

Greek:

α	thermal diffusivity = $k / \rho\, c_p$	
β	constant in Collins-Graves rheology model	-
ε	wall roughness	m
$\dot{\gamma}$	shear rate	s^{-1}
η	high shear viscosity	Pas
μ$_{app}$	apparent viscosity	Pas
μ$_{pl}$	plastic viscosity (Bingham fluid)	Pas
π	3.1416	-
ρ	mass density	kg / m^3
σ	surface tension	Pa
τ	shear stress	Pa
θ	cylindrical coordinate (rad), readings in Fann viscometer	-
τ$_o$, τ$_y$	yield shear stress (yield point)	Pa
ν	kinematic viscosity = μ / ρ	

Subscripts referring to:

a, ann	annulus
app	apparent
bit	drill bit
c	cuttings
dc	drill collar
d	parasitic pressure drop minus Dp$_{bit}$ in the circulating system
e	equivalent
eff	effective (viscosity)
F	Fanning

fl   fluid

h   hydraulic diameter ($d_o - d_i$)

i   initial or to arbitrary number or to inner

m   mud

M   Moody

max   maximum

mud   drilling mud

NL   no load

o   outer

p   pipe

pl   plastic (referring to the Bingham model)

r   radial position

Re   Reynolds

s   sphere

w   water or to the wall of pipe

y   yield

x,y,z   Cartesian axis

0   value at start point

1,2   value at inlet/outlet of the system

300,600 rotational speed of the Fann viscometer (rpm)

10.2   Abbreviations and explanations

1D   one dimensional

ADE   applied drilling engineering (SPE textbook)

BHA   bottom hole assembly

BHT   bottom hole temperature

CEC   Cation exchange capacity

CMC   Carboxyl Methyl Cellulose

CSG   casing

DC   drill collar

DP/DS   drill pipe/drill string

ECD   equivalent circulating density

GPM   gallons pr. minute

GYP   Gypsum (added to the mud)

HHP   hydraulic horse power

Hp   Horsepower

HTHP   high temperature high pressure

HWDP   heavy weight drill pipe

IADC   International Association of Drilling Contractors

ID   inner diameter

IF   impact force

LAB   linear alkyl benzene

LCM   Lost Circulation Material

Lithology   The description of a sedimentary rock. Sedimentary rocks can be classified according to grain size, color and hardness characteristic criteria to describe the lithology. A sandstone has river facies (appearance) when it has the typical lithological moves of river deposits.

MBT   Methylene Blue Test

MMS   mixed metal systems

MW   molecular weight, mud weight

MWD   measure while drilling

NS   North Sea

OBM   oil based mud, including LT(low toxic) and PO(pseudo oil) BM

OD   outer diameter

OFU   oil field units

O/W   oil water ratio

PAC   poly anionic cellulose

PDM   positive displacement motor

PHPA   partially hydrolyzed poly anion

PPB   pounds pr. barrel

PPG   pounds pr. gallon

Rheology   Rheology is the science of matter deformation and flow properties. Measuring quantities such as viscosity, elasticity and yield point. Viscosity describes the material flow behavior and elasticity describes the structure of the material.

ROP   Rate Of Penetration

SBM   synthetic oil based mud (= POBM)

SI   system international

SG   specific gravity (water = 1.00)

SPE   Society of Petroleum Engineers

TJ   tool joint

TVD   True Vertical Depth

WBM   water based mud

WOB   weight on bit

WOC   waiting on cement

YP   yield point (identical with t_0 and t_y)

10.3   Definitions

moment	= torque = T	(Nm)
momentum	= M	(Nm)
energy	= work	(W)
heat exchange rate	= Q	
power	= $\dot{w}$ = P	(W/s)
Isothermal process	= process at constant T	
Adiabatic process	= process where no heat is transferred	
Isentropic process	= reversible, adiabatic (entropy is constant)	
A priori	= valid independent on previous observations; non-analytic.	
Ideal fluid	= a fluid where $\mu = 0$ *and* $\rho = konst$	

$div\ a$ $= \dfrac{\partial a_x}{\partial x} + \dfrac{\partial a_y}{\partial y} + \dfrac{\partial a_z}{\partial z} = \nabla \vec{a}$ = divergence of a vector

$grad\ \varphi$ $= \vec{i}\dfrac{\partial \varphi}{\partial x} + \vec{j}\dfrac{\partial \varphi}{\partial y} + \vec{k}\dfrac{\partial \varphi}{\partial z} = \nabla \varphi$ = Gradient of a scalar field ϕ = a vector field

Natural convection   = heated fluid adjacent to the wall rises due to buoyancy.

Forced convection   = mass transferred heat when liquid is pumped through a pipe

Speed of sound in gas $= c = \sqrt{k\dfrac{p}{\rho}} = \sqrt{kRT}$

Speed of sound in liquid or solids $= c = \sqrt{E/\rho}$

Elastisity or compressibility modulus $= E_v = -V\dfrac{dp}{dV} = \rho\dfrac{dp}{d\rho}$ $(E_{water} = 2.1\cdot10^9\ N/m^2)$

Coefficient for thermal expansion $= \alpha_T = \dfrac{1}{V}\cdot\dfrac{dV}{dT} = -\dfrac{1}{\rho}\dfrac{d\rho}{dT}$ $(\alpha_{T_{water}} = 1.53\cdot10^{-4}\ K^{-1})$

10.4 Continuity, momentum and energy equation in microscopic and macroscopic form

Continuity equation:

Microscopic

General form

$$-\frac{\partial \rho}{\partial t} = \nabla \cdot (\rho v)$$

Cartesian coordinates

$$-\frac{\partial \rho}{\partial t} = \frac{\partial}{\partial x}(\rho v_x) + \frac{\partial}{\partial y}(\rho v_y) + \frac{\partial}{\partial z}(\rho v_z)$$

Cylindrical coordinates

$$-\frac{\partial \rho}{\partial t} = \frac{1}{r}\frac{\partial}{\partial r}(\rho v_r) + \frac{1}{r}\frac{\partial}{\partial \theta}(\rho v_\theta) + \frac{\partial}{\partial z}(\rho v_z)$$

Macroscopic

$$\frac{d\int v\rho dV}{dt} = -\Delta\rho\bar{v}A = \rho_1\bar{v}_1 A_1 - \rho_2\bar{v}_2 A_2$$

Momentum equation

Microscopic

General form $\quad \rho\dfrac{Dv}{Dt} = \rho g - \nabla p - \nabla \cdot \pi$

Cartesian coordinates
(only x-component)

$$\rho\left(\frac{\partial v_x}{\partial t} + v_x\frac{\partial v_x}{\partial x} + v_y\frac{\partial v_x}{\partial y} + v_z\frac{\partial v_x}{\partial z}\right) = -\frac{\partial P}{\partial x} + \mu\left(\frac{\partial^2 v_x}{\partial x^2} + \frac{\partial^2 v_x}{dy^2} + \frac{\partial^2 v_x}{dz.^2}\right) + \rho g_x$$

Cylindrical coordinates

(only the r-component)

$$\rho\left(\frac{\partial v_z}{\partial t} + v_z\frac{\partial v_r}{\partial r} + \frac{v_\theta}{r}\frac{\partial v_z}{\partial \theta} + v_z\frac{\partial v_z}{\partial z}\right)$$

$$= -\frac{\partial p}{\partial z} + \mu\left[\frac{\partial}{\partial r}\left(\frac{1}{r}\frac{\partial}{\partial r}(rv_z)\right) + \frac{1}{r^2}\frac{\partial^2 v_z}{\partial \theta^2} + \frac{\partial^2 v_z}{\partial z^2}\right] + \rho g_z$$

For steady state laminar flow, this expression reduces to

$$\frac{\partial p}{\partial z} = \frac{\mu}{r}\cdot\frac{\partial}{\partial r}(r\cdot\frac{\partial v_z}{\partial r}) + \rho g_z$$

Macroscopic $\quad \dfrac{d}{dt}\displaystyle\int \rho dV = \rho_1\bar{v}_1^2 A_1 - \rho_2\bar{v}_2^2 A_2 + p_1 A_1 - p_2 A_2 - F + Mg$

F is the resultant shear force acting on the system, M the total mass flow $\left(\int \rho dV\right)$. The steady state, one dimensional pipe flow the macroscopic expression reduces to: $p_1 A_1 - p_2 A_2 - F = Mg\sin\theta$.

Energy equation

Microscopic

Conservation of energy: $\quad \dfrac{\partial Q}{\partial t} - k\nabla^2 T = 0$ (for incompressible flow)

Macroscopic

$$\left(\frac{p}{\rho g} + \frac{\bar{v}^2}{2g} + z\right)_{in} + h_{pump} = \left(\frac{p}{\rho g} + \frac{\bar{v}^2}{2g} + z\right)_{out} + h_{friction}$$

First bracket-term is called useful or total head. $\dfrac{p}{\gamma} + z$ is called the hydraulic head while $\bar{v}^2/2g$ the velocity head.

10.5 Hydraulic friction loss equations

	Newtonian model	Bingham model	Power law model
Lam. pipe	$\Delta p_p = \dfrac{32\bar{v}\mu L}{d^2}$	$\Delta p_p = \dfrac{32\mu_{pl}\cdot L\cdot\bar{v}}{d^2} + \dfrac{16L\tau_o}{3d}$	$\Delta p_p = 4K\left(\dfrac{8\bar{v}}{d}\cdot\dfrac{3n+1}{4n}\right)^n\cdot\dfrac{L}{d}$
Lam. annulus	$\Delta p_a = \dfrac{48\bar{v}\mu L}{(d_o-d_i)^2}$	$\Delta p_a = \dfrac{48\mu_{pl}\cdot L\cdot\bar{v}}{(d_o-d_i)^2} + \dfrac{6L\tau_o}{d_o-d_i}$	$\Delta p_a = 4K\left(\dfrac{12\bar{v}}{d_o-d_i}\cdot\dfrac{2n+1}{3n}\right)^n\cdot\dfrac{L}{d_o-d_i}$
Turb. Pipe. ann.	$\Delta p = \dfrac{0{,}092\cdot\rho_m^{0,8}\cdot\bar{v}^{1,8}\cdot\mu^{0,2}\cdot L}{d_h^{1,2}}$	$\Delta p = \dfrac{0{,}073\rho_m^{0,8}\cdot\bar{v}^{1,8}\cdot\mu_{pl}^{0,2}\cdot L}{d_h^{1,2}}$	$\Delta p = a\cdot N_{\mathrm{Re}}^{-b}\cdot\dfrac{4L}{d_h}\cdot\dfrac{1}{2}\rho\bar{v}^2 \quad \begin{array}{l} a=(\log n+3{,}93)/50 \\ b=(1{,}75-\log n)/7 \end{array}$
Eff. viscosity, pipe	$\mu_{eff}=\mu$	$\mu_{eff} = \mu_{pl} + \dfrac{\tau_o d}{6\bar{v}}$	$\mu_{eff} = \left(\dfrac{8\bar{v}}{d}\cdot\dfrac{3n+1}{4n}\right)^n\cdot\dfrac{Kd}{8\bar{v}}$
Eff. visc. ann.	$\mu_{eff}=\mu$	$\mu_{eff} = \mu_{pl} + \dfrac{\tau_o(d_o-d_i)}{8\bar{v}}$	$\mu_{eff} = \left(\dfrac{12\bar{v}}{d_h}\cdot\dfrac{2n+1}{3n}\right)^n\cdot\dfrac{Kd_h}{12\bar{v}}$
Shear rate pipe	$\dot{\gamma} = \dfrac{8\bar{v}}{d}$	$\dot{\gamma} = \dfrac{8\bar{v}}{d} + \dfrac{\tau_o}{3\mu_{pl}}$	$\dot{\gamma} = \left(\dfrac{8\bar{v}}{d}\cdot\dfrac{3n+1}{4n}\right)$
Shear rate ann.	$\dot{\gamma} = \dfrac{12\bar{v}}{d_y-d_i}$	$\dot{\gamma} = \dfrac{12\bar{v}}{d_o-d_i} + \dfrac{\tau_o}{2\mu_{pl}}$	$\dot{\gamma} = \left(\dfrac{12\bar{v}}{d_o-d_i}\cdot\dfrac{2n+1}{3n}\right)$
General NR$_{e,pipe}$	$N_{\mathrm{Re}} = \dfrac{d^n\cdot\bar{v}^{2-n}\cdot\rho}{K_p\cdot(8^{n-1})}$	$K_p = K\cdot\left(\dfrac{3n+1}{4n}\right)^n$	*Fanning f_{lam} = 16/ N_{Re}*
General NR$_{e,ann}$	$N_{\mathrm{Re}} = \dfrac{d^n\cdot\bar{v}^{2-n}\cdot\rho}{K_a\cdot(12^{n-1})}$	$K_a = K\cdot\left(\dfrac{2n+1}{3n}\right)^n$	*Fanning f_{lam} = 24/ N_{Re}*

10.6 Determine Rheological Constants – Regression Analysis

Generally, the best fit is evaluated through the least squares method. In this method, the best fit is considered to be that instance of the model for which the sum of squared of the difference between an observed value and the value given by the model has the lowest value.

Regression analysis can broadly be divided into two categories – linear regression and nonlinear regression. In linear regression, a straight line is fitted to the observed data values while a nonlinear model is fitted in case of nonlinear regression.

For the project, linear regression is used for the Newtonian and the Bingham plastic model while nonlinear regression is used for the Power Law and the Herschel-Bulkley model to calculate the rheological constants.

Tools for Regression Analysis:

Specialist programs such as Microcal Origin, Sigma Plot or Graphpad Prism are available for regression analysis. These programs are capable of fitting user-input functions to data. However these programs are expensive. Also these programs are difficult for the novice to learn as they are aimed at experienced users with mathematical background.

An alternative method to fit non-linear functions is to use Microsoft Excel. Excel is included in the computer package as part of the Microsoft Office and hence requires no additional expense.

Excel offers a user friendly interface, flexible data manipulation, built-in mathematical functions and instantaneous graphing of data.

Excel also contains the SOLVER function which can be used to fit data with non-linear functions. In addition, Excel can directly be used for linear regression analysis.

Linear Regression Using Excel:

For linear regression analysis using MS Excel, the data have to be put in the spreadsheet using two columns – one for the independent variable and the other for the dependent variable: shear rate and shear stress respectively. Afterwards 'Data Analysis' has to be chosen from the 'Tools Menu' and the option 'Regression' has to be selected from the dialog box for performing linear regression.

In linear regression, a linear function is used to describe the relationship between the independent and the dependent variables. The linear function can be in the following form:

$$y = mx + c$$

The parameters m and c are calculated by:

$$m = \frac{n \cdot \sum xy - \sum x \cdot \sum y}{n \cdot \sum x^2 - (\sum x)^2}$$

$$c = \frac{\sum y \cdot \sum x^2 - \sum x \cdot \sum xy}{n \cdot \sum x^2 - (\sum x)^2}$$

The coefficient of determination (denoted by r^2 for linear regression and R^2 for nonlinear regression) expresses the proportion of variance in the dependent variable explained by the independent variable and is defined as:

$$r^2 = 1 - \frac{\sum (y - y_{model})^2}{\sum (y - y_{mean})^2}$$

The closer the r^2 value is to 1, the better the fit. It is to be noted that for determining apparent viscosity for the Newtonian model using linear regression provided by the MS Excel the 'Constant is zero' box in the 'Regression' dialog box has to be checked. For the Binghamian model, this need not to be done since the intercept in this case is not zero.

Nonlinear Regression Using Excel (this section was written by D. Chowdhury in his MSc)

A method called 'Iterative Nonlinear Least Squares Fitting' can be used for nonlinear regression analysis. Like linear regression, this minimizes the value of the squared sum (SS) of the difference between data and fit. However unlike linear regression, it is an iterative or cyclical process. In this case, an initial estimate of the parameter values is made based on prior experience of the data or a sensible guess based on knowledge of the function used to fit the data.

The first iteration involves computing the SS based on the initial parameter values. The second iteration involves changing the parameter values by a small amount and recalculating the SS. This process is repeated many times to ensure that changes in the parameter values result in the smallest possible value of SS.

Several different algorithms can be used in non-linear regression including the Gauss-Newton, the Marquardt-Levenberg, the Nelder-Mead and the steepest descent methods. However, SOLVER uses another iteration protocol. It is based on the robust and reliable generalized reduced gradient (GRG) method.

All of these algorithms have similar properties. They all require the user to input the initial parameter values and use these values to provide a better estimate of the parameters employing an iterative process. All of these methods should yield the same parameter values with the same set of data.

For determining the rheological constants using nonlinear regression analysis, the initial values of the constants are determined by using the field approach. Nonlinear regression has been used for the Power Law and the Herschel – Bulkley model.

The procedure for nonlinear regression using MS Excel is outlined as follows:

- Insert the experimental values for shear rate and shear stress in two columns of the spread sheet
- Calculate shear stress using the formula for the corresponding model (i.e. Power Law or the Herschel – Bulkley model) in the third column using the rheological constant values those were calculated by adopting the field approach
- Calculate the mean of the experimental shear stress
- Calculate the degrees of freedom by subtracting the number of parameters or rheological constants in the model from the number of data points
- Calculate the standard error in shear stress by using the following formula:

$$S.E = \sqrt{\frac{\sum (y - y_{model})^2}{df}}$$

In Excel this formula must be expressed as an array formula by pressing Ctrl+Sift+Enter.

- Calculate the R^2 value
- Calculate the confidence interval (CI) of the fit at a significance level of 95 % by inserting the following built in formula for the critical t value:
- tinv(0.05,df)

- Calculate the upper confidence limit by adding CI to y_{model} and lower confidence limit by subtracting CI from y_{model}
- Open the solver function and iterate to maximize R^2 by changing the parameter values

Figure 10-1, 2 and 3 show images of the spreadsheet which has been used for regression analysis to determine the rheological constants taking data for all the six rotational speeds of the Fann viscometer into consideration. In addition, it also shows the improved curves obtained from the regression analysis.

	A	B	C	D	E	F	G	H	I	J
1	**Experimental Results**									
2	Rotor Speed	Dial Reading	Shear Rate	Shear Stress	Initial values of rheological constants using field approach:					
3	RPM	degree	(s^{-1})	(Pa)	Bingham		Power Law		Herschel-Bulkley	
4	600	38	1021.80	19.29	τ_o (Pa)	7.11	k	0.43	τ_0 (Pa)	2.2839
5	300	26	510.90	13.20	μ_p (cp)	12	m	0.5475	k	0.2019
6	200	22	340.60	11.17					m	0.6398
7	100	15	170.30	7.61						
8	6	5	10.22	2.54						
9	3	4	5.11	2.03						
10										
11	**Bingham Model (Linear regression)**									
12	Shear Rate	Shear Stress	Using Regression Analysis		Model Shear Stress		R^2			
13	(s^{-1})	(Pa)	τ_o (Pa)	μ_p (Pas)	(Pa)		0.945			
14	1021.80	19.29			20.64					
15	510.90	13.20			12.11					
16	340.60	11.17	3.57102	0.01671	9.26					
17	170.30	7.61			6.42					
18	10.22	2.54			3.74					
19	5.11	2.03			3.66					

bingham / newton / **Sheet1**

Figure 10-1: Data and regression analysis of the Bingham model.

	A	B	C	D	E	F	G	H	I	J
21	**Power Law Model (Noninear regression)**									
22	Shear Rate	Shear Stress	Model Shear Stress	Upper CI	Lower CI		**K**	**0.67127**		
23	(s^{-1})	(Pa)	(Pa)				**m**	**0.48211**		
24	1021.80	19.29	18.96	19.31	18.60		Mean	9.305		
25	510.90	13.20	13.57	13.93	13.21		df	4.000		
26	340.60	11.17	11.16	11.52	10.80		SE	0.483		
27	170.30	7.61	7.99	8.35	7.63		R^2	**0.996**		
28	10.22	2.54	2.06	2.42	1.70		Critical t	0.741		
29	5.11	2.03	1.47	1.83	1.12		CI	0.358		
30										
31	**Herschel-Bulkley Model (Noninear regression)**									
32	Shear Rate	Shear Stress	Model Shear Stress	Upper CI	Lower CI		**τo**	**1.15069**		
33	(s^{-1})	(Pa)	(Pa)				**k**	**0.36165**		
34	1021.80	19.29	19.26	19.42	19.10		**m**	**0.56477**		
35	510.90	13.20	13.39	13.56	13.23		Mean	9.305		
36	340.60	11.17	10.89	11.05	10.73		df	3.000		
37	170.30	7.61	7.73	7.90	7.57		SE	0.212		
38	10.22	2.54	2.49	2.66	2.33		R^2	**0.999**		
39	5.11	2.03	2.06	2.22	1.90		Critical t	0.765		
40								CI	0.162		

bingham / newton / **Sheet1**

Figure 10-2. Regression analysis of Power-Law and Herschel-Bulkley model.
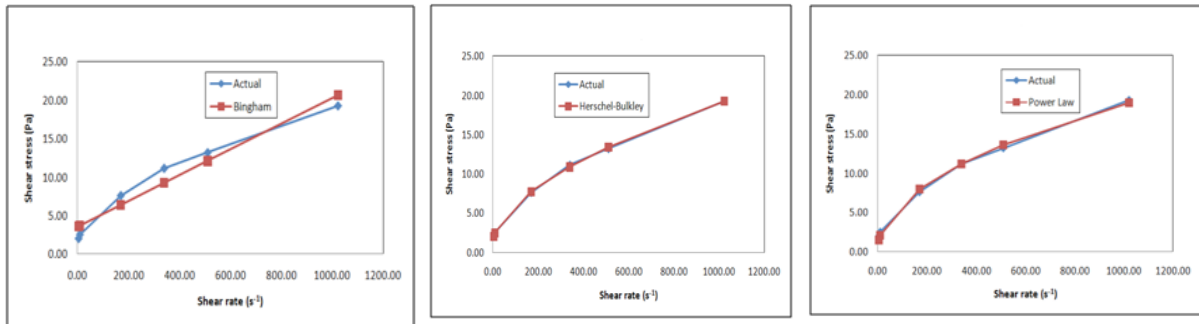

Figure 10-3: Regressed results for Bingham model, Power-Law model and Herschel-Bulkley model

10.7   Unit conversion factors

Variable		Symbol	Oil Field Units	Engineering	SI	OFU · factor = SI
	Mass	m	lb	kg	kg	0.4536
	Density	ρ	lb/gal (PPG)	kg/l	kg/m^3	119.8264
Fluid	Viscosity	μ	cP	cP	Pa·s	10^{-3}
	Yield Point	τ_y	lbf/100 ft^2	m bar	Pa	0.4788026
	Additives		lb/bbl (PPB)	g/l	kg/m^3	2.853010
	Depth	D	ft	m	m	0.3048
	Diameter hole	d_{well}	in	mm	m	0.0254
Geo-	Diameter nozzle	d_{nozzle}	1/32nd in	mm	m	.00079375
metry	Volume	V	ft^3	l	m^3	2.8315·10^{-5}
	Volume	V	gal	l	m^3	3.785412·10^{-3}
	Volume	V	bbl	l	m^3	0.158987
	Flow rate	q	gal/min (GPM)	1/min	m^3/s	6.309020·10^{-5}
	Velocity	v	ft/min	m/min	m/s	5.08·10^{-3}
Opera-	Force	F	lb$_f$	kg$_f$	N	4.448
tional	Force	F	dyne		N	10^{-5}
	Force	F	kilogram-force	kilopond	N	9.81
	Pressure	p	psi	bar	Pa	6894.76
	Power	P	Hp	KW	W	745.7
	Power	P	Hp	Hp	W	735.5
	Temperature	T	^{o}F	^{o}C	^{o}K	(^{o}F-32)/1.8

10.8   Viscosity and density of water vs. temperature

T, °C	p, kg/m^3	μ, Pa*s (*E-3)
0	1000	1.788
10	1000	1.307
20	998	1.003
30	996	0.799
40	992	0.657
50	988	0.548
60	983	0.467
70	978	0.405
80	972	0.355
90	965	0.316
100	958	0.283